MECHANISM OF OXYGEN ACTIVATION AND HYDROXYLATION BY THE AROMATIC AMINO ACID HYDROXYLASES

A Dissertation

by

JORGE ALEXANDER PAVON

Submitted to the Office of Graduate Studies of
Texas A&M University
in partial fulfillment of the requirements for the degree of

DOCTOR OF PHILOSOPHY

May 2009

Major Subject: Biochemistry

MECHANISM OF OXYGEN ACTIVATION AND HYDROXYLATION BY THE AROMATIC AMINO ACID HYDROXYLASES

A Dissertation

by

JORGE ALEXANDER PAVON

Submitted to the Office of Graduate Studies of
Texas A&M University
in partial fulfillment of the requirements for the degree of

DOCTOR OF PHILOSOPHY

Approved by:

Co-Chairs of Committee,	Paul F. Fitzpatrick
	Gary R. Kunkel
Committee Members,	J. Martin Scholtz
	Frank M. Raushel
Head of Department,	Gregory D. Reinhart

May 2009

Major Subject: Biochemistry

ABSTRACT

Mechanism of Oxygen Activation and Hydroxylation by the Aromatic Amino Acid Hydroxylases.

(May 2009)

Jorge Alexander Pavon, B.A., Rutgers University

Co-Chairs of Advisory Committee: Dr. Paul F. Fitzpatrick
Dr. Gary R. Kunkel

The aromatic amino acid hydroxylases phenylalanine hydroxylase (PheH), tyrosine hydroxylase (TyrH) and tryptophan hydroxylase (TrpH) utilize tetrahydropterin and molecular oxygen to catalyze aromatic hydroxylation. All three enzymes have similar active sites and contain an iron atom facially coordinated by two histidines and a glutamate. The three enzymes also catalyze the benzylic hydroxylation of 4-methylphenylalanine. The intrinsic primary and α-secondary isotope effects for benzylic hydroxylation and their temperature dependences are nearly identical for the three enzymes, suggesting that the transition states, the tunneling contributions and the reactivities of the iron centers are the same. When molecular oxygen and the tetrahydropterin are replaced by hydrogen peroxide (H_2O_2), these enzymes catalyze the hydroxylation of phenylalanine to form tyrosine and meta-tyrosine with nearly identical second order rate constants. When the H_2O_2-dependent reaction is carried out with cyclohexylalanine or 4-methylphenylalanine, the products are 4-HO-cyclohexylalanine and 4-hydroxymethylphenylalanine, respectively. These experiments provide further evidence that the intrinsic reactivities of the iron centers in these enzymes are the same.

Wild-type PheH and the uncoupled mutant protein V379D exhibit normal and inverse isotope effects, respectively, with deuterated phenylalanines. When the reaction is monitored by stopped-flow absorbance spectroscopy, three steps are visible. The first step is the reversible binding of O_2, the second step is 5-7 fold faster than the turnover number, setting a limiting value for the rate constant for O_2 activation, and the last step is non-enzymatic. There is no burst in the pre-steady state formation of tyrosine. These results are consistent with formation of the new C-O bond to form tyrosine as the rate-limiting step of the reaction.

The reaction of TrpH with both tryptophan and phenylalanine was studied by stopped-flow absorbance spectroscopy and rapid-quench product analysis. With either amino acid as substrate, four steps can be distinguished. The first step is the reversible binding of O_2 to the Fe(II) center; this results in an absorbance signature with a maximum at 420 nm. This O_2 complex decays with a rate constant that is 18-22 fold faster than the turnover number with either amino acid, setting a the lower limit for the rate constant for O_2 activation. The rate constant for the third step agrees well with the pre-steady state of formation of 5-hydroxytryptophan or tyrosine from rapid-quench product analysis. The rate constant for the fourth step agrees well with the turnover number. Overall, these results show that O_2 activation is fast and turnover with each amino acid is limited by hydroxylation and release of a product, with the former step being about 4-fold faster than the latter.

DEDICATION

This dissertation is dedicated to my parents for giving me the gift of life and the opportunity to follow my dreams.

ACKNOWLEDGEMENTS

I would like to thank my advisor and co-chair, Dr. Paul F. Fitzpatrick, for allowing me to be part of his laboratory, for his knowledge, guidance, support and for making my research enjoyable. I would also like to thank all the lab members, past and present; especially Dr. Michael P. Valley, whose work ethic I tried to emulate very early. He told me to read 5-7 research articles every week and more importantly to learn to love your research. I would especially like to thank Michaela Huynh; for the past six months she has been an outstanding researcher partner. She played an important role in chapters III and VI of this dissertation. I would also like to thank Dr. William Park and Dr. Greg Reinhart for everything they have did for me. I would also like to thank past and present committee members: co-chair, Dr. Gary Kunkel, Dr. J. Martin Scholtz, Dr. Frank Raushel and Dr. Michael P. Kladde. I would like to thank Dr. Martin Bollinger and Dr. Carsten Krebs for allowing me to do experiments in their laboratories and discussing subtle details about transient kinetics and Mössbauer spectroscopy with me.

Finally, I would like to thank my parents and Dr. Roger Lalancette; without them I would never have gone to graduate school. My parents have always been there for me; they forced me to stay in high school. They taught me to work hard, to be tough on myself, to have goals in life and more importantly to remember that anything worth having in life should never come easy. I would like to thank all my friends at Texas A&M. Last, but certainly not least, my brothers Robert, Davis, David and my sister

Diana; I learned a lot from all you, especially to always be happy even when everything seems to go wrong.

NOMENCLATURE

TyrH	tyrosine hydroxylase
PheH	phenylalanine hydroxylase
TrpH	tryptophan hydroxylase
Δ117PheH	catalytic core of phenylalanine hydroxylase lacking 116 residues from the N-terminus
$TrpH_{102-416}$	catalytic core of tryptophan hydroxylase lacking 101 and 28 residues from the amino and carboxyl termini respectively
NDO	oxygenase component of napthalene 1,2 dioxygenase
BZDOS	oxygenase component of benzoate 1,2-dioxygenase
DHPR	dihydropteridine reductase
TauD	α-ketoglutarate dependent dioxygenase
HPPD	(4-hydroxyphenyl) pyruvate dioxygenase
Dopa	dihydroxyphenylalanine
5-HO-trp	5-hydroxytryptophan
6-$MePH_4$	6-methyl-tetrahydropterin
6Me7,8PH_2	6-methyl-7,8-dihydropterin
5Me5DPH_4	6-methyl-5-deazatetrahydropterin
q6$MePH_2$	quinonoid 6-methyldihydropterin
4a-6$MePH_3OH$	4a-hydroxypterin
NDA	naphthalene-2,3-dicarboxaldeyde
CBI	1-cyanobenz[f]-isoindole

ESI	electrospray negative ion mode mass spectrometry
EDTA	ethylenediamine tetraacetic acid
NTA	nitrilotriacetic acid
DTT	dithiothreitol
Hepes	N-(2-hydroxyethyl) piperazine-N'-2-ethane-sulfonic acid
PKU	phenylketonuria

TABLE OF CONTENTS

CHAPTER Page

LIST OF FIGURES

FIGURE Page

FIGURE Page

FIGURE Page

FIGURE Page

LIST OF TABLES

CHAPTER I

INTRODUCTION

Many important biological transformations of aromatic and aliphatic compounds entail the insertion of one or both atoms from molecular oxygen into an un-activated carbon-hydrogen bond (*1-3*). These biological transformations are typically carried out by proteins that contain an essential metal cofactor coordinated by several amino acid residues (non-heme) or a porphyrin ring (heme). The metal is utilized to activate O_2 from its un-reactive triplet ground state to the reactive singlet ground state in order to oxidize a target organic molecule (*1, 3-5*).

The general mechanism that these enzymes share to activate O_2 for substrate oxidation involves the binding of O_2 to the coordinated metal atom; for most non-heme and heme-dependent enzymes the metal atom is iron. Once bound to the metal center, the electronic configuration of O_2 changes, favoring its irreversible reduction to yield a high valence metal-oxygen complex. For the iron-dependent enzymes, several high valence iron-oxygen complexes have been proposed over the years (Scheme 1). These include the binding of O_2 to form a ferrous-dioxygen complex. An iron-(II)-superoxo or an iron-(III)-superoxo forms from the ferrous-dioxygen complex where one electron is provided by an external source for the former. An additional electron yields an iron-(II)-peroxo or iron-(III)-peroxo species. A ferryl-oxo intermediate, Fe(IV)O or Fe(V)O, has

---

This dissertation follows the style of *Biochemistry*.

been proposed to be formed following protonation(s) of the distal oxygen and cleavage of the O-O bond in either (Scheme 1) (*1, 2, 6*). Ferryl-oxo intermediates are considered to be the most potent oxidizing species found in nature, capable of catalyzing a wide range of biological transformations including but not limited to hydroxylation, halogenation, cyclization, isomerization, epoxidation, decarboxylation and heteroatom-dealkylation (*1, 2, 7, 8, 9*).

Scheme 1

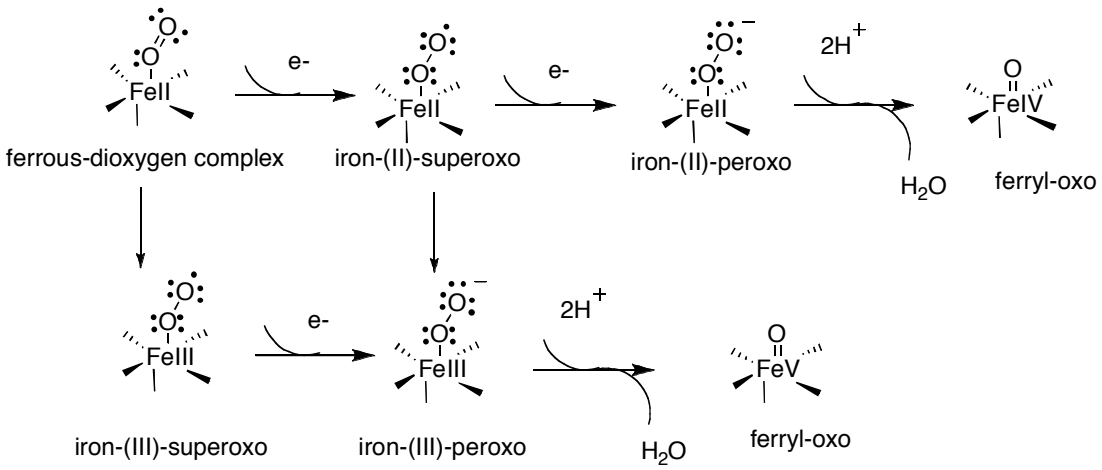

Ferryl-oxo intermediates are considered to be the products of oxygen activation for most non-heme and heme dependent enzymes; however, the mechanism, sequence of events and external source of electrons can vary drastically even among non-heme enzymes. Over the years a tremendous amount of effort has gone into elucidating the mechanism of oxygen activation and hydroxylation for the family of heme-dependent cytochrome P450 due to the wide range of biological transformations that it can catalyze (*1, 4*). The mechanisms of the non-heme iron-dependent enzymes are less well understood. For these enzymes, nature decided to employ as the metal ligand not a

porphyrin ring, but the side chains of histidine, aspartate or glutamine residudes. These residues typically form a structural motif where one face of the iron atom is facially coordinated by 2-histidines and one glutamate or aspartate. Three water molecules in the substrate free enzyme occupy the other face of the iron. This motif, called the 2-His-1-carboxylate facial triad ($(His)_2$(Asp/Glu)-facial triad motif), is found in a wide range of non-heme dependent enzymes and is vital for the activation of O_2 (*6, 10*).

The four most studied families of enzymes containing the $(His)_2$(Asp/Glu)-facial triad motif are the α-ketoacid dependent enzymes (*11, 12*), the extradiol dioxygenases (*13, 14*), the Rieske dioxygenases (*15, 16*) and the pterin-dependent aromatic amino acid hydroxylases (*17, 18*). In the α-ketoacid dependent enzymes two electrons for the activation of O_2 are supplied through the oxidative decarboxylation of an α-ketoacid (co-substrate). This co-substrate, usually α-ketoglutarate, can chelate to the metal center directly. The other oxygen atom from O_2 is inserted into the substrate (*11, 12*). The extradiol dioxygenases are important in the degradation of a large number of aromatic catechols. These enzymes typically oxidize catechol compounds by cleaving carbon-carbon bonds and incorporating both atoms from O_2 into the aromatic substrate (*13, 14*). In these enzymes the catechol substrate serves the role of both substrate and co-substrate, since both oxygen atoms from O_2 end up in the product in the form of a ketone and/or an aldehyde. The Rieske dioxygenases catalyze the important conversion of aromatic compounds into cis-dihydrodiols. The initial di-hydroxylation of aromatic compounds is considered to be essential for the conversion of unreactive aromatics into useful carbon sources. These enzymes require a reductase partner that delivers two

electrons from an external source, usually NADH, into an iron-sulfur cluster of the dioxygenase component. The iron-sulfur cluster subsequently delivers one electron at a time to its iron center (*15, 16*). Finally, the pterin-dependent aromatic amino acid hydroxylases catalyze aromatic hydroxylation, utilizing a tetrahydropterin (co-substrate) to supply two electrons (*17-19*).

As emphasized above, hydroxylation of the aromatic rings of organic compounds is an essential transformation in biology. The heme dependent enzyme cytochrome P450 (*1, 4*) and the flavoprotein hydroxylases (*20*) catalyze many of these important

Scheme 2

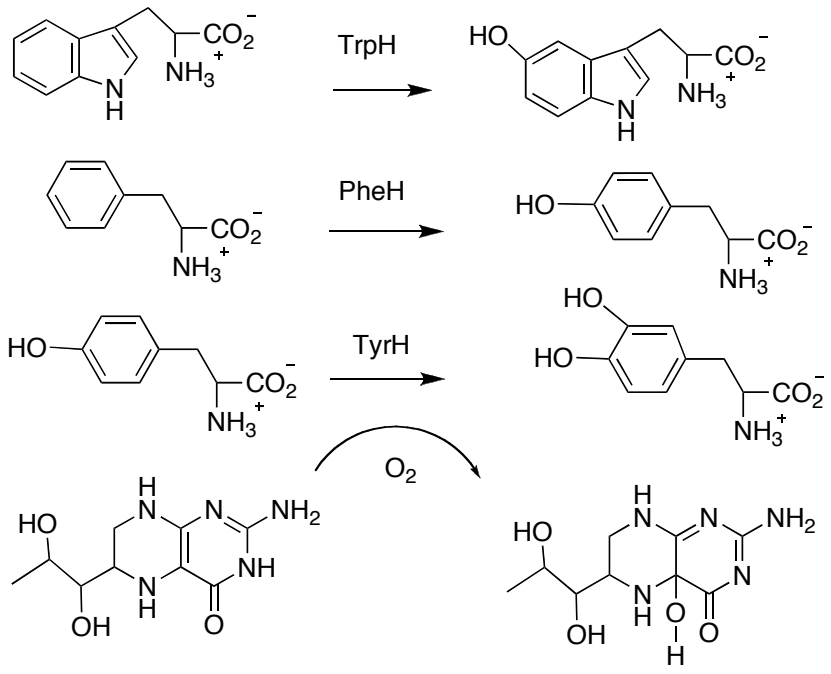

hydroxylation reactions. For the hydroxylation of aromatic amino acids, however, nature uses the $(His)_2(Asp/Glu)$-facial triad and a folate derivative (terahydropterin). The three enzymes PheH, TyrH and TrpH form the small family of aromatic amino acid

hydroxylases (*3, 5, 17, 18*). PheH, TyrH and TrpH catalyze a similar reaction, hydroxylation of the side chain of an aromatic amino acid (Scheme 2).

In vivo tetrahydropbiopterin (BH_4) supplies two electrons. In contrast to most flavoprotein hydroxylases, BH_4 is not tightly bound in the active site, but is a co-substrate that binds and dissociates during turnover. The pterin product of the enzymatic reaction is a 4a-hydroxypterin (Scheme 2) (*21, 22*). The 4a-hydroxypterin dehydrates to water and the quinonoid dihydropterin, which is recycled back to the reduced form by the enzyme dihydropterine reductase using NADH (*23*).

PheH in the liver catalyzes the first step in the catabolism of excess phenylalanine (*24*). Mutations result in phenylketonuria (PKU), a disorder that can result in metal retardation (*25*). TyrH in the adrenal gland and the brain catalyzes the hydroxylation of tyrosine to 3,4-dihydroxyphenylalanine (dopa) (*26*). The hydroxylation of tyrosine to form dopa is the first committed step in the biosynthesis of the neurotransmitters dopamine, epinephrine and norepinephrine. Mutations in TyrH have been associated with Parkinson's disease (*27*). TrpH in the digestive track and the central nervous system catalyzes the hydroxylation of trytptophan to form 5-hydroxytryptophan (5-HO-trp) (*28*). Mutant forms of TrpH have been implicated in several physiological and neurological disorders (*29*). The mammalian forms of the aromatic amino acid hydroxylases share significant structural similarity (*30*). All three contain oligomerization, regulatory and catalytic domains and at least one phosphorylation site, usually a serine residue, important for regulation. The phosphorylation site(s) of each enzyme is located in the regulatory domain of 100-160

residues. The regulatory domains of the three aromatic amino acid hydroxylases have low sequence similarity; this is consistent with the different mechanisms of regulation of each enzyme in vivo (*19*). In contrast, the catalytic domains of about 300 amino acids are homologous, with similar structures (Figure 1 (A)) (*31-33*) This similarity extends to their active sites, where each enzyme has a non-heme iron bound in a $(His)_2(Glu)$-facial triad and three water molecules (Figure 1 (B)). In rat TyrH the three residues that make up the facial triad are His331, His336 and Glu376; in human PheH they are His285, His290 and Glu330; and the corresponding residues in chicken TrpH are His273, His278 and Glu318 (*32-34*).

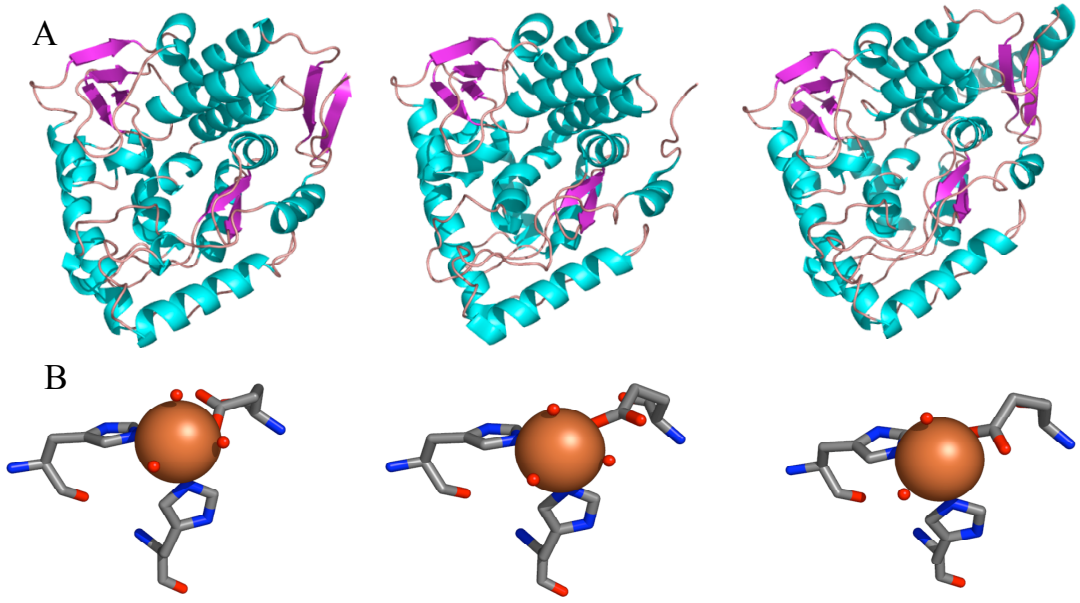

Figure 1: A. Crystal structures of the catalytic domains of PheH (left), TrpH (center) and TyrH (right). B. The non-heme iron center bound in the 2-his-1-carboxylate facial triad for PheH (left), TrpH (center) and TyrH (right). Water molecule are shown as red spheres.

Given the similar structures of the three enzymes, the assumption can be made that they share a common catalytic mechanism. Accordingly, experimental results obtained with all three enzymes have been used to formulate the chemical mechanism shown in Scheme 3 for TrpH (*18, 19*). The reaction is initiated following the formation of a quaternary complex between the enzyme and substrates. The first step is binding of O_2 to the $(His)_2(Glu)$-facial-Fe(II) center. This complex reacts with the co-substrate tetrahydropterin to yield an oxygen-bridged iron-pterin intermediate (4a-peroxypterin-iron).

Scheme 3

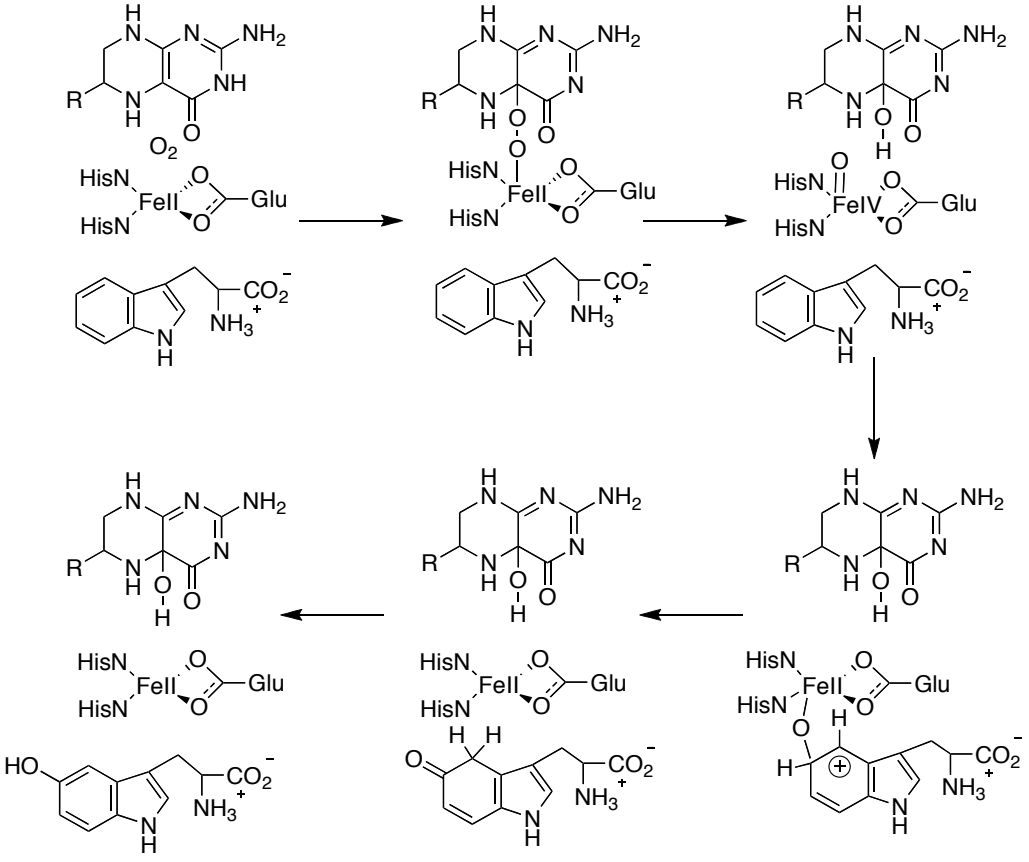

The $^{18}(k_{cat}/K_m)$ value for TyrH is independent of the pH and the amount of productive turnover, suggesting that the first irreversible step does not involve amino acid hydroxylation (*35*), although the basis for the effect is still unsettled (*36*). The magnitude of the $^{18}(k_{cat}/K_m)$ effect is greater than the upper limit for the equilibrium binding of O_2 to an Fe(II) center and lower than the established upper limit for an outer sphere electron transfer (*37*). The $^{18}(k_{cat}/K_m)$ for TyrH is likely to be a product of the equilibrium binding of O_2 and a kinetic isotope effect for the first irreversible step. The latter is likely to be an irreversible inner sphere electron transfer as the 4a-peroxypterin-iron intermediate forms. Heterolytic cleavage of the oxygen-oxygen bond and addition of a proton to the 4a-peroxypterin-iron yields the high valence Fe(IV)O intermediate and 4a-hydroxypterin, the first product.

The Fe(IV)O intermediate subsequently oxidizes the amino acid via electrophilic aromatic substitution, resulting in a new carbon-oxygen bond. Steady state kinetic isotope effects on the turnover number ($^{D}k_{cat}$) with wild-type TrpH and mutant forms of PheH and TyrH are inverse (0.9-0.95) (*38-40*). This is consistent with formation of a carbocation as the hybridization of the carbon undergoing hydroxylation changes from sp^2 to sp^3. In addition, when a series of para-substituted amino acids was used as substrates for TyrH, the relative amounts of hydroxylated products yielded a negative ρ value (*41*). This shows that electron-donating substituents activate the ring of the amino acid. This is consistent with the electrophilic nature of the reaction, in that unproductive turnover results from the unproductive decay of the Fe(IV)O intermediate due to the decreased reactivity of the aromatic amino acids with electron-withdrawing substituents.

Experimental and computational evidence support the involvement of a Fe(IV)O intermediate as the hydroxylating intermediate for these enzymes (*18, 38, 42-45*). The Fe(IV)O intermediate in TyrH has been detected by freeze-quench Mössbauer spectroscopy (*45*). Its spectrum resembles those for several members of the α-ketoglutarate dependent dioxygenase family, where substrate oxidation in most cases occurs via hydrogen atom abstraction (*46, 47*).

CHAPTER II

INTRINSIC ISOTOPE EFFECTS ON BENZYLIC HYDROXYLATION BY THE AROMATIC AMINO ACID HYDROXYLASES: EVIDENCE FOR HYDROGEN TUNNELING, COUPLED MOTION AND SIMILAR TRANSITION STATE STRUCTURES*

INTRODUCTION

Phenylalanine hydroxylase (PheH), tyrosine hydroxylase (TyrH) and tryptophan hydroxylase (TrpH) form a small family of non-heme iron monooxygenases (*19, 23*). These enzymes catalyze the insertion of a oxygen atom from molecular oxygen into the aromatic side chain of their corresponding substrates using a tetrahydropterin to reduce the other oxygen atom to the level of water (Scheme 2) (*18*). The three aromatic amino acid hydroxylases share significant sequence and structure similarity. Each enzyme has an N-terminal regulatory domain containing one or more phosphorylated serine residues. The regulatory domains for the eukaryotic enzymes share little identity, in accordance with the need for different regulatory properties. In addition these enzymes contain a C-terminal tetramerization domain. The catalytic domains for the three enzymes are homologous, suggesting that all three enzymes share a common catalytic mechanism.

The three aromatic amino acid hydroxylases contain one iron atom per subunit, which is coordinated by a conserved glutamate and two histidine residues. This arrangement of iron ligands has also been found in a number of other non-heme iron mono and dioxygenases and has been termed the 2-his-1-carboxylate facial triad (*10, 48*). A proposed chemical mechanism for the aromatic amino acid hydroxylases is shown in Scheme 3 (*18*). The chemical mechanism can be divided into two partial reactions. After a quaternary complex is formed between the enzyme and substrates, tetrahydropterin and oxygen react to form an oxygen bridged iron-pterin species. Heterolytic cleavage of the oxygen-oxygen bond and addition of a proton forms a ferryl-oxo species and 4a-hydroxypterin. Electrophilic aromatic substitution, cleavage of the iron oxygen bond, NIH shift and rearomatization of the amino acid forms the hydroxylated amino acid product and regenerates the ferrous enzyme for another round of catalysis. Studies with substrate analogues and deuterium, solvent and ^{18}O kinetic isotope effects for TyrH suggest the rate liming step in the reaction is the formation of the hydroxylating intermediate (*35, 49, 50*).

Over the years experimental and computational evidence suggest that the hydroxylating intermediate for the aromatic amino acid hydroxylases is a ferryl-oxo species resembling those of the heme based cytochrome P-450 in reactivity (*18, 44, 45*). Consistent with such an expectation, all three aromatic amino acid hydroxylases catalyze benzylic hydroxylation of methylated aromatic amino acids (*51-53*). In the case of TyrH the intrinsic kinetic deuterium isotope effects for this reaction are consistent with the removal of a hydrogen atom with significant rehybridization of the methyl carbon in the

transition state (*52*). In the present study a detailed determination of the intrinsic primary and α-secondary deuterium isotopes for all three enzymes has been performed, using 4-methylphenylalanines with one, two and three deuterium atoms in the methyl group. This study has allowed us to compare the reactivity of the ferryl-oxo intermediate Fe(IV)O in the three enzymes. In addition questions about transition state structure and quantum mechanical tunneling are addressed.

EXPERIMENTAL PROCEDURES

Materials. 6-Methyltetrahydroptein ($6MePH_4$) was from B. Schircks Laboratories (Jona Switzerland). Sodium cyanide and boric acid were from Sigma-Aldrich Chemical Co. (Milwaukee WI). Napththalene-2,3-dicarboxaldehyde (NDA) was from Invitrogen (Carlsbad CA). 4-Methylphenylalanine was purchased from PepTech Corporation (Burlington MA). The synthesis of methyl-deuterated phenylalanines has been described (*52*). The amino acids were further purified using a μBondapak C^{18} column (14 x 300 mm) with a 6% acetonitrile mobile phase.

Protein purification. The catalytic domain of rat phenylalanine hydroxylase (Δ117PheH) was purified as previously described (*54*), with the exception that the enzyme was resuspended in 30 mM potassium phosphate buffer, pH 7.0, instead of 75 mM sodium phosphate, before loading onto the hydroxyapatite column. Recombinant rat phenylalanine hydroxylase was purified according to the protocol of Shiman et al. (*55*), as modified by Daubner et al. (*56*). Excess phenylalanine was removed from the purified enzyme by dialysis against 80 mM HEPES, 10% glycerol, pH 7.0. The catalytic

core of rabbit tryptophan hydroxylase ($TrpH_{102-416}$), a variant of the wild type lacking 101 and 28 residues from the amino termini and carboxyl termini, respectively, was provided by Dr. Graham R. Moran. The enzyme was dialyzed into 80 mM MOPS, 10% glycerol, pH 7.0. Wild type rat tyrosine hydroxylase was a generous gift of Dr. Patrick Frantom.

Methods. Standard assay conditions for determination of the percent of benzylic hydroxylation were 25 mM sodium phosphate buffer, pH 7.0, 30 μM ferrous ammonium sulfate, 1.2 mM 4-methylphenylalanine, 10 μM enzyme and 150 μM $6MePH_4$. Reactions were run for 2-3 minutes in a volume of 100 μL. $6MePH_4$ was used at a concentration 15-fold greater than the enzyme concentration in order to minimize the amount of auto-oxidation of the tetrahydropterin; in addition 150 μM $6MePH_4$ resulted in the largest ratio of hydroxylated amino acid products to tetrahydropterin consumed. The reactions between 3 and 30 °C were initiated by the addition of $6MePH_4$. Between 35 and 60 °C the reactions were initiated with enzyme. Reactions were quenched after 1-3 minutes between 25-60 °C, and after 4-5 minutes between 3-20 °C to assure that all the $6MePH_4$ had been consumed. The subsequent identification and separation procedures have been previously described (*52*).

Samples for mass spectrometry were made following the same standard conditions, except 0.8-1.5 mM $6MePH_4$ and 2.0 mM 4-methylphenylalanine in 250 μL were used, and the reaction was quenched by the addition of 200 μL of 10 mM sodium borate pH 9.2. Aliquots of 500 μL were injected onto a Nova-Pak C^{18} column (2.1 x 150 mm). The HPLC elution conditions were 5 minutes at 100% water followed by a 3 min

gradient to 85% water/15% acetonitrile and finally a 36 min linear gradient to 80% water/20% acetonitrile, at 0.15 ml/min. Products were detected using 470 and 530 nm excitation and emission wavelengths, respectively. The peak corresponding to 4-hydroxymethylphenylalanine was collected and analyzed by negative ion electrospray-time of flight mass spectrometry at the Laboratory of Biological Mass Spectrometry (LBMS) Texas A&M. The ratios of the (*m*-1) peaks resulting from loss or retention of deuterium were corrected for ^{13}C contributions and used in the calculation.

RESULTS

Products with 4-methyl-phenylalanine. 4-methyl-phenylalanine was used as substrate for wild type TyrH, PheH, and mutant forms of PheH and TrpH lacking the N-terminal regulatory domains, respectively (Δ117PheH and $TrpH_{102-416}$). The products were labeled with NDA and sodium cyanide, separated by HPLC and identified as the N-substituted 1-cyanobenz[f] isoindole (CBI) derivatives (*57*). The stoichiometry of the reaction was independent of the deuterium content in the methyl group. The amount of productive turnover (the ratio of amino acid hydroxylation to tetrahydropterin oxidation) was 51.4 ± 4.2 for Δ117PheH, 46.5 ± 0.9 for $TrpH_{102-416}$, 33.2 ± 1.3 for TyrH and 35.5 ± 1.7 for PheH. The products were quantified and the percentage of benzylic hydroxylation was determined by comparison with synthetic standards. Figure 1 shows the distribution of products obtained for each enzyme. The percentages of benzylic hydroxylation were 22.1 ± 2.4, 54.9 ± 0.4, 54.5 ± 0.8, 39.7 ± 2.2 for TyrH, PheH and Δ117PheH and $TrpH_{102-416}$ respectively. For TyrH the dominant product is 3-hydroxy-4-

methylphenylalanine; this is consistent with this enzyme having greater specificity for the meta position of the aromatic ring. It has been reported previously that PheH is poor in hydroxylating tyrosine (*54*), and Figure 2 shows that for this enzyme the percentage of 3-hydroxy-4-methylphenylalanine is also extremely low. In addition, for PheH deletion of the first 116 amino acids responsible for the regulatory properties of the enzyme has no effect on the product composition.

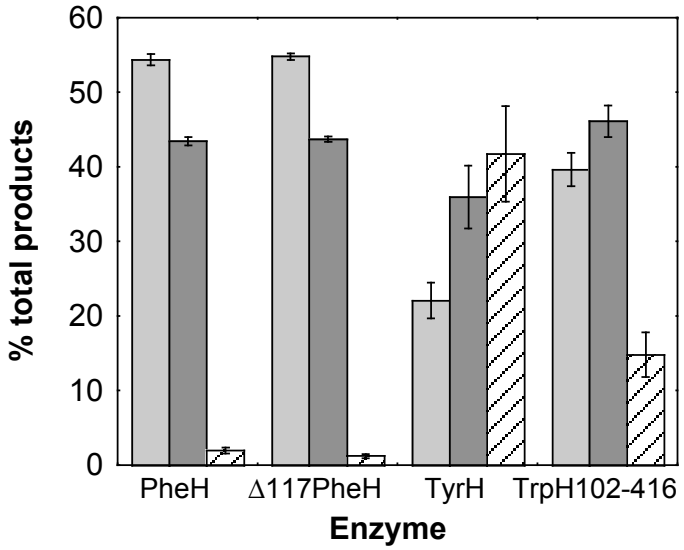

Figure 2: Product distribution with 4-methylphenylalanine as substrate for the aromatic amino acid hydroxylases: 4-hydroxymethylphenylalanine (grey), 3-methyl-4-hydroxyphenylalanine (dark grey), 3-hydroxy-4-methylphenylalanine (stripes).

Isotope effects. The isotope effects on the percent of benzylic hydroxylation were determined from the fraction of 4-hydroxymethylphenylalanine formed from 4-methyl-phenylalanine versus that from deuterated 4-methylphenylalanines. The use of 4-methylphenylalanines containing one, two or three deuterium atoms in the methyl group allowed the determination of the intrinsic primary and α-secondary isotope effects for the benzylic hydroxylation reaction. The effects of isotopic substitution on the

relative amounts of the three amino acid products were analyzed using the model shown in Scheme 4 (*58, 59*). In this model, all substrates bind before the enzyme proceeds through the first irreversible step (*35, 50*). Partitioning occurs and different amino acid

Scheme 4

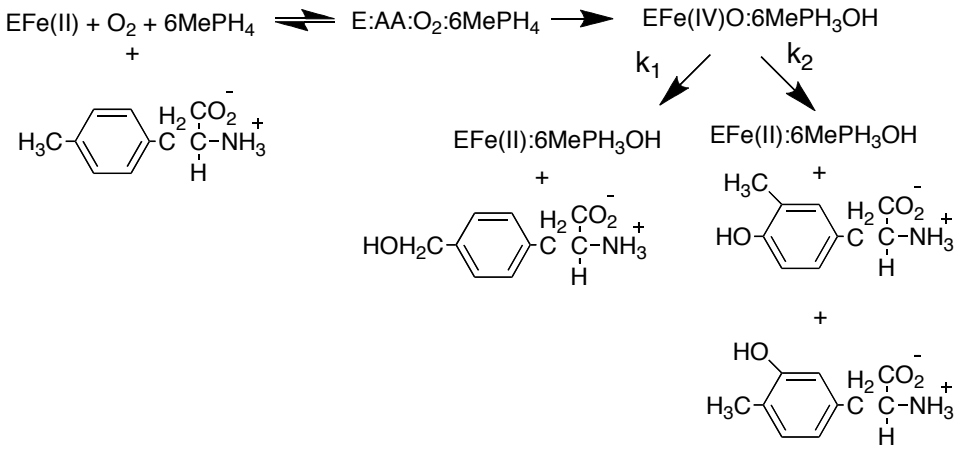

products are formed after the hydroxylating intermediate Fe(IV)O is formed. 4a-6MePH$_3$OH denotes the product 4a-hydroxypterin. For the model in Scheme 4, k_1 denotes the rate constant for benzylic hydroxylation and k_2 the net rate constant for aromatic hydroxylation at the 3 and 4 positions. The fraction of 4-hydroxymethyl-phenylalanine produced is $k_1/(k_1 + k_2)$.

The step with rate constant k_1 should be the only step sensitive to isotopic substitution, so that increasing the deuterium content of the methyl group will decrease the magnitude of k_1, leaving k_2 constant. Equation 1 relates the isotope effect on the percent of benzylic hydroxylation to the intrinsic isotope effect on k_1. The value of k_{1H}/k_2 was determined from the products with non-deuterated 4-methylphenylalanine.

The deuterium isotope effects for benzylic hydroxylation of deuterated 4-methyl-phenylalanines are listed in Table 1. These isotope effects are similar in magnitude for TyrH, PheH, Δ117PheH and $TrpH_{102-416}$. In addition they show similar increases as the deuterium content in the methyl group increases, consistent with a decrease in k_1 due to isotopic substitution.

Table 1: Intrinsic Kinetic Isotope Effects on Benzylic Hydroxylation by the Aromatic AminoAcid Hydroxylases

Enzyme	Substrate		
	4-$CH_2{}^2H$-phenylalanine	4-CH^2H_2-phenylalanine	4-C^2H_3-phenylalanine
PheH	1.63 ± 0.14	2.84 ± 0.25	12.4 ± 1.1
Δ117PheH	1.92 ± 0.19	2.66 ± 0.25	12.1 ± 1.1
TyrH	2.26 ± 0.33	3.07 ± 0.45	13.8 ± 1.2
$TrpH_{102-416}$	2.04 ± 0.27	2.77 ± 0.36	13.0 ± 1.7

Standard assay conditions were 25 mM sodium phosphate buffer pH 7.0, 30 μM ferrous ammonium sulfate, 1.2 mM 4-methylphenylalanine, 10 μM enzyme and 150 μM $6MePH_4$. Reactions were performed at least 6 times.

$$^{D}(\%\ 4\text{-}CH_2OH\text{-}phe) = \frac{^{D}k_1 + k_{1H}/k_2}{1 + k_{1H}/k_2} \qquad (1)$$

These isotope effects are combinations of primary and α-secondary isotope effects. When the trideuterated substrate is used, the deuterium isotope effect is a product of a primary and two α-secondary effects $^{D}k(^{\alpha D}k)^2$. When the monodeuterated or dideuterated substrate is used, the product 4-hydroxymethylphenylalanine can result from loss of deuterium or hydrogen. For the monodeuterated substrate abstraction of a

hydrogen atom will show a α-secondary isotope effect ($^{\alpha D}k$), while abstraction of a deuterium atom will show a primary isotope effect (^{D}k). Similarly, for the dideuterated substrate abstraction of a hydrogen atom will show two α-secondary isotope effects $(^{\alpha D}k)^2$, and a primary and a α-secondary isotope effect when a deuterium atom is abstracted $^{D}k(^{\alpha D}k)$. The 4-hydroxymethylalanines formed from the monodeuterated and dideuterated substrates by TyrH, Δ117PheH and $TrpH_{102-416}$ were collected from the HPLC and analyzed by mass spectrometry, allowing the ratios of products due to C-H versus C-D cleavage to be calculated. These values are listed in Table 2.

Table 2: Relative Amounts of Hydrogen versus Deuterium Loss from 4-Methylphenylalanine upon Benzylic Hydroxylation by the Aromatic Amino Acid Hydroxylases

Enzyme	(371)/(370) 4-$CH_2{}^2H$-phenylalanine	(372)/(371) 4-CH^2H_2-phenylalanine	Ratios[b]
Δ117PheH	16.8 ± 0.8	2.7 ± 0.1	6.2 ± 0.2
TyrH	15.8 ± 0.9	2.8 ± 0.1	5.6 ± 0.4
$TrpH_{102-416}$	20.0 ± 0.5	2.8 ± 0.1	7.0 ± 0.2

[b]Ratio of product formed due to hydrogen loss to the product due to deuterium loss. Standard assay conditions were 25 mM sodium phosphate buffer, pH 7.0, 30 μM ferrous ammonium sulfate, 2.0 mM 4-methylphenyl-alanine, 10 μM enzyme and 0.8-1.5 mM 6-$MePH_4$. 4-Methylphenylalanines were identified as cyanobenz[f] isoindole (CBI) derivatives (Shah J. A. 1999). Product ratios were determined by ESI mass spectrometry.
[b]Ratio of 4-hydroxy-methylphenylalanines arising from 4-$CH_2{}^2H$-phenylalanine and 4-CH^2H_2-phenylalanine.

Equations 2 and 3 show the relationships between the isotopic compositions of the 4-hydroxymethylphenylalanine products and the intrinsic primary and α-secondary isotope effects (*58, 60*). Accordingly, the data of Table 2 and the corresponding kinetic

$$\frac{\text{4-CDHOH-phe}}{\text{4-CH}_2\text{OH-phe}} = \frac{2\,{}^{D}k}{{}_{\alpha D}k} \qquad (2)$$

$$\frac{\text{4-CD}_2\text{OH-phe}}{\text{4-CDHOH-phe}} = \frac{{}^{D}k}{2\,{}_{\alpha D}k} \qquad (3)$$

Isotope effects obtained from trideuterated 4-methylphenylalanine could be used for the calculation of the intrinsic primary and α-secondary kinetic isotope effects for benzylic hydroxylation by TyrH, Δ117PheH and $TrpH_{102\text{-}416}$ (Table 3). The results from the two partially deuterated substrates are different, but similar results were obtained for the three enzymes. Intrinsic primary isotope effects of about 10 and α-secondary isotope effects of about 1.15 were calculated for monodeuterated 4-methylphenylalanine. In contrast intrinsic primary isotope effects less than 8 and α-secondary isotope effects of 1.3 or greater were calculated for dideuterated 4-methylphenylalanine.

Table 3: Intrinsic Isotope Effects on Benzylic Hydroxylation by the Aromatic Amino Acid Hydroxylases

Substrate		Δ117PheH	WT TyrH	$TrpH_{104-416}$
4-C^2H_3-phe	Overall isotope effect	12.1 ± 1.1	13.8 ± 1.2	13.0 ± 1.7
4-$CH_2{}^2H$-phe	Primary isotope effect	9.5 ± 0.4	9.5 ± 0.6	10.9 ± 0.4
	Secondary isotope effect	1.12 ± 0.05	1.20 ± 0.08	1.09 ± 0.03
4-CH^2H_2-phe	Primary isotope effect	7.1 ± 0.2	7.6 ± 0.3	7.5 ± 0.1
	Secondary isotope effect	1.31 ± 0.03	1.35 ± 0.05	1.31 ± 0.02

Calculated from the overall isotope effect and the data in Table 2 using equations 2 and 3.

*Temperature dependence of the isotope effects***.** The primary isotope effects for TyrH, Δ117PheH and $TrpH_{102-416}$ are greater than the upper limit of about 7 predicted by transition state theory. Such large kinetic isotope effects are often interpreted as an indication of quantum mechanical tunneling of the hydrogen atom (*61, 62*). One criterion used to detect hydrogen tunneling in hydrogen transfer reactions is the effect of temperature on the kinetic isotope effect (*62-64*). Kinetic isotope effects on the benzylic hydroxylation reaction as a function of temperature were determined for each enzyme using trideuterated 4-phenylphenylalanine. Figure 3 shows the temperature dependence of the intrinsic kinetic isotope effect for Δ117PheH and $TrpH_{102-416}$. The data were fit to the Arrhenius equation (Equation 4) to obtain the isotope effects on the Arrhenius pre-exponential factors and the differences in activation energies for TyrH, PheH, Δ117PheH and $TrpH_{102-416}$ (Table 4).

$$\ln({}^{D}k) = \ln(A_H/A_D)+\Delta E_{act}/RT \qquad (4)$$

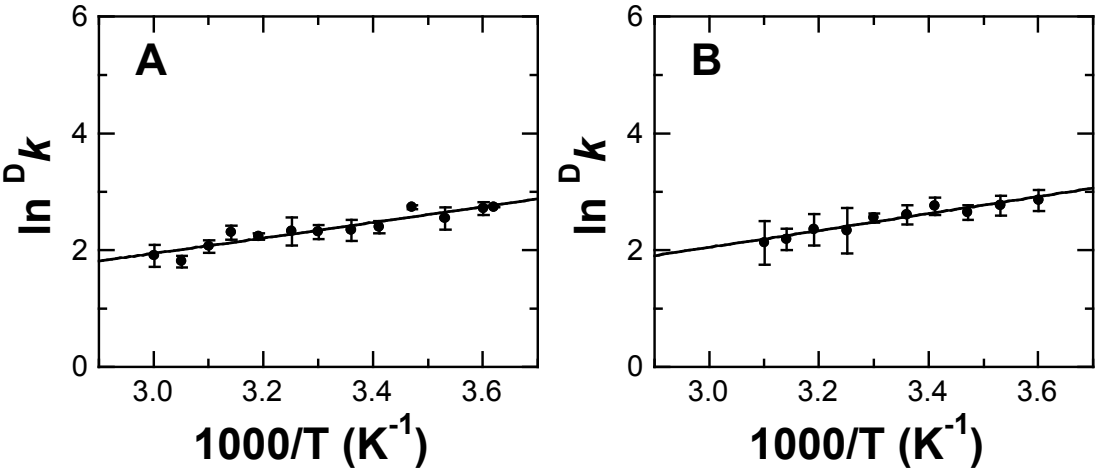

Figure 3: Deuterium kinetic isotope effects as a function of temperature for the catalytic cores of PheH (A) and TrpH (B). Reactions at each temperature were performed 3-4 times. Lines are from fits to the Arrhenius equation.

Table 4: Isotope Effects on Pre-Exponential Factors and Differences in Activation Energies for Benzylic Hydroxylation by the Aromatic Amino Acid Hydroxylases

Enzyme	A_H/A_D	ΔE_{act} (kcal/mol)
PheH[a]	0.18 ± 0.08	2.4 ± 0.3
Δ117PheH[b]	0.13 ± 0.06	2.6 ± 0.3
TyrH[c]	0.11 ± 0.05	2.9 ± 0.3
$TrpH_{102-416}$[d]	0.10 ± 0.05	2.9 ± 0.3

Experimental temperature range [a]5-60 °C, [b]3-60 °C, [c]5-35 °C and [d]5-50 °C. Reactions at each temperature were performed 3-4 times.

DISCUSSION

The aromatic amino acid hydroxylases PheH, TyrH and TrpH are capable of catalyzing benzylic and aromatic hydroxylation of 4-methylphenylalanine. The products vary from one enzyme to the next, establishing that their active site architectures are different. For PheH, deletion of the regulatory domain of the enzyme has no effect on the distribution of products. It has previously been shown that the substrate specificities of these enzymes are determined by residues in the catalytic domain (*54*). The present study establishes that for mechanistic purposes the catalytic cores of the enzymes are suitable.

The analysis of products arising from 4-methylphenylalanines containing one, two, or three deuterium atoms in the methyl group has allowed the determination of the intrinsic primary and secondary isotope effects on the benzylic hydroxylation reaction. The data in Table 1 clearly show that the amount of benzylic hydroxylation decreases as the deuterium content in the methyl group increases, consistent with previously published results (*52*). The intrinsic isotope effects are clearly very similar among the enzymes. When the trideuterated substrate is used the enzyme has no choice but to cleave the carbon deuterium bond. The value and magnitude of this isotope effect is clearly very similar among the three enzymes, requiring that the hydroxylating intermediate be of similar reactivity in the three enzymes (Table 1).

One of the initial goals of this study was to determine independent values of the intrinsic primary and α-secondary kinetic isotope effects for benzylic hydroxylation by all three aromatic amino acid hydroxylases. It was anticipated that the rule of geometric

mean (RGM) would be valid for this reaction (*62, 65*). Comparison of equations 2 and 3 shows that the ratio of products obtained from the monodeuterated versus dideuterated substrates should be equal to four if the RGM applies (*60*). The ratios were greater than four in all cases (Table 2). This unexpected result leads to different intrinsic primary and α-secondary isotope effects on benzylic hydroxylation when the dideuterated and monodeuterated substrates are used (Table 3). When one deuterium is present in the methyl group the isotope effects are likely to be the intrinsic effects. However, when a second deuterium is present the motion of the primary hydrogen is coupled to the motion of the second deuterium, resulting in an inflated α-secondary isotope effect and a decreased primary effect (*66, 67*). Computational studies have shown that large secondary isotope effects exceeding their corresponding equilibrium effects can result from a combination of coupled motion and quantum mechanical tunneling (*68*). Alternatively, it could simply be that when one deuterium is present in 4-methyl-phenylalanine, the transition state is symmetrical, leading to the maximum value of the primary isotope effect and a moderate α-secondary effect. When two deuterium atoms are present in the methyl group, the transition state is late, leading to a smaller primary isotope effect, and a larger secondary effect. The latter explanation would be consistent with the results in Table 3. However, secondary isotope effects of 1.31 and 1.35 exceed the expected equilibrium isotope effect which is considered the theoretical limit for the secondary isotope effects, ruling out this possibility (*69*).

The large intrinsic primary and secondary deuterium kinetic isotope effects are consistent with a mechanism involving hydrogen atom abstraction. Primary and

α-secondary kinetic isotope effects have been determined for benzylic hydroxylation reactions by dopamine β-monooxygenase and peptidyglycine α-amidating enzyme (*1, 70-72*). The similarity of the values reported for those enzymes and the aromatic amino acid hydroxylases may reflect similar transition state structures and a similar hydroxylating intermediates proposed to be high-valence metal ferryl-oxo-compounds (*18, 73*).

The heme-containing cytochromes P-450 catalyze benzylic as well as aliphatic hydroxylation with very large primary and α-secondary kinetic isotope effects (*26-28*). The mechanism proposed for the cytochrome P-450 family has changed over the years, but a radical abstraction and recombination mechanism referred to as the oxygen rebound mechanism first proposed by Groves has been widely accepted (*1, 74*). Scheme 5 shows the proposed mechanism for benzylic hydroxylation by the aromatic amino acid hydroxylases proposed by Frantom et al. (*52*). This mechanism is a variation of the oxygen rebound mechanism. Here, the putative Fe(IV)O intermediate (*38, 41, 45, 75*), abstracts a hydrogen atom from the benzylic position of the substrate. 4-Hydroxy-methylphenylalanine and the ferrous enzyme are obtained upon radical recombination. The intrinsic primary and α-secondary effects seen with monodeuterated 4-methyl-phenylalanine support a mechanism for all the aromatic amino acid hydroxylases in which the transition state for hydrogen atom abstraction is symmetrical with rehybridization towards planarity during carbon-hydrogen bond cleavage.

Scheme 5

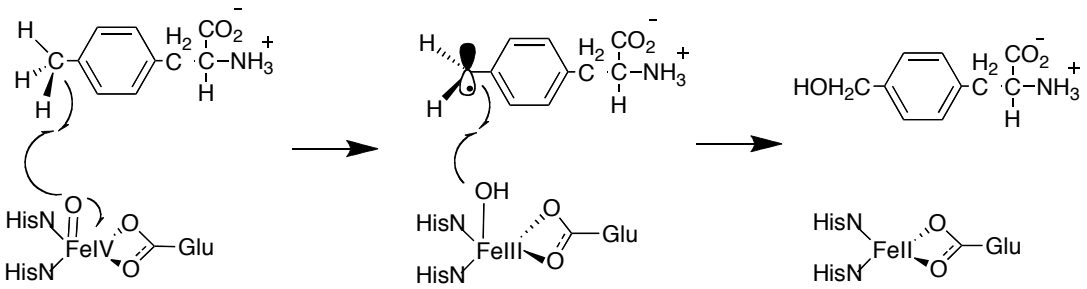

The intrinsic primary and α-secondary kinetic isotope effects for TyrH, Δ117PheH and $TrpH_{102-416}$ (Table 3) suggest that the Fe(IV)O intermediate for the aromatic amino acid hydroxylases has similar reactivity to the heme based oxidant in cytochrome P-450. Several intermediates over the years have been proposed for the aromatic amino acid hydroxylases (*76-79*). However; it is expected that only an intermediate as reactive as the Fe(IV)O will be able to activate benzylic carbon-hydrogen bonds (85 kcal/mol) (*80*), such as the ones found in 4-methylphenylalanine. The ability of all of the aromatic amino acid hydroxylases to catalyze benzylic hydroxylation suggests not only that a high valence Fe(IV)O species with identical reactivity is a common intermediate, but the magnitude and similarity of the isotope effects reported here also suggest that transition state structure for this reaction is nearly identical in the three enzymes.

The large primary isotope effects (Table 3) exceed the value of 7 at 30 °C expected for a simple bond-stretch formalism and suggest quantum mechanical tunneling of the hydrogen atom in the transfer event (*61, 81*). Furthermore, the secondary kinetic isotope effects with the dideuterated substrate exceed the equilibrium

isotope effect and under certain conditions this is often an indication of hydrogen tunneling (*82*). However, large secondary isotope effects and intrinsic primary isotope effects of 7 or greater are not a definite indication of quantum mechanical tunneling (*83*). A frequent probe of quantum mechanical tunneling is comparison of the temperature dependence for H and D transfer reactions (*61, 62*). Transition state theory predicts that in the absence of tunneling, effects on the Arrhenius pre-exponential factor will fall in the range of 0.7-1.4, and the differences in activation energies should not exceed 1.4 kcal mol^{-1} (*62-64, 84*). The tunneling contribution at low temperature affects H transfer more than D transfer, resulting in crossing of the Arrhenius plots and values for the Arrhenius pre-exponetial factor less than unity and differences in activation energies greater than those predicted by zero point energy differences (*61, 81*). For all three aromatic amino acid hydroxylases, the isotope effects on the Arrhenius pre-exponential factors and the differences in activation energies are outside the range predicted by classical transition state theory. The values for all three enzymes agree well, suggesting that the extent of tunneling is very similar. These results, in addition to the large kinetic isotope effects, establish that quantum mechanical tunneling contributes to catalysis to the same extent for all the aromatic amino acid hydroxylases. The tunneling event can be formalized as moderate in which protium tunnels to a much greater extent than deuterium (*85, 86*).

In conclusion, the data presented here establish that all three aromatic amino acid hydroxases use a radical mechanism to hydroxylate the benzylic carbon of 4-methyl-phenylalanine, with coupled motion and quantum mechanical tunneling contributions. The magnitude and similarity of these isotope effects along with the temperature

dependence of the isotope effects suggest that the transition state structures are very similar among the three enzymes.

CHAPTER III

DEMONSTRATION OF A PEROXIDE SHUNT FOR THE AROMATIC AMINO ACID HYDROXYLASES

INTRODUCTION

Phenylalanine hydroxylase (PheH), tyrosine hydroxylase (TyrH) and tryptophan hydroxylase (TrpH) are non-heme iron monooxygenases (*19, 23*). These enzymes catalyze the insertion of a oxygen atom from molecular oxygen into the aromatic side chain of their corresponding substrates using two electrons from tetrahydropterin to reduce the other oxygen atom from O_2 to the level of water (Scheme 2) (*18*). The three aromatic amino acid hydroxylases share significant sequence and structure similarity. The crystal structures of the isolated catalytic domains are very similar (Figure 1 (A)) (*31-33*), a similarity that extends to their active sites where each has a iron atom facially coordinated by two histidines, a glutamate and three water molecules (Figure 1 (B)). This arrangement of ligands to the iron is found in a diverse number of non-heme iron mono and dioxygenases that irreversibly activate O_2 for substrate oxidation and has been termed the 2-his-1-carboxylate facial triad (*10, 48*).

The chemical mechanism proposed for the aromatic amino acid hydroxylases is shown in Scheme 3 (*18*). A reactive quaternary complex is formed between the enzyme and substrates. Following this the first chemical step is a reaction between tetrahydropterin, oxygen and the iron center to form oxygen bridged iron-pterin intermediate (4a-peroxypterin-iron). Heterolytic cleavage of the oxygen-oxygen bond

and addition of a proton to the 4a-peroxypterin-iron forms a Fe(IV)O intermediate and 4a-hydroxypterin, the first product. The Fe(IV)O intermediate reacts with the side chain of the aromatic substrate through electrophilic aromatic substitution, forming a new carbon oxygen bond (*38, 41*). Following cleavage of the iron oxygen bond, an NIH shift and tautomerization yield the second product, the hydroxylated amino acid. Experimental and computational evidence support the involvement of a Fe(IV)O intermediate as the hydroxylating intermediate for these enzymes (*18, 38, 42-44*). The Fe(IV)O intermediate in TyrH has recently been detected by freeze-quench Mössbauer spectroscopy. In addition, the Fe(IV)O intermediate decays concomitantly with dihydroxyphenylalanine formation (*45*). These experiments convincingly showed that the hydroxylating intermediate for these enzymes is a high valence Fe(IV)O species. This intermediate resembles those in several members of the α-ketoglutarate dependent dioxygenase family, where hydroxylation reactions in most cases occur via hydrogen atom abstraction (*46, 47*).

The experimental evidence is strong regarding the nature of the Fe(IV)O as the hydroxylating intermediate, ruling out earlier proposals for a 4a-peroxypterin or a 4a-peroxypterin-iron as hydroxylating intermediates (*77, 79*). The mechanism in Scheme 3 shows that one oxygen atom is sufficient to hydroxylate the side chain of the amino acid. Consequently, formation of the Fe(IV)O intermediate should be feasible by supplying both electrons and oxygen to the resting enzyme in the form of hydrogen peroxide or another peroxide donor. It has been possible in the cases of the heme based enzyme cytochrome P450 and the non-heme dinuclear enzyme methane monooxygenase to

replace molecular oxygen and electrons supplied from the reductase components with hydrogen peroxide to catalyze the same hydroxylations reactions (*87, 88*).

In this work we investigate the ability of the aromatic amino acid hydroxylases to effectively activate hydrogen peroxide for hydroxylation reactions. The results rule out hydroxylating intermediates involving tetrahydropterin. In addition, the ability of all three enzymes TyrH, PheH and TrpH to use hydrogen peroxide as electron and oxygen donor provides further evidence that the intrinsic reactivity of the iron centers in these enzymes is the same.

EXPERIMENTAL PROCEDURES

Materials. 6-Methyltetrahydropterin ($6MePH_4$) and 6-methyl-7,8-dihydropterin ($6Me7,8PH_2$) were from B. Schircks Laboratories (Jona Switzerland). L-Tyrosine, L-meta-tyrosine, L-phenylalanine, L-tryptophan, D,L-5-hydroxytryptophan, dihydroxy-phenylalanine (dopa), ethylenediamine tetraacetic acid (EDTA), nitrilotriacetic acid (NTA), glycerol, sodium chloride, sodium hydroxide, monobasic and dibasic sodium phosphate, sodium cyanide and boric acid, cumene hydroperoxide, peracetic acid, sodium periodate, and t-butyl hydroperoxide were from Sigma-Aldrich Chemical Co. (Milwaukee WI). Ferrous ammonium sulfate, ammonium sulfate, ferric chloride, (30% v/v) hydrogen peroxide and Hepes were from Fisher (Pittsburgh, PA). Napththalene-2,3-dicarboxaldehyde (NDA) was from Invitrogen (Carlsbad CA). The analytical GEMINI reverse-phase C18 column was purchased from Phenomenex (Torrance California). The synthesis and purification of 6-methyl-5-deazatetrahydropterin ($5Me5DPH_4$) has

been described previously (*89*). The synthesis and purification of 4-hydroxymethyl-phenylalanine, 3-hydroxy-4-methyl-phenylalanine and 3-methyl-4-hydroxyphenyl-alanine have been described previously (*52*). L-Cyclohexylalanine, L-$^{2}H_{11}$-cyclohexyl-alanine and 4-OH-cyclohexylalanine were provided by Aram J. Panay of this laboratory.

Enzymes. The growth, expression and purification of the wild-type catalytic domain and the active site mutants V379D and F263A of rat PheH (Δ117PheH), the catalytic core of rabbit TrpH ($TrpH_{102-416}$) and apo wild-type rat TyrH and the active site mutants S395A, E332A have been described previously (*39, 43, 54, 90-92*). To produce the apo-enzymes, following purification TyrH, PheH and the mutant proteins were precipitated with 60 percent ammonium sulfate. The enzymes were resuspended in 150 mM Hepes/NaOH, 200 mM sodium chloride, 20% glycerol, 20 mM NTA, and 20 mM EDTA, pH 7.0. TrpH was precipitated with 50 percent ammonium sulfate and subsequently resuspended in 100 mM Hepes/NaOH, 200 mM ammonium sulfate, 2 mM dithiothreitol, 20% glycerol, 20 mM NTA, and 20 mM EDTA, pH 7.0. The enzymes were subsequently dialyzed multiple times against the same buffers lacking the metal chelators.

To determine the activity of the apo-enzymes with respect to the holo-enzymes, the formation of the hydroxylated amino acid product was monitored by HPLC under k_{cat} conditions in the absence or presence of ferrous ammonium sulfate. For these assays the concentration of the enzymes was between 5 and 10 μM. The percent activity for the apo-enzyme with respect to the holo-enzyme was 12, 0 and 5 for PheH, TrpH and TyrH, respectively.

Peroxide shunt reactions. The standard conditions for the peroxide shunt reactions were 20 to 100 μM enzyme, 80 to 400 uM ferrous ammonium sulfate, 1 to 50 mM of L-phenylalanine, 5-30 mM H_2O_2, 150 mM Hepes buffer and 100 mM NaCl, pH 7.0 at 30 °C. Stock solutions of 1 M H_2O_2 were typically prepared in 100 mM Hepes, pH 7.0. The concentration was verified using the absorbance at 240 nm where the extinction coefficient of H_2O_2 is 39.4 M^{-1} cm^{-1} (*93*). The peroxide shunt reactions were initiated by adding H_2O_2. For some experiments H_2O_2 was first added to the reaction component and after one minute the reaction was initiated by adding L-phenylalanine. The volumes of the peroxide shunt reactions were typically 2 to 4 mL, with reaction times ranging from 30 seconds to an hour. The reactions were terminated by mixing a 500 μL aliquot with 500 μL of 5 M HCl.

For anaerobic reactions, standard assay conditions were followed. A tonometer was made anaerobic by alternating vacuum and argon gas cycles for 10-15 min at 5 °C. H_2O_2 from the 1 M stock solution was placed in the side arm of the tonometer. At this point the temperature of the tonometer was changed to 30 °C and additional vacuum and argon cycles were performed for 5 minutes. The reaction was initiated by mixing H_2O_2 with the enzyme solution under argon. At indicated times, the valve of the tonometer was opened very rapidly under positive pressure releasing 500 μL of the reaction into 500 μL of 5 M HCl.

Steady state kinetic isotope effects with L-cyclohexylalanine and L-$^2H_{11}$-cyclohexylalanine. Peroxide shunt reactions were performed with L-cyclohexylalanine and L-$^2H_{11}$-cyclohexylalanine for PheH and TyrH. The reaction conditions were 50 μM

enzyme, 300 μM ferrous ammonium sulfate, 150 mM sodium phosphate, 100 mM NaCl, pH 7.0 in 1 mL at 25 °C. The concentrations of protiated and deuterated cyclohexylalanine varied from 10-50 mM, whereas H_2O_2 was 20 or 30 mM. The reactions were quenched by removing 100 μL and mixing it with 200 μL of methanol and 700 μL of sodium borate, pH 11. The precipitated enzyme was removed by centrifugation at 15000 g and the 1-cyanobenz[f]-isoindole (CBI) derivatives were formed by adding 200 μL of 50 mM naphthalene-2,3-dicarboxaldeyde (NDA) and 200 μL of 50 mM sodium cyanide (*94*). Control reactions revealed that 100 mM of H_2O_2 did not prevent the formation of the (CBI) cyclohexylalanine derivatives. Steady state kinetic isotope effects measurements were also performed with TyrH and PheH under normal turnover conditions: 4 mM $6MePH_4$, 4 mM L-cyclohexylalanine or L-$^2H_{11}$-cyclohexylalanine (saturating conditions), 15 μM ferrous ammonium sulfate, 10 μM enzyme, 100 mM NaCl and 100 mM Hepes/NaOH, pH 7.0, at 30 °C. The reactions were quenched by removing 20-50 μL and mixing it with 200 μL of methanol and 780 or 750 μL of sodium borate, pH 11. The CBI derivatives were formed following the protocol described above for the H_2O_2 reactions. The amount of 4-HO-cyclohexylalanine was identified and quantified using authentic 4-HO-cyclohexylalanine and converting it to a CBI derivative following the protocol outlined above.

Product analysis by HPLC. The amino acids in the reaction samples were separated on a Waters HPLC 600E multisolvent delivery system. The reaction samples were centrifuged at 15000 g to remove the precipitated enzyme. The entire sample was injected onto a C18 Phenomenex HPLC column (250 x 4.60 mm). Tyrosine, meta-

tyrosine and phenylalanine, or 4-hydroxymethyl-phenylalanine and 4-methylphenyl-alanine were separated with a mobile phase of 15 mM sodium phosphate, pH 7.0, 1% of tetrahydrofuran, at a flow rate of 1.0 ml/min. The amino acids were detected using a Waters 2475 Multi λ Fluorescence Detector with excitation at 270 nm and emission at 310 nm. The cyclohexylalanine and 4-HO-cyclohexylalanine CBI derivatives were separated with an isocratic solution containing 50% 15 mM sodium phosphate, pH 7.0, 1% tetrahydrofuran, and 50 % acetonitrile at a flow rate of 1.0 ml/min. In this case L-cyclohexylalanine and 4-hydroxy-cyclohexylalanine were detected by setting the fluorescence detector at 420 nm excitation and 520 nm emission.

RESULTS

Products from peroxide shunt reactions with aromatic substrates. Addition of excess H_2O_2 and phenylalanine to the ferrous forms of PheH, TyrH and TrpH resulted in the formation of significant amounts of hydroxylated amino acids. Figure 4 shows a representative HPLC chromatograph when PheH and ferrous iron are incubated with 10 mM L-phenylalanine and H_2O_2; tyrosine and meta-tyrosine are the only amino acid products.

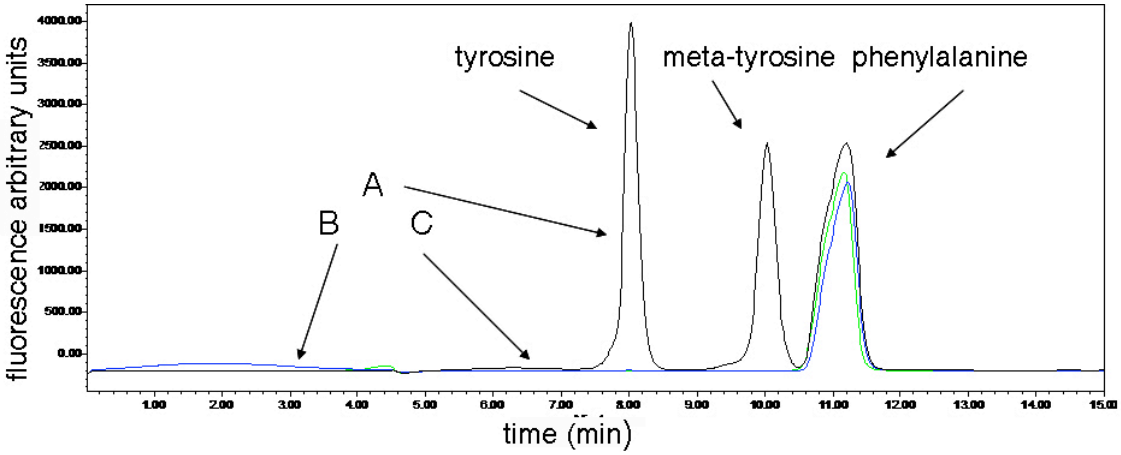

Figure 4: Chromatographs of a typical reaction quenched after 10 min when 10 mM of H_2O_2 and L-phenylalanine are incubated with (A) 50 μM PheH•300 μM Fe(II), (B) 500 μM Fe(II), or (C) 50 μM PheH.

Control experiments under the same conditions with apo-PheH or ferrous iron and no enzyme yielded no hydroxylated amino acids. The same experiments were carried out with TyrH and TrpH and the results were nearly identical, with a slight variation in the distribution of products. All three enzymes have a preference for tyrosine over meta-tyrosine tyrosine. The ratios of tyrosine to meta-tyrosine are 1.5, 1.2, 1.6 for PheH, TyrH and TrpH respectively. This shows that the reaction is not very specific; even though the three enzymes make two products from phenylalanine all three prefer the para position to the meta-position.

Single oxygen and peroxide donors including sodium periodate, cumene hydroperoxide, peracetic acid, and t-butyl hydroperoxide were also tested for their ability to support the hydroxylation of phenylalanine, since these have been successfully used for the heme-based cytochrome P450 family (*95-97*). No amino acid products with PheH, TyrH or TrpH were obtained from these reactions when the concentrations of

each donor ranged from 1 to 50 mM.

The ability of H_2O_2 to support hydroxylation of tyrosine by TyrH and tryptophan by TrpH was also investigated. These reactions did not yield hydroxylated amino acid products. The reason for this is unclear, but it is reasonable to propose that H_2O_2 and the Fe(II) center react. It is possible that the hydroxylation reaction occurs and dopa and 5-hydroxytryptophan are formed, but they rapidly react with H_2O_2. When dopa and 5-hydroxytryptophan (100 or 500 μM) are incubated with 5-10 mM of H_2O_2 for 2 min, neither could be detected, by fluorescence or absorbance spectroscopy nor could new products. Consequently, reactions with L-tyrosine and L-tryptophan were not investigated further.

Kinetics of the peroxide shunt reactions. Having established phenylalanine as the only aromatic amino acid that can yield hydroxylated aromatic amino acids from the peroxide shunt reactions, the kinetics of this reaction were further investigated. The initial rate of the reaction was determined for all three enzymes by measuring the formation of tyrosine and meta-tyrosine with time. Figure 5 (A) shows an overlay of several HPLC chromatographs for reactions in which 20 mM phenylalanine and 20 mM H_2O_2 were incubated with 50 μM of ferrous TrpH. Tyrosine and meta-tyrosine are formed in a time-dependent manner (Figure 5 (A)). When the same experiment was performed by varying the concentration of phenylalanine, plots of the total product yield versus time fit well to straight lines with intercepts that pass through the origin (Figure 5 (B)). The apparent first order rate constant for phenylalanine hydroxylation increases with the concentration of phenylalanine from 0.0089 min^{-1} to 0.22 min^{-1} for 1 and 50

mM of phenylalanine, respectively. It is worth noting that for the three enzymes the total product yield at concentrations higher than 20 mM of phenylalanine exceeds one equivalent; this shows that the reaction can be catalytic under certain conditions. Identical experiments to those shown in Figures 5 (A-B) were performed for TyrH and PheH by varying the concentration of phenylalanine at a constant concentration of H_2O_2. (Figure 5 (C)) shows plots of the rates versus the concentration of L-phenylalanine for all three enzymes. In all three cases the data fit well to a straight line with no evidence of saturation. The magnitudes of the second order rate constants for the three enzymes are nearly identical: 6.4 ± 0.3, 5.3 ± 0.7 and 4.3 ± 0.1 M^{-1} min^{-1} for PheH, TyrH and TrpH, respectively. The values are similar and suggest that the rate-limiting step with H_2O_2 is likely to be the same for the three enzymes (vide infra). It is worth noting that time points of one min or less did not yield products even when the concentration of phenylalanine was 50 mM, consistent with the slow activation of H_2O_2. The effect of H_2O_2 on the second order rate constant was further investigated by varying the concentration of L-phenylalanine at fixed levels of H_2O_2 for PheH and TrpH. Figure 6 shows a plot of the apparent second order rate constants versus the concentration of H_2O_2 for PheH and TrpH. The data show saturation behavior with an apparent K_m value for H_2O_2 of 25 ± 16 mM and 18 ± 11 mM for PheH and TrpH, respectively.

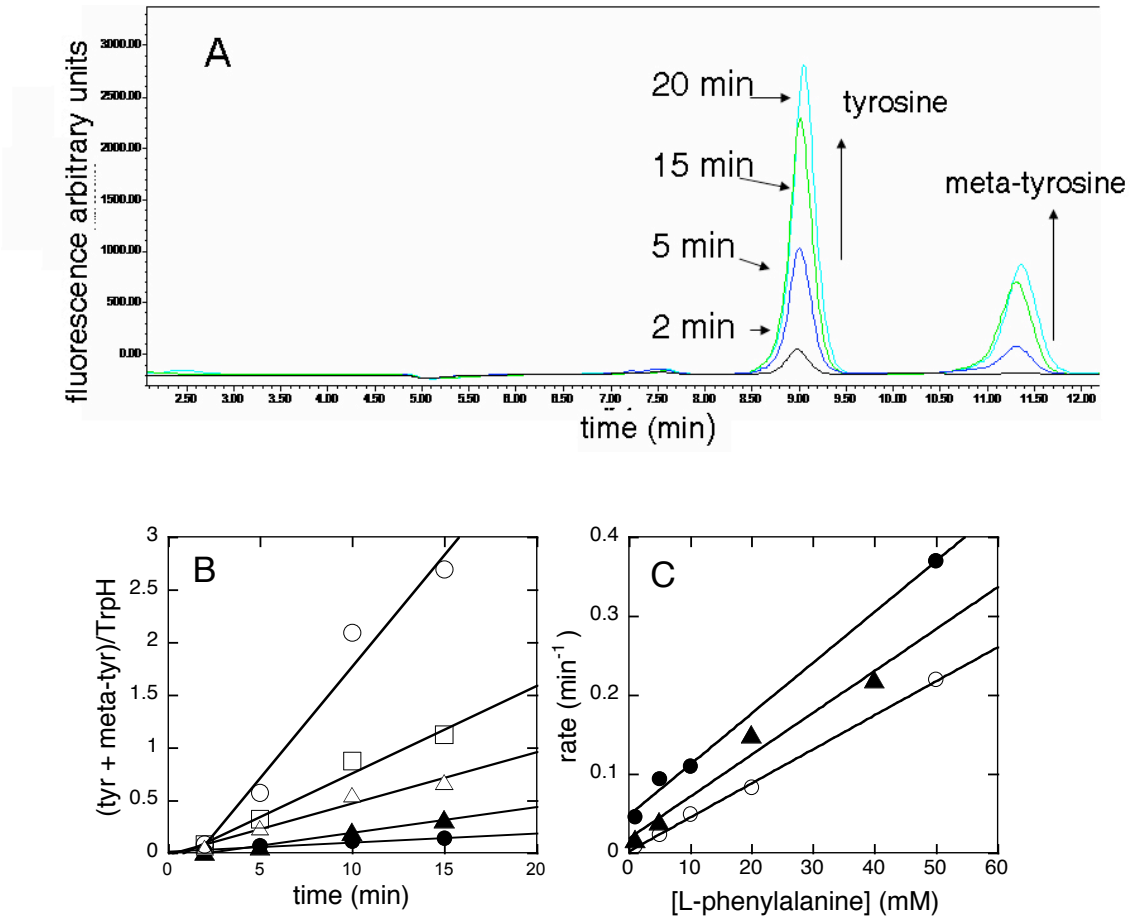

Figure 5: Kinetics of phenylalanine hydroxylation. A. Time course for the formation of tyrosine and meta-tyrosine when 20 mM H_2O_2 and phenylalanine are incubated with 50 μM ferrous TrpH. B. Effect of phenylalanine concentration on the rate of hydroxylation by TrpH: (●) 1 mM, (▲) 5 mM, (Δ) 10 mM, (❑) 20 mM and (❍) 50 mM. C. Plot of the initial rate versus the concentration of phenylalanine for PheH (●), TyrH (▲) and TrpH (❍).

To determine if the slow turnover rate with H_2O_2 is the result of enzyme inactivation, the rate of tyrosine formation was determined for PheH and TrpH with 200-1000 μM $6MePH_4$, 200-1000 μM L-phenylalanine, 15 μM ferrous ammonium sulfate, 2-5 μM enzyme, 100 mM NaCl and 100 mM Hepes/NaOH, pH 7.0, at 25 °C (standard assay conditions). Initially, stock solutions of PheH and TrpH were incubated with 0, 10, 20, 50, 70 and 100 mM of H_2O_2 at 5 °C. After one hour each enzyme

sample was assayed under standard conditions for its ability to form tyrosine. These experiments revealed that the rate of tyrosine formation was unaffected when the concentration of H_2O_2 was less than 70 mM. As an additional control experiment, reactions were performed for PheH in which after 0, 5, 10 and 20 minutes of a typical peroxide shunt reaction 2 μM of enzyme was sampled for its ability to make tyrosine under standard assay conditions. The initial rate of tyrosine formation was unaffected by the extent of the peroxide shunt reaction.

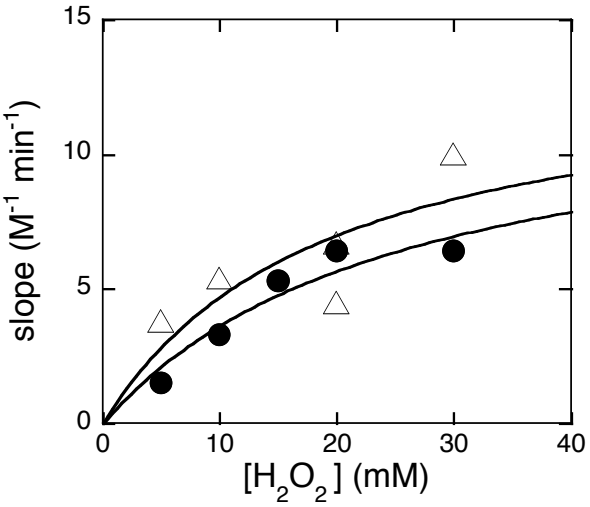

Figure 6: Effect of H_2O_2 concentration on the slopes of the lines in Figure 5 (C) for PheH (●) and TrpH (Δ). The slopes (apparent second order rate constants) were obtained by varying the concentration of phenylalanine versus different fixed levels of H_2O_2. The lines are fits to the Michaelis Menten equation.

The peroxide shunt reactions were typically carried out for 30 minutes. When reactions were continued for longer time a decrease in the total product yield was typically found between 20 and 30 min. Therefore, the calculation of the initial rate was

limited to 15-20 min. The time when deviation from linearity occurred depended on the initial concentrations of phenylalanine and H_2O_2, suggesting that H_2O_2 degrades tyrosine and meta-tyrosine in a reaction that is slow relative to turnover. The products from the degradation are presumed to be oxidized amino acids, which are undetectable under the standard HPLC conditions (see above). The kinetics of the oxidation reactions were not pursued due to the anticipated complexity of the reaction. In order to verify that degradation of tyrosine and meta-tyrosine does not occur in the quenched samples, tyrosine and meta-tyrosine (100 μM) were first mixed with 2.5 M HCl; following this 0 or 50 mM H_2O_2 was added to the acidic solution. These samples were incubated at 30 °C for one hour and then injected onto the HPLC. The total amounts of products were the same (not shown), suggesting that H_2O_2 does not degrade the amino acids under acidic conditions.

The degradation of tyrosine and meta-tyrosine by H_2O_2 suggests that the reaction with H_2O_2 might appear to be slow due to the continuous degradation of the hydroxylated aromatic amino acids. In order to validate the kinetics in Figures 5 (A-C) and 6, the effect of the enzyme concentration on the product yield with time was analyzed. Figure 7 show typical time courses when 20, 50 or 100 μM of PheH were incubated with 20 mM H_2O_2 and 20 mM L-phenylalanine. A plot of the product yield versus time is linear with time at all enzyme concentrations, but the yield decreases faster when the concentration of PheH in the reaction is higher (Figure 7).

This shows that H_2O_2 degrades tyrosine and meta-tyrosine faster when their concentrations in solution are higher. This analysis also reveals that the product yield up

to at least fifteen minutes is equivalent for all concentrations of PheH, suggesting that no significant degradation of tyrosine and meta-tyrosine has occurred. The dependence of the initial rate on enzyme concentration validates the analyses in Figures 5 (A) and 6 and suggests that the lower product yield at higher concentrations of PheH is not due to inactivation of PheH by H_2O_2.

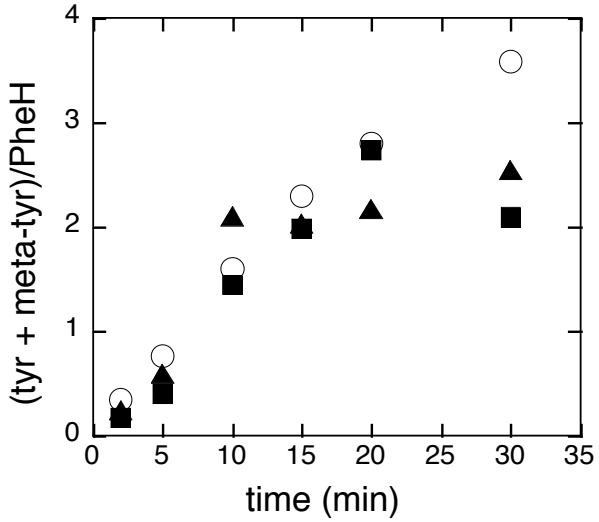

Figure 7: Enzyme concentration dependence of the total product yield in the H_2O_2 shunt reaction for PheH. The standard conditions were as described in the experimental procedures section. The concentrations of H_2O_2 and phenylalanine were 20 mM, whereas PheH was 20 μM (○), 50 μM (■) or 100 μM (▲).

The peroxide shunt reactions were performed in the absence of O_2 to determine if aerobic conditions are a reason for the slow reaction rate. Aerobic and anaerobic reactions were performed simultaneously to eliminate discrepancies from reaction conditions. These reactions were performed following standard conditions with 20 mM H_2O_2 and phenylalanine whereas PheH was 50 μM. A plot of the total product yield

versus time for the anaerobic reaction yielded an apparent rate of 0.17 ± 0.02 min^{-1}, whereas the value under aerobic conditions is 0.16 ± 0.01 min^{-1}; these values are effectively identical (Figure 8). This suggests that the slow turnover with H_2O_2 is not due to the oxidation of the Fe(II) center by O_2 or another species generated between O_2 and H_2O_2, but more importantly it shows that O_2 is not required at all.

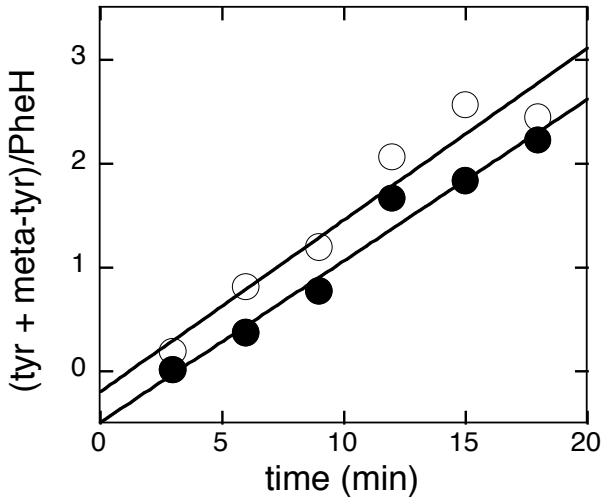

Figure 8: Time course of the formation of tyrosine and meta-tyrosine when 20 mM H_2O_2 and phenylalanine are incubated with 50 μM ferrous PheH (●) aerobically or (○) anaerobically. The lines are fits to linear equations.

Effect of 6-methyl-7,8-dihydropterin and 6-methyl-5-deazatetrahydropterin on the peroxide shunt reactions. Peroxide shunt reactions were also carried under the standard assay conditions described above, but 50 to 2000 μM 6Me7,8PH_2 or 5Me5DPH_4 were included with 50 μM ferrous PheH or TyrH and 10 mM phenylalanine. These reactions were initiated with 20 mM of H_2O_2. The initial rate, the total product

yield, and the ratio of tyrosine to meta-tyrosine were identical to those obtained in the absence of the pterin analogs (data not shown) for both enzymes.

Peroxide shunt reactions for active site mutants of TyrH and PheH. Active site mutants of TyrH and PheH that affect the hydroxylation of the amino acid more than the oxidation of $6MePH_4$ (decouple the reaction) were tested for their ability to catalyze the hydroxylation of phenylalanine using H_2O_2. The TyrH mutant E332A has been previously characterized as an enzyme with a higher K_m value for $6MePH_4$ for which only 2.5 percent of the reducing equivalents from $6MePH_4$ are used for productive turnover (*92*). The TyrH mutant S395A is not impaired in its ability to activate O_2 since it forms the 4a-hydroxypterin (4a-$6MePH_3OH$) at a normal catalytic rate, but it is unable to form dopa from tyrosine (*43*). In the case of PheH, the mutants V379D and F263A have low turnover rates and higher K_m values for phenylalanine. The coupling efficiencies with respect to $6MePH_4$ for the PheH mutants V379D and F263A are 27 and 15 percent, respectively (*39, 91*). Standard peroxide shunt reactions were carried out using concentrations of the mutant enzymes of 25 μM, 10 mM H_2O_2 and 20 mM phenylalanine. For V379D-PheH, F263A-PheH, E332A-TyrH and S395A-TyrH the reactions yielded no products after more than 30 minutes (data not shown). The results with the mutant enzymes clearly show that mutations that decouple catalysis under normal turnover conditions can drastically affect the ability of the enzymes to use H_2O_2 as oxygen and electron donor. This suggests that the mechanism of uncoupling under normal turnover may be similar with H_2O_2.

L-Cyclohexylalanine and 4-methylphenylalanine as substrates for PheH and TyrH. 4-Methylphenylalanine, 4-C^2H_3-methylalanine, L-cyclohexylalanine and L-$^2H_{11}$-cyclohexylalanine were used as substrates for TyrH and PheH with H_2O_2 in order to determine if the hydroxylating intermediate can catalyze aliphatic and benzylic hydroxylation. The reaction was also studied under normal turnover conditions ($6MePH_4$, O_2) with L-cyclohexylalanine and L-$^2H_{11}$-cyclohexylalanine. TyrH, TrpH and PheH can catalyze the $6MePH_4$ and O_2 dependent hydroxylation of 4-methylphenyl-alanine to form 4-hydroxymethyl-phenylalanine, 3-hydroxy-4-methyl-phenylalanine and 3-methyl-4-hydroxy-phenylalanine (*42, 52*). In addition, TyrH and PheH can catalyze the $6MePH_4$ and O_2-dependent hydroxylation of cyclohexylalanine to form 4-HO-cyclohexylalanine; no additional products were identified by HPLC. The k_{cat} values for the hydroxylation of L-cyclohexylalanine were 10.0 ± 0.5 and 5.0 ± 0.2 min^{-1} for TyrH and PheH, respectively at 30 °C. The stoichiometry of this reaction with respect to $6MePH_4$ and the concentration dependence with L-cyclohexylalanine were not investigated. When the reaction was carried out with L-$^2H_{11}$-cyclohexylalanine, the k_{cat} values were nearly identical to those obtained with the protiated substrate, yielding a kinetic isotope effect on the k_{cat} value of unity. The intrinsic deuterium kinetic isotope effect for cleavage of a CH bond of the methyl group of 4-methylphenylalanine for TyrH and PheH is 10 (*42, 52*). For cyclohexylalanine the isotope effect is expected to be of similar magnitude; this suggests that steps other than hydroxylation limit turnover with this substrate.

Peroxide shunt reactions were subsequently carried out with PheH and TyrH with 5 or 10 mM 4-methylphenylalanine or 4-C^2H_3-phenylalanine and 30 mM of H_2O_2. The only product detected was 4-hydroxymethyl-phenylalanine. A kinetic isotope effect from the ratio of 4-hydroxymethyl-phenylalanine arising from the protiated and deuterated substrate will not be the intrinsic effect due to the inability to quantify the products from aromatic hydroxylation (*58, 59*). Despite this caveat limiting kinetic isotope effects of 2 and 1.4 were obtained for PheH and TyrH, respectively. The peroxide shunt reactions were carried out with PheH and TyrH by varying the concentration of cyclohexylalanine from 10 to 50 mM while the concentration of H_2O_2 was 30 mM. For these experiments the initial rate of the reaction was determined for up to 40 min; the product yield for this reaction never reached one equivalent. This shows that with cyclohexylalanine the peroxide shunt reaction for TyrH and PheH is considerably more uncoupled than with phenylalanine.

Control experiments revealed that as high as 100 mM H_2O_2 does not degrade cyclohexylalanine or 4-HO-cyclohexylalanine. Figure 9 (A) shows an HPLC chromatograph of a reaction quenched after 20 min when PheH and H_2O_2 are incubated with L-cyclohexylalanine (A) or L-$^2H_{11}$-cyclohexylalanine (B). A plot of the initial rate of the reaction (Figure 9 (B)) shows that just as the case is with L-phenylalanine, L-cyclohexylalanine displays second order kinetics with no evidence for saturation.

For PheH the second order rate constant with L-cyclohexylalanine is 0.17 ± 0.06 M^{-1} min^{-1}, while the value with L-$^2H_{11}$-cyclohexylalanine is 0.083 ± 0.002 M^{-1} min^{-1} (Figure 9 (B)). A kinetic isotope effect on the second order rate constant of about 2 can

be calculated from these data. For TyrH the value of the second order rate constant at 50 mM L-cyclohexylalanine is 0.28 M^{-1} min^{-1}, whereas the value with L-$^{2}H_{11}$-cyclohexyl-alanine is about 0.18 M^{-1} min^{-1}, yielding a kinetic isotope effect of about 1.5. These

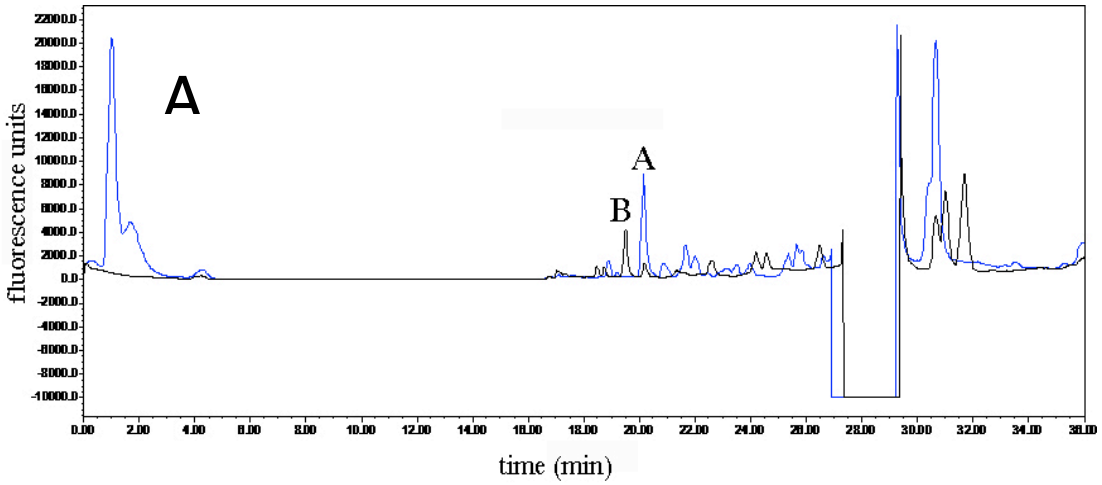

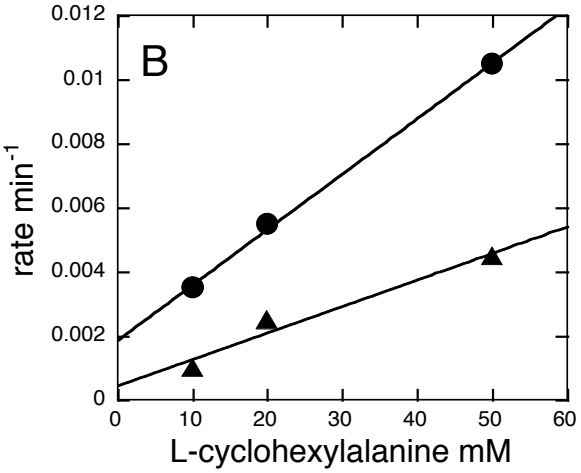

Figure 9: A. Chromatographs of a reaction quenched after 20 min when 30 mM H_2O_2 and L-cyclohexylalanine (A) or L-$^{2}H_{11}$-cyclohexylalanine (B) are incubated with 100 μM ferrous PheH B. A plot of the initial rate for a peroxide shunt reaction with L-cyclohexylalanine (●) or L-$^{2}H_{11}$-cyclohexylalanine (▲).

isotope effects for both enzymes are similar and slightly greater then unity, but the magnitudes suggest that they are not intrinsic. The ability of PheH and TyrH to catalyze hydroxylation of cyclohexylalanine with H_2O_2 suggests that the hydroxylating intermediate formed via a peroxide shunt may be the same high valence Fe(IV)O intermediate used under normal turnover.

DISCUSSION

The aromatic amino acid hydroxylases PheH, TyrH and TrpH form a unique class in the monooxygenase family of enzymes that share the $(His)_2$-(Asp/Glu) facial triad. These enzymes require a tetrahydropterin and a mononuclear iron center to activate O_2 for the hydroxylation of an amino acid (*10, 18, 98*). In this study we investigated and successfully generated a system in which the enzymatic aromatic hydroxylation of phenylalanine does not require molecular oxygen and tetrahydropterin. The rationale for these experiments is simple: if the two electron reduced form of O_2, H_2O_2, can support aromatic hydroxylation, a hydroxylating intermediate involving tetrahydropterin can be ruled out. It is worth noting that studies involving H_2O_2 as oxygen and electron donor were unsuccessfully attempted in the past for TyrH and PheH (*99*), and earlier experiments in which H_2O_2 and tyrosine were the only substrates for TyrH were not convincing (*100*).

Currently, strong experimental evidence is available from freeze-quench Mössbauer spectroscopy supporting the involvement of an Fe(IV)O intermediate in aromatic hydroxylation by TyrH (*45*). A 4a-peroxypterin was attractive for some time

as the hydroxylating intermediate in the catalytic cycle of the aromatic amino acid hydroxylases, considering that a 4a-peroxyflavin, structurally similar to the 4a-peroxypterin, has been shown to be the hydroxylating intermediate for aromatic hydroxylation in the flavoproteins phenol hydroxylase and p-hydroxybenzoate hydroxylase (*101-103*). In addition, the formation of hydrogen peroxide from $6MePH_4$ and O_2 during unproductive turnover when tyrosine, p-fluorophenylalanine, or p-chlorophenylalanine is used as a substrate for PheH is consistent with the intermediacy of a 4a-peroxypterin (*78*). A 4a-peroxypterin or a 4a-peroxypterin-iron species (*77*) (Scheme 3) is likely to be an intermediate in the catalytic cycle of aromatic hydroxylation, but the studies presented here convincingly rule out their direct role as hydroxylating intermediates.

The ability of the aromatic amino acid hydroxylases to effectively use H_2O_2 as oxygen substitute and electron donor with phenylalanine also supports several elements of the mechanism in Scheme 3. The role of ferrous iron and the catalytic aspect of the H_2O_2 dependent reaction suggest that the Fe(II) center can be regenerated after one turnover since no additional reductants are present. Ferrous iron and H_2O_2 can react in solution to form reactive oxygen species (Fenton chemistry) (*104*). The possibility exists that reactive oxygen species generated from Fenton chemistry could be responsible for the hydroxylation of aromatic amino acids. However, the results presented here argue strongly against a non-enzymatic source for the hydroxylation of phenylalanine. For one, the results with apo-wild type enzymes, ferrous iron in solution and active site mutants of PheH and TyrH that completely eliminate the activity with

H_2O_2 strongly support a reaction that is strictly enzyme catalyzed. Secondly, non-enzymatic Fenton chemistry would likely yield products not seen in the enzyme catalyzed reaction. Given that the only products obtained from the peroxide shunt reaction with phenylalanine are tyrosine and meta-tyrosine, and their relative ratios (Figure 4) depend on the enzyme, it can be concluded that the reaction is enzyme-catalyzed. In addition, no hydroxylated aromatic amino acids are obtained with single oxygen or larger peroxide donors that have been shown previously to support hydroxylation in cytochrome P450. This reinforces the notion that the reaction with H_2O_2 is enzyme-catalyzed, since these peroxide donors can readily donate hydrogen peroxide. In addition, this shows that the aromatic amino acid hydroxylases have drastically different active sites than the P450 enzymes where oxygen donors with larger organic substituents can be accommodated.

The low rate of turnover with H_2O_2 can be the result of multiple factors. Under normal turnover, all three aromatic amino acid hydroxylases are readily saturated with their respective substrate with K_m values in the low micromolar range (*49, 56, 90*). The data in Figure 5 (C) show that saturation with respect to phenylalanine cannot be achieved for any of the enzymes. This shows that phenylalanine binds weakly or non-productively and/or the reaction occurs through a state for which the enzymes are not structurally optimized (vide infra). Furthermore, the non-saturation behavior with respect to phenylalanine suggests that binding of the amino acid is at least partially rate limiting. The inability to observe saturation kinetics with respect to phenylalanine, along with the high non-physiological concentrations of amino acid and H_2O_2 required

to effectively generate the peroxide shunt, suggests that the reaction proceeds through a state, which is not relevant under normal turnover. In view of the fact that the second order rate constants are nearly identical (Figure 5 (C)) and that tyrosine and meta-tyrosine are the only products, it can also be concluded the rate determining step and the substrate specificities with H_2O_2 are likely to be the same for all three enzymes.

The ability of PheH to hydroxylate the meta position of phenylalanine is surprising, considering that PheH is unable to make meta-tyrosine from phenylalanine and dopa from tyrosine (*91, 105*). This shows that tetrahydropterin, in addition to delivering reducing equivalents for O_2 activation, has significant effects on the architecture of the active site of PheH, allowing the reaction to be specific for the para position of phenylalanine. The k_{cat}/K_m value for phenylalanine under normal turnover is 600,000 fold faster than the second order rate constant with H_2O_2. This suggests that tetrahydropterin has additional important roles in catalysis. A role may be to induce structural changes that enhance the rate of chemical steps. It is reasonable to propose that tetrahydropterin is required to be in the active site for each enzyme to be readily saturated with the amino acid, fast turnover and substrate specificity. It should be noted that agreement on the order of substrate binding has not been reached for all three enzymes yet. The results obtained here suggest that under normal turnover tetrahydropterin needs to be bound before the amino acid, and the former contributes to the binding site of the latter. This is consistent with the available crystal structures for PheH, TyrH and TrpH in complex with tetrahydropterin (*31, 106, 107*) and suggests that these binary complexes may be catalytically relevant and not necessarily inhibitory

complexes. The inability of the pterin analogs to affect the peroxide shunt reactions is unexpected. Inhibition studies have established previously that 6Me7,8PH_2 and 5Me5DPH_4 bind PheH and TyrH competitively with respect to a tetrahydropterin (*49, 89, 108, 109*). At this point the simplest explanation for this inconsistency is that upon H_2O_2 binding the dissociation of tetrahydropterin is enhanced and the peroxide shunt reaction proceeds from a state in which tetrahydropterin cannot access the active site.

A comparison of the crystal structures of PheH and TrpH with only tetrahydropterin bound versus structures for the ternary complexes shows significant structural differences. For PheH the structure with both tetrahydropterin and an amino acid bound shows significant conformational changes, especially on the surface loop containing residues 132-148. This surface loop is in close contact to the iron center only in the structure of the ternary complex (*110, 111*). The crystal structure of TrpH becomes more compact upon binding of tryptophan and imidazole (*112*). The latter is proposed to substitute for tetrahydropterin in the structure. In addition, the loop region containing Leu124-Asp139 moves in close contact to residues Ile367-Thr369 (*112*). In the case of TyrH no structure is available for the ternary complex, but fluorescence anisotropy studies reveal that binding of tetrahydropterin alone has significant effects on the surface loop containing residues 178-193 (*89*). These residues correspond to residues 132-148 in PheH. More importantly, X-ray absorption spectroscopy on PheH shows that the coordination number of the Fe(II) center changes from 6 to 5 when L-phenylalanine and a tetrahydropterin are bound. It has been proposed that this coordination change allows the three water molecules coordinating the Fe(II) center in

the resting state to be released as glutamate 330 becomes bidentate, creating a binding site for O_2 (*113*). These crystallographic, fluorescence and X-ray spectroscopy studies establish that significant structural changes in the enzymes and the Fe(II) center are dependent on both substrates or tetrahydropterin alone. Therefore, it is reasonable to propose that H_2O_2 and phenylalanine alone cannot induce the movements of the surface loops and/or the required coordination change of the Fe(II) center.

The results derived thus far from the reactions of H_2O_2 for the aromatic amino acid hydroxylases are comparable to results obtained in previous studies with the oxygenase components of the mononuclear iron enzymes napthalene 1,2 dioxygenase (NDO) and benzoate 1,2-dioxygenase (BZDO). These two enzymes also share the $(His)_2(Asp/Glu)$-facial triad motif and catalyze aromatic hydroxylation, but do not require a tetrahydropterin (*114, 115*). Unlike the aromatic amino acid hydroxylases, the reactions of NDO and BZDO with H_2O_2 allow at maximum one turnover. This is attributed to the requirement for an additional electron for the re-reduction of the Fe(III) center to the ferrous state. This reduction step appears to be essential for product release. When H_2O_2 is the oxygen and the electron donor, the extra electron is not available (*114, 115*). In the present work we show that all three aromatic amino acid hydroxylases can perform more than one turnover when the concentration of L-phenylalanine is above 20 mM. This firmly suggests that the Fe(II) center can be regenerated. Abortive oxidation of the Fe center likely occurs during turnover, but the data suggest that it is slow relative to turnover. For both NDO and BZDO, the concentration of H_2O_2 required to initiate the reaction is 20-50 mM, comparable to that

used in these studies. This suggests that the mononuclear non-heme centers in NDO, BZDO and the aromatic amino acid hydroxylases are similar in that the affinity for H_2O_2 is weak. Similarity, BZDO requires higher concentrations of benzoate with H_2O_2 in comparison to normal turnover conditions. Unlike the aromatic amino acid hydroxylases, saturation kinetics are observed with respect to benzoate (*114*). One way to interpret this difference is to assume that significant structural changes may not be required to create a binding site for benzoate in BZDO; thus saturation kinetics are observed. As noted above, this is consistent with the hypothesis that in addition to delivering the two electrons, tetrahydropterin has essential roles in enhancing the affinity of the amino acid for each aromatic amino acid hydroxylase.

The steady state deuterium kinetic isotope effect for the hydroxylation of L-cyclohexylalanine by TyrH and PheH under normal turnover (6MePH$_4$, O_2) and with H_2O_2 were measured in order to compare the nature of the transition state for both reactions. The only product detected under normal turnover and with H_2O_2 is 4-HO-cyclohyxylalanine; it is reasonable to propose that the same hydroxylating intermediate is involved. However, the magnitude of the deuterium isotope effects does not allow us to draw definite conclusions regarding the nature of the transition state for the hydroxylation reaction. Hydroxylation reactions for non-heme systems with aliphatic substrates are thought to proceed via hydrogen atom abstraction and radical rebound by high valence Fe(IV)O intermediates (Scheme 5) (*116, 117*). The intrinsic deuterium kinetic isotope effect for this reaction is expected to be 10-13 with a normal secondary component if one assumes a symmetrical transition state. The $^{D}k_{cat}$ value is unity; the

simplest explanation for this is that a step following hydroxylation limits k_{cat} for TyrH and PheH. The deuterium isotope effect on the second order rate constant with H_2O_2 is greater than unity for both enzymes, but less than the expected value of 10 or 13. One way to interpret this is to assume that the rate-limiting step has changed with H_2O_2. As noted above, the kinetic behavior for the reactions with H_2O_2 strongly suggests that tetrahydropterin not only delivers two electrons for O_2 activation, but also affects substrate binding and the rate of catalysis to allow for effective turnover. It is very likely that steps following hydroxylation also depend on the structural changes imposed by tetrahydropterin. Therefore, if product release or a conformational change coupled to product release is rate limiting under normal turnover, this step is very likely to be different with H_2O_2. We proposed that the rate-limiting step for the peroxide shunt reaction is activation of H_2O_2 (vide infra). However, the second order rate constants with phenylalanine for TyrH and PheH are about 18-35 fold faster than those obtained with cyclohexylalanine. If activation of H_2O_2 were rate limiting, then one would expect the magnitude of the second order rate constants to be nearly identical or perhaps similar in magnitude. One way to reconcile these results is to assume that the formation of the hydroxylating intermediate does not depend on the identity of the amino acid. The difference in magnitude of the second order rate constants may reflect significantly more unproductive decay of the Fe(IV)O intermediate with cyclohexylalanine coupled to a slower rate constant for aliphatic hydroxylation versus aromatic hydroxylation.

The nearly identical kinetic behavior of the peroxide shunt reaction for all three enzymes suggests that the rate-determining step is the same for all three enzymes.

Scheme 6 shows a proposed chemical mechanism for the hydroxylation of phenylalanine with H_2O_2. In Scheme 6 pathway A amino acid binding is required for the activation of H_2O_2. We have proposed that an iron-hydroperoxo intermediate forms following binding of H_2O_2 to the Fe(II) center. With the available data the involvement of the iron-hydroperoxo intermediate as the actual hydroxylating intermediate cannot be ruled

Scheme 6

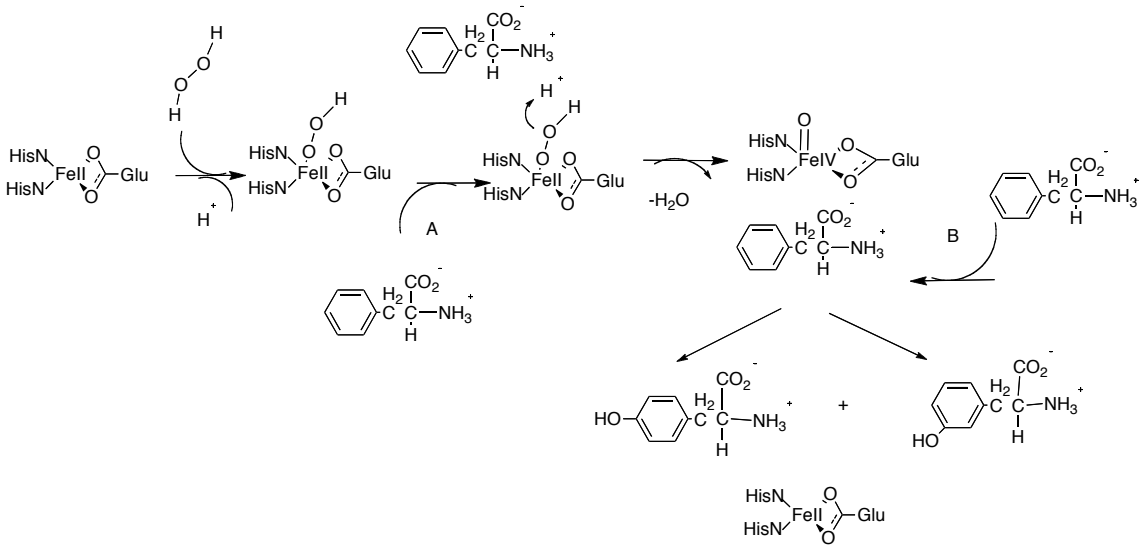

out. Nevertheless, experimental data from model complexes that mimic the active site of non-heme enzymes suggest that iron-hydroperoxo intermediates are likely to be non-reactive in hydroxylation reactions (*118*). Therefore, protonation of the distal oxygen of the iron-hydroperoxo has to occur, followed by water release to form the high valence Fe(IV)O intermediate, a step that is expected to be irreversible. One of the factors that is likely to contribute to the rate limitation of the reaction with H_2O_2 is the heterolytic cleavage of the O-O bond from the iron-hydroperoxo intermediate (Scheme 6). Under

normal turnover, the O-O bond will be cleaved from the 4a-peroxypterin-iron species; the leaving group in this case is the 4a-6MePH$_3$OH (pK$_a$ 6.8) (*119*). With H_2O_2 the leaving group is water (pK$_a$ 15.74); this makes the 4a-6MePH$_3$OH a much better leaving group than H_2O. We can speculate that under normal turnover protonation may not be required for cleave of the O-O bond of the 4a-peroxypterin-iron intermediate. Protonation of the distal oxygen of the iron-hydroperoxo is essential with H_2O_2 because hydroxide would be a poor leaving group and that step may in fact contribute significantly to the rate limitation. Scheme 6 pathway A predicts that activation of H_2O_2 requires phenylalanine; if activation of H_2O_2 is fully rate limiting the kinetics of this reaction should display saturation with respect to phenylalanine, inconsistent with what is observed kinetically.

The available data do not rule out a mechanism where the activation of H_2O_2 is substrate independent, for this reason Scheme 6 pathway B needs to be considered. In pathway B the Fe(IV)O intermediate forms with the same steps as for A, but without the requirement of the amino acid. Scheme 6 pathway B shows that the amino acid can bind only after the Fe(IV)O intermediate has formed, react to yield tyrosine, meta-tyrosine and the resting enzyme. Pathway B is appealing because it accounts for the non-saturation behavior with respect to the amino acid and is consistent with the activation of H_2O_2 as fully rate-limiting. Furthermore, it can also account for the suppressed isotope effects with L-cyclohexylalanine if substrate binding or the access of the amino acid to the Fe(IV)O intermediate is slow relative to hydrogen atom abstraction.

The results presented here suggest that H_2O_2 can effectively replace tetrahydropterin and O_2 and form the same high valence Fe(IV)O intermediate involved in aromatic hydroxylation during normal turnover. The kinetics of the reactions with H_2O_2 are identical for all three enzymes, showing that the iron centers in all three enzymes are essentially identical. Furthermore, the high concentrations of substrates required and the slow nature of the reaction suggest that a non-physiological state is operative in which the rate-limiting step is activation of H_2O_2.

CHAPTER IV

INSIGHTS INTO THE CATALYTIC MECHANISMS OF PHENYLALANINE AND TRYPTOPHAN HYDROXYLASE FROM KINETIC ISOTOPE EFFECTS ON AROMATIC HYDROXYLATION*

INTRODUCTION

Phenylalanine hydroxylase (PheH), tyrosine hydroxylase (TyrH) and tryptophan hydroxylase (TrpH) form a small family of non-heme iron monooxygenases (*19*). These enzymes catalyze the insertion of an oxygen atom from molecular oxygen into the aromatic side chain of their corresponding substrates, utilizing a tetrahydropterin to reduce the other oxygen atom to the level of water (Scheme 2) (*18*). The three aromatic amino acid hydroxylases show significant sequence and structural similarity, especially in their catalytic cores. Structures are now available for the isolated catalytic domains of all three enzymes, clearly showing the structural homology (Figure 1 (A)) (*31, 33, 120*). This homology extends to the active site where each contains an iron atom coordinated by a glutamate and two histidine residues (Figure 1 (B)). This arrangement of iron ligands has also been found in a number of other non-heme iron mono and dioxygenases and has been termed the 2-his-1-carboxylate facial triad (*10, 121*).

The chemical mechanism proposed for the aromatic amino acid hydroxylases is shown in Scheme 3 (*18*). After all the substrates are bound, tetrahydropterin, oxygen and the Fe(II) center react to form a high valence ferryl-oxo intermediate (Fe(IV)O) and 4a-hydroxypterin the first product. An electrophilic substitution reaction between the Fe(IV)O intermediate and the amino acid proceeds through a cationic intermediate, which undergoes a 1,2 hydrogen (NIH) shift and tautomerization to yield the hydroxylated amino acid product and the ferrous enzyme.

In the mechanism of Scheme 3, the rate constant for the formation of the new carbon-oxygen bond upon attack of the Fe(IV)O species should increase 10-15% upon deuterium substitution at the site of hydroxylation, resulting in a $^{D}k_{cat}$ value of about 0.9 if this step is fully rate limiting. The basis for it is a hybridization change from sp^2 to sp^3 results in a stiffer bond and the heavier C-D bond prefers the stiffer bond (*69, 122*). In the case of TrpH, an inverse isotope effect is seen under k_{cat} conditions (*38*). In contrast, with wild-type TyrH no isotope effect is found when 3,5-$^{2}H_2$-tyrosine is used as substrate (*49*). In this case, an isotope effect could be unmasked by taking advantage of mutant enzymes which oxidize excess tetrahydropterin relative to the amount of amino acid hydroxylated (*40*). Several active site mutants of TyrH yield $^{D}k_{cat}$ values similar to the value for TrpH, consistent with these two aromatic amino acid hydroxylases sharing the same chemical mechanism. In the case of wild-type PheH, a normal kinetic isotope effect on k_{cat} of 1.45 has been reported (*123*), suggesting a different rate limiting step for PheH or perhaps a different chemical mechanism than that of the other two hydroxylases. In the present study an approach similar to that taken for TyrH was

carried out with Δ117PheH, employing mutant enzymes and kinetic isotope effects to probe individual steps in the catalytic mechanism.

EXPERIMENTAL PROCEDURES

Materials. Oligonucleotides were synthesized on an Applied Biosystems Model 380B DNA synthesizer by the Gene Technology Laboratory of the Biology Department of Texas A&M University. 6-Methyltetrahydropterin ($6MePH_4$) was from B. Schircks Laboratories (Jona, Switzerland). L-Tyrosine, L-phenylalanine, L-tryptophan, D,L-phenylalanine, sheep dihydropteridine reductase (DHPR), NADH, sodium cyanide, boric acid and 5-hydroxytryptophan (5-HO-trp) were from Sigma-Aldrich Chemical Co. (Milwaukee, WI). Naphthalene-2,3-dicarboxaldehyde (NDA) was from Invitrogen (Carlsbad, CA). L-$^2H_5$-Phenylalanine and $^2H_5$-indole-tryptophan were from Cambridge Isotope Co., MA. Dithiothreitol (DTT) was from Inalc (Milano, Italy). D,L-[4-^{2}H]-Phenylalanine and D,L-[3,5-$^2H_2$]-phenylalanine were synthesized as previously described (*124*). All other reagents were of the highest purity commercially available.

Construction of vectors, enzyme expression and purification. Site directed mutagenesis of the catalytic domain of rat phenylalanine hydroxylase (Δ117PheH) was carried out with the Stratagene QuikChange Kit using *Pfu* DNA polymerase and the plasmid ptzRPH5 (*54*). Δ117PheH and the mutants E280A, F263A and V379D were expressed and purified as previously described, with one modification (*54, 91*). The ammonium sulfate pellet was resuspended in 30 mM potassium phosphate, 10% glycerol, pH 7.0, before loading onto the hydroxyapatite column. The enzymes were

eluted from this column with a linear gradient of 30 to 450 mM potassium phosphate, pH 7.0, and stored in 80 mM Hepes/NaOH, 15% glycerol, pH 7.0. $TrpH_{102-416}$, a variant of rabbit tryptophan hydroxylase lacking 101 and 28 residues from the amino and carboxyl termini, was purified as previously described (*90*), with several modifications. The plasmid pEWOHΔ101ΔH was used to transform *E. coli* strain C41(DE3), a strain derived from BL21(DE3) which grows to a higher cell density (*125*). A single colony was used to inoculate one hundred milliliters of LB broth (100 μg/mL ampicillin) and allowed to grow at 37 °C for 5 hours; ten mL of the one hundred mL culture was used to inoculate one liter of LB broth (100 μg/mL ampicillin). The culture was grown until the cell density reached an A_{600} of 0.9. The temperature was decreased to 18 °C, and the cells were permitted to grow until the cell density reached an A_{600} of 1.2. At this point isopropyl-β-thiogalactoside was added to a final concentration of 100 μM. After 12 hours the cells were harvested by centrifugation as previously described (*90*). The cells were resuspended in a 8-fold volume with respect to the cell weight of 80 mM Hepes/NaOH, 100 mM ammonium sulfate, 2 mM DTT, pH 7.1. Nucleic acids were removed by addition of polyethyleneimine to a final concentration of 0.1%. Prior to the hydroxyapatite column, the ammonium sulfate pellet was resuspended in 50 mM potassium phosphate, 10% glycerol, 100 mM ammonium sulfate, 2 mM DTT, pH 7.1. The enzyme was then eluted with a linear gradient of 50 to 400 mM potassium phosphate, 10% glycerol, 100 mM ammonium sulfate, 2 mM DTT, pH 7.1. The purified enzyme was stored in 15% glycerol, 100 mM ammonium sulfate, 2 mM DTT, 50 mM

Hepes/NaOH, pH 7.0, after the addition of a stoichiometric amount of ferrous ammonium sulfate.

Enzyme assays. Tyrosine formation from phenylalanine was measured by monitoring the initial rate of the absorbance change at 275 nm due to the formation of tyrosine (ε_{275} = 1.34 mM^{-1} cm^{-1}) (*54, 126*). The assays contained 200 μM $6MePH_4$ and 10-800 μM L-phenylalanine in 60 μg/ml catalase, 5 mM DTT, 15 μM ferrous ammonium sulfate, 80 mM Hepes/NaOH, pH 7.0, at 25 °C. When racemic phenyl-alanine was used, the concentration range was 20-1600 μM. Control experiments with D-phenylalanine established that concentrations of the nonphysiological stereoisomer up to 1 mM had no effect on the activity of any of the enzymes.

Initial rates of $6MePH_4$ oxidation were determined using a coupled assay with DHPR and NADH, monitoring the decrease in absorbance at 340 nm due to the oxidation of NADH (ε_{340} = 6.22 mM^{-1} cm^{-1}) (*54, 78*). The assay conditions were 10-800 μM L-phenylalanine for Δ117PheH and $TrpH_{102-416}$ and 10-2000 μM L-phenylalanine for Δ117PheH V379D, 0.05-1 μM enzyme, 100-200 μM $6MePH_4$, 60 μg/ml catalase, 200-250 μM NADH, 0.2-0.5 units/ml DHPR, 15 μM ferrous ammonium sulfate, 80 mM Hepes/NaOH, pH 7.0, at 25 °C.

Initial rates of formation of 5-hydroxytryptophan from tryptophan were monitored on a Applied Photophysics SX-18MV stopped-flow fluorometer (*127*). The sample was excited at 315 nm along a 10 mm path and the emission was passed through a 335 nm cutoff filter. The assay conditions were 20-2000 μM L-tryptophan, 200 μM $6MePH_4$, 1.5 μM Δ117PheH, 7 mM DTT, 50 μg/ml catalase, 10 μM ferrous ammonium

sulfate, 80 mM Hepes/NaOH, pH 7.0, at 25 °C. These conditions were obtained by mixing two syringes of equal volumes. Syringe 1 contained 400 μM $6MePH_4$, 12 mM DTT, tryptophan, and 80 mM Hepes/NaOH, pH 7.0. Syringe 2 contained 100 μg/ml catalase, 3 μM Δ117PheH, 20 μM ferrous ammonium sulfate, 2 mM DTT and 80 mM Hepes/NaOH, pH 7.0. The amount of 5-hydroxytryptophan formed was determined by comparison with a standard curve obtained under the same conditions.

To measure directly the stoichiometry of amino hydroxylation relative to $6MePH_4$ oxidation, an HPLC-based assay similar to that described previously (*41, 52*) was performed. The conditions were 1.2 mM D,L-phenylalanine or 500 μM L-phenylalanine, 10 μM enzyme, 40-100 μM $6MePH_4$, 25 mM potassium phosphate, pH 7.0, at 30 °C in 100 μL. The reactions were initiated with $6MePH_4$; after 3 minutes they were quenched with 400 μL of 10 mM sodium borate, pH 9.2. To this were added 100 μL of 10 mM sodium cyanide and 40 μL of 10 mM naphthalene-2,3-dicarboxaldehyde (NDA) to form the 1-cyanobenz[f]-isoindole (CBI) derivatives (*94*). Fifty μL of the reaction were injected onto a Nova-Pak C18 column (2.1 x 150 mm). The CBI derivatives of tyrosine and phenylalanine were separated with a gradient of 30-35% acetonitrile and 70-65% 12.5 mM potassium phosphate, pH 6.8, containing 1% THF, with fluorescence detection using excitation and emission wavelengths of 420 and 490 nm, respectively. The amount of tyrosine was quantified by comparison with a standard curve obtained under the same conditions. Samples for mass spectrometry were made following the same protocol, except that 4 mM $6MePH_4$, 8 mM [4-^{2}H]- or [3,5-$^2H_2$]-phenylalanine, 100 μM enzyme and 100 μM ferrous ammonium sulfate in 300 μL were

used, and the reaction was quenched by the addition of 100 μL of 100 mM sodium borate, pH 9.2. Fifty μL of 100 mM sodium cyanide and 100 μL of 50 mM NDA were added, and precipitated protein was removed by centrifugation. The entire reaction mixture was then injected onto the Nova-Pak C18 column, and the CBI derivatives of tyrosine and phenylalanine were separated with an isocratic mobile phase of 85% water and 15% acetonitrile. The peak corresponding to tyrosine eluted at 18 minutes and was detected with excitation and emission wavelengths of 470 and 590, nm respectively. The CBI-tyrosine was collected and analyzed by negative ion electrospray-time of flight mass spectrometry at the Laboratory of Biological Mass Spectrometry at Texas A&M University. The ratios of the (*m*-1) peaks resulting from loss or retention of deuterium were corrected for ^{13}C contributions and used in calculations of the isotope effects.

Data analysis. The Michaelis-Menten equation was used to determine k_{cat}, k_{cat}/K_m and K_m values when initial rates were measured as a function of the concentration of a single substrate, using the program KaleidaGraph (Synergy Software, Reading PA). Steady-state kinetic isotope effects were determined using Igor Pro (WaveMetrics, Lake Oswego, OR) to fit the data to equation 5. Equation 5 describes data for which there is an isotope effect on the k_{cat} value only. Here, v is the initial rate, k_{cat} is the turnover number, A is the substrate concentration, K_m is the Michaelis constant for the varied substrate, F_i is the mole fraction of deuterium in the substrate, E_v is the isotope effect on $k_{cat.}$ Isotope effects on the ratio of productive hydroxylation to total $6MePH_4$ consumption were calculated by direct comparison of the amount of tyrosine formed with phenylalanine versus deuterated phenylalanine.

$$v = \frac{k_{cat}A}{K_m + A*(1+F_i*(E_V-1))} \qquad (5)$$

RESULTS

Steady state kinetics of Δ117PheH and isotope effects. The catalytic core of rat PheH, Δ117PheH, was chosen instead of the wild-type rat enzyme because the former does not need to be pre-activated with phenylalanine, lysolecithin or limited proteolysis, and it shows Michaelis-Menten kinetics (*54*). In addition, the stoichiometry of tyrosine formed with respect to $6MePH_4$ oxidized is one. The kinetic parameters for this enzyme reported here (Table 5) are not statistically different from values published previously (*54*). To determine if hydroxylation is rate-limiting in Δ117PheH as is the case in TrpH (*38*), isotope effects on tyrosine formation were measured using ring-deuterated phenylalanines; the results are summarized in Table 6. The data fit best to equation 1, in which there is an isotope effect on k_{cat} only. With Δ117PheH there are significant normal kinetic isotope effects with [4-^{2}H]-, [3,5-$^2H_2$]-, and $^2H_5$-phenylalanine, in agreement with the previous results for the wild-type rat enzyme (*123*). In the case of $^2H_5$-phenylalanine, the isotope effect is greater than the isotope effects obtained with [4-^{2}H]- and [3,5-$^2H_2$]-phenylalanine (Table 6).

Table 5: Steady State Kinetic Parameters for Δ117PheH and Δ117PheH-V379D

Parameter	Δ117PheH		Δ117PheH-V379D	
	Tyrosine formation[a]	$6MePH_4$ oxidation[b]	Tyrosine formation[a]	6-$MePH_4$ oxidation[b]
k_{cat} (min^{-1})	513 ± 23	471 ± 50	18 ± 1	67 ± 4
K_{phe} (μM)	120 ± 18	127 ± 53	420 ± 48	625 ± 85
k_{cat}/K_{phe} (μM^{-1} min^{-1})	4.3 ± 0.7		0.043 ± 0.004	
K_{6MePH4}[c] (μM)	83 ± 9		63 ± 9	

[a]Determined from initial rates of tyrosine formation in 80 mM Hepes/NaOH, 5 mM DTT, 15 μM ferrous ammonium sulfate, 60 μg/mL catalase, 200 μM $6MePH_4$, pH 7.0, at 25 °C. [b]Determined from initial rates of $6MePH_4$ oxidation in 80 mM Hepes/NaOH, 15 μM ferrous ammonium sulfate, 60 μg/mL catalase, 200-250 μM NADH, 0.2-0.5 units of DHPR, 200 μM 6-$MePH_4$, pH 7.0, 25 °C. [c]Determined from initial rates of tyrosine formation in 80 mM Hepes/NaOH, 5 mM DTT, 15 μM ferrous ammonium sulfate, 60 μg/mL catalase, 500 μM L-phenylalanine for Δ117PheH or 1000 μM phenylalanine for Δ117PheH V379D, pH 7.0, at 25 °C.

Characterization of mutant enzymes and kinetic isotope effects. In the case of TyrH, the active site mutants E326A and F309A, in which tetrahydropterin oxidation is largely uncoupled from amino acid hydroxylation, show inverse kinetic isotope effects on both steady state kinetics and the uncoupling, in contrast to the wild type enzyme (*40*). The homologous mutations E280A and F263A were prepared in Δ117PheH, yielding enzymes that were 30% and 15% coupled with respect to tetrahydropterin oxidation. Kinetic isotope effects of unity were found on the ratio of amino acid hydroxylation to $6MePH_4$ consumption for all the enzymes. These results suggest that the uncoupling occurred prior to formation of the Fe(IV)O intermediate for these enzymes (vide infra). In the case of E280A the kinetic isotope effects on initial rates of tyrosine formation with [4-^{2}H]-, [3,5-$^2H_2$]-, and $^2H_5$-phenylalanine as substrates were normal and comparable to those with Δ117PheH (results not shown).

Table 6: Kinetic Isotope Effects on the Hydroxylation of Deuterated Phenylalanines[a]

Enzyme	4-^{2}H-phenylalanine	3,5-$^2H_2$-phenylalanine	$^2H_5$-phenylalanine
Δ117PheH	1.19 ± 0.06	1.12 ± 0.04	1.41 ± 0.05
Δ117PheH-V379D	0.92 ± 0.03	1.07 ± 0.05	0.98 ± 0.09
$TrpH_{102-416}$	0.96 ± 0.07	1.04 ± 0.06	1.01 ± 0.04

[a]Conditions as for Table 5.

The V379D mutation was initially identified in a screen for PheH active site mutants with an increased ability to hydroxylate tyrosine (*91*). As is the case with the intact protein (*91*), the mutation of Val379 to aspartate affects several kinetic parameters for the hydroxylation of phenylalanine by Δ117PheH (Table 5). The k_{cat} value is 30-fold lower, the k_{cat}/K_{phe} value is about 100-fold lower and there is a 3-fold increase in the K_{phe} value. The K_{6MePH4} value is not altered significantly by the mutation, suggesting that the mutation of valine 379 has little effect on the binding of the tetrahydropterin. For Δ117PheH-V379D the k_{cat} value for $6MePH_4$ oxidation is about four times that for tyrosine formation, consistent with only 27% of the total $6MePH_4$ being consumed in productive hydroxylation. In contrast to Δ117PheH, Δ117PheH-V379D shows a significantly inverse isotope effect with [4-^{2}H]-phenylalanine as substrate (Table 6). The value matches those obtained with mutant TyrH proteins and with wild-type TrpH (*38, 40*). This suggests that the three aromatic amino acid hydroxylases share the same chemical mechanism for aromatic hydroxylation, but the isotope effect is masked in PheH by other chemical steps. An inverse isotope effect was only obtained when the site of hydroxylation was deuterated, suggesting that a change in hybridization from sp^2 to

sp^3 occurs exclusively at the para position. When [3,5-$^2H_2$]-phenylalanine is used as a substrate for Δ117PheH-V379D, there is a normal deuterium isotope effect; the value is identical within experimental error to that for Δ117PheH.

Isotope effects on the stoichiometry of amino acid hydroxylation and 6MePH$_4$ oxidation. The stoichiometry of 6MePH$_4$ oxidized relative to tyrosine formed was determined by measuring the amount of tyrosine after a limiting amount of 6MePH$_4$ had been consumed. The changes in stoichiometry when [4-^{2}H]-, [3,5$^2H_2$]- and $^2H_5$-phenylalanines are used as substrates for Δ117PheH and Δ117PheH-V379D yield the isotope effects on the stoichiometry (Table 7). There was no isotope effect on the stoichiometry with Δ117PheH, consistent with the ratio of 6MePH$_4$ oxidation to amino acid hydroxylation being one. In contrast inverse isotope effects on the stoichiometry were found for Δ117PheH V379D with both [4-^{2}H]- and $^2H_5$-phenylalanine as substrates. Both isotope effects match the isotope effect on k_{cat} obtained with [4-^{2}H]-phenylalanine.

Table 7: Kinetic Isotope Effects on the Stoichiometry of Tyrosine Formation[a]

Enzyme	4-^{2}H-phenylalanine	3,5-$^2H_2$-phenylalanine	$^2H_5$-phenylalanine
Δ117PheH	1.01 ± 0.03	1.00 ± 0.07	1.01 ± 0.02
Δ117PheH-V379D	0.96 ± 0.03	1.06 ± 0.05	0.93 ± 0.04

[a]Assay conditions: 25 mM potassium phosphate, pH 7.0, 500 μM L-phenylalanine, or 1.2 mM D,L-phenylalanine, 10 μM enzyme, 40-100 μM 6-MePH$_4$ at 30 °C.

Deuterium content of products. The deuterium contents of the tyrosine products arising from [4-^{2}H]- and [3,5$^2H_2$]-phenylalanine were determined by mass spectrometry. When [4-^{2}H]- phenylalanine is used as substrate for Δ117PheH (Table 8) about seventy-

five percent of the deuterium in the substrate is retained in the product, in excellent agreement with previous results for the wild type non-recombinant enzyme (*128, 129*). In the case of [3,5-$^2H_2$]-phenylalanine, about one-eight of the product has lost one of the two deuterium atoms present in the substrate. The mutation of Val379 to aspartate has no effect on the deuterium retention in the products (Table 8), suggesting that steps after oxygen addition to the phenyl ring of phenylalanine are not significantly altered in the mutant protein.

Table 8: Ratio of Deuterium to Hydrogen in Tyrosine upon Hydroxylation of Deuterated Phenylalanine[a]

Enzyme	4-^{2}H-phenylalanine	3,5-$^2H_2$-phenylalanine
Δ117PheH	3.79 ± 0.19	6.81 ± 0.46
Δ117PheH-V379D	3.68 ± 0.12	6.27 ± 0.26

[a]Conditions: 25 mM potassium phosphate pH 7.0, 100 μM ferrous ammonium sulfate, 8 mM D,L-phenylalanine, 100 μM enzyme and 4 mM 6-MePH_4 at 30 °C. Amino acid products were purified by HPLC as the N-substituted cyanobenz[f]isoindole derivatives. Deuterium content was determined by negative mode ESI mass spectrometry.

Tryptophan as a substrate for Δ117PheH. Tryptophan is a good substrate for wild-type PheH (*56, 130*). Δ117PheH has a k_{cat} value of 33 ± 2 min^{-1} and a K_{trp} value of 700 ± 80 μM when 5-hydroxy-tryptophan formation is followed, and values of 47 ± 6 min^{-1} and 1000 ± 290 μM for 6-MePH_4 oxidation. This yields a stoichiometry of 0.70 ± 0.10, suggesting that 6MePH_4 oxidation and tryptophan hydroxylation are mostly coupled. The use of $^2H_5$-indole-tryptophan as a substrate for Δ117PheH yields a $^Dk_{cat}$ value of 0.89 ± 0.04, consistent with a change of hybridization from sp^2 to sp^3 at the transition state for an electrophilic aromatic substitution reaction (*38*). The inverse

isotope effect on the k_{cat} value is consistent with the rate constant for the attack of the hydroxylating intermediate on the indole ring of tryptophan in Δ117PheH being slower than all other first order steps.

Kinetic isotope effects with phenylalanine as a substrate for $TrpH_{102-416}$. L-Phenylalanine is also a substrate for $TrpH_{102-416}$, with k_{cat} values equal for $6MePH_4$ oxidation and tyrosine formation this shows that all the reducing equivalents from $6MePH_4$ oxidation are used for productive turnover (*90*). In the present work k_{cat} values of 127 ± 6 min^{-1} for tyrosine formation and 131 ± 14 min^{-1} for $6MePH_4$ oxidation were found; these are somewhat higher than previously published results (*90*). Ring-deuterated phenylalanines were also used as substrates for $TrpH_{102-416}$; the resulting isotope effects are given in Table 6. $TrpH_{102-416}$ shows considerable substrate inhibition at phenylalanine concentrations higher than 200 μM, greatly limiting the precision of the $^{D}k_{cat}$ value. Despite the lack of precision, the values for $TrpH_{102-416}$ are clearly in better agreement with those for Δ117PheH-V379D.

DISCUSSION

The results presented here provide evidence that all three aromatic amino acid hydroxylases share the same chemical mechanism, but differ in the identity of the rate-limiting step. In the case of TrpH, the inverse deuterium kinetic isotope effect on k_{cat} and the sensitivity of k_{cat} to the amino acid substrate establish that hydroxylation of the indole ring of tryptophan is rate-limiting (*38, 51*). In the case of wild-type TyrH, the lack of an isotope effect on the k_{cat} value with [3,5-$^{2}H_2$]-tyrosine, ^{18}O kinetic isotope

effects, and the insensitivity of k_{cat} to the amino acid substrate suggest that oxygen activation or a product release step limits turnover (*35, 49, 50*). In the case of PheH, a kinetic isotope effect of 1.45 with $^{2}H_{5}$-phenylalanine previously suggested a different rate-limiting step and possibly a different chemical mechanism for PheH (*123*).

In the present study it was possible to unmask the isotope effect on the electroplilic aromatic substitution reaction hydroxylation of PheH using a mutant enzyme, Δ117PheH-V379D. The theory of unmasking kinetic isotope effects by partitioning of intermediates via branched pathways has been described previously (*40, 59, 131*). Scheme 7 illustrates the basic kinetic scheme for the analysis. The enzyme binds all three substrates and proceeds through the first irreversible step to form a high-valence ferryl-oxo intermediate, Fe(IV)O. With some amino acid substrates or mutant proteins there is a branch point after formation of this Fe(IV)O intermediate which leads to unproductive consumption of tetrahydropterin. In such a case the reaction can follow either the productive hydroxylation pathway with net rate constant k_1 or the unproductive pathway with net rate constant k_2. If it is assumed that hydroxylation and unproductive breakdown of the intermediate are irreversible events, a reasonable assumption, rate constant k_1 will be sensitive to deuterium substitution on the amino acid and k_2 will not. The stoichiometry of tyrosine formed relative to $6MePH_4$ consumed is then $k_1/(k_1 + k_2)$. Deuterium substitution on the amino acid can change the net rate constant k_1, thus changing the stoichiometry. If $k_2 >> k_1$ the isotope effect on the stoichiometry will yield the intrinsic isotope effect directly; the isotope effect will also be expressed on the k_{cat} value because the change in the contribution of the unproductive pathway will result in a

change in the rate of formation of the hydroxylated amino acid (*40, 131*).

Scheme 7

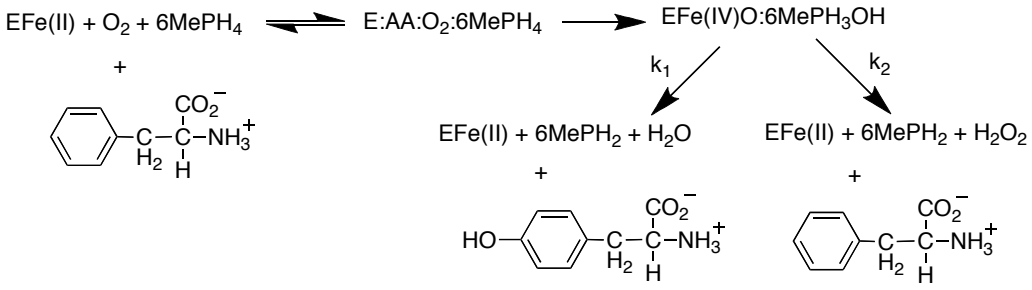

Val379 does not interact directly with the amino acid substrate, but the crystal structures of PheH with an amino acid analog (thienylalanine) and tetrahydropbiopterin (BH_4) bound indicate that valine 379 is in the active site, in close proximity to thienylalanine and the $(His)_2(Glu)$-facal-triad (Figure 10) (*132, 133*). It is reasonable to

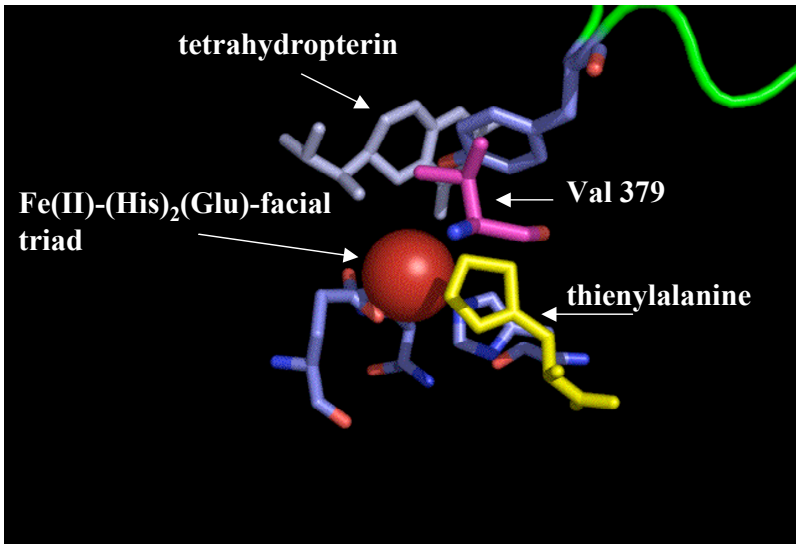

Figure 10: Structure of the active site of PheH. The $(His)_2(Glu)$-facial triad (Fe center red sphere), (BH_4 purple) and substrate analog (thienylalanine yellow) (PDB file 1KW0). The structure shows that Val379 (pink) stacks against thienylalanine and in close proximity to the $(His)_2(Glu)$-facial triad.

propose that mutating this residue could have detrimental effects on the activation of O_2 and the electrophilic aromatic substitution reactions. Accordingly, mutating Val379 toaspartate in Δ117PheH alters the stoichiometry of the reaction, so that more $6MePH_4$ is oxidized relative to tyrosine formed. This is consistent with the introduction of a branched pathway in which the high-valence Fe(IV)O intermediate is breaking down unproductively more frequently than it reacts with the aromatic ring. This mutant enzyme also exhibits an inverse isotope effect, consistent with the predictions of Schemes 3 and 7. An inverse isotope effect is seen only when deuterium is present at the site of hydroxylation, establishing that attack of the hydroxylating intermediate, or the formation of a new C-O bond occurs exclusively at the para position of the amino acid; this rules out the formation of an arene intermediate as was once proposed for PheH (*134*). The inverse isotope effect with Δ117PheH-V379D agrees well with those previously reported for mutant forms of TyrH and TrpH (*38, 40*), establishing that the three aromatic amino acid hydroxylases share similar transition states for aromatic hydroxylation. Thus, the isotope effect for the reaction of the Fe(IV)O intermediate with the phenyl ring of phenylalanine in the wild-type enzyme is masked by another isotope-sensitive step.

The minimal mechanism of Scheme 7 predicts that the isotope effect on k_{cat} will vary between one and the intrinsic inverse isotope effect if the isotope effect is due solely to the initial reaction of the hydroxylating intermediate with the amino acid substrate to form the new carbon-oxygen bond. However, for wild-type enzyme and Δ117PheH, normal isotope effects are seen with ring-deuterated phenylalanines. A

normal isotope effect will occur in a step in which a C-D bond is cleaved; for the mechanism of Scheme 3, there are two such steps, the NIH shift and the subsequent tautomerization to form the aromatic amino acid product. Computational studies done on PheH are consistent with the mechanism of Scheme 3, with the initial cation undergoing a zero-barrier NIH shift to form a dienone intermediate (*44*). This will result in the NIH shift being fast and isotope insensitive. The same computational studies indicate that the subsequent tyrosine formation from the dienone is associated with a large energy barrier, so that this step will be isotope-sensitive; this conclusion is confirmed by the retention of deuterium in the product tyrosine shown in Table 8. The normal $^{D}k_{cat}$ values with Δ117PheH can then be attributed to the isotope-sensitive tautomerization of the amino acid being partially rate limiting for the overall reaction.

The results presented here can be used to estimate the relative values of the rate constants for hydroxylation and the subsequent tautomerization. Scheme 8 shows a minimal mechanism for the reaction of a hydroxylating intermediate with the aromatic ring of phenylalanine to form tyrosine. In Scheme 8, attack of the Fe(IV)O intermediate occurs with net rate constant k_1 to form a cationic intermediate. The subsequent NIH shift is likely to be fast and isotope-insensitive, as noted above. The rate constants k_{21} and k_{22} are for the possible cleavages of the two different CH bonds during tautomerization and are subject to primary kinetic isotope effects. Equations 6 and 7 relate the isotope effects on k_{22} and k_{21} to $^{D}k_{cat}$ for [4-^{2}H]- and [3,5-$^{2}H_2$]-phenylalanine, respectively.

$$ {}^{D}k_{cat} = \frac{\dfrac{{}^{D}k_{22}\left(1+\dfrac{k_{21}}{k_{22}}\right)}{1+{}^{D}k_{22}\left(\dfrac{k_{21}}{k_{22}}\right)} + \dfrac{{}^{D}k_{1}}{k_{1}}(k_{22}+k_{21})}{1+\dfrac{{}^{D}k_{1}}{k_{1}}(k_{22}+k_{21})} \qquad (6) $$

$$ {}^{D}k_{cat} = \frac{\dfrac{{}^{D}k_{21}\left(1+\dfrac{k_{22}}{k_{21}}\right)}{1+{}^{D}k_{21}\left(\dfrac{k_{22}}{k_{21}}\right)} + \dfrac{k_{21}+k_{22}}{k_{1}}}{1+\dfrac{k_{21}+k_{22}}{k_{1}}} \qquad (7) $$

Scheme 8

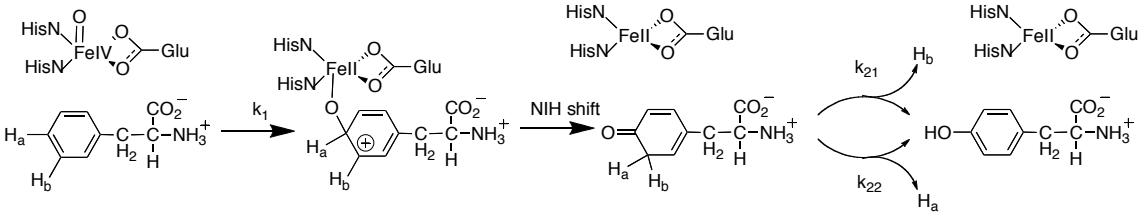

The magnitudes of ${}^{D}k_{21}$, ${}^{D}k_{22}$, and k_{21}/k_{22} can be estimated from the isotopic contents of the tyrosine produced from [4-^{2}H]- and [3,5-$^{2}H_2$]-phenylalanine. The ratios of tyrosine formed by loss of hydrogen versus deuterium are related to the rate constants and the isotope effects by equations 8 and 9. In the case of [4-^{2}H]-phenylalanine, H_a is deuterium, so that loss of deuterium with rate constant k_{22} will exhibit an isotope effect. Accordingly, the ratio R_1 of the product containing one deuterium (P_D) to that containing only hydrogen (P_H) is given by equation 8. Similarly, for [3,5-$^{2}H_2$]-phenylalanine,

where H_b is deuterium, the ratio R_2 of the product with two deuteriums to that with one is given by equation 9. Values of R_1 and R_2 were determined by mass spectrometry and are given in Table 8.

$$P_D/P_H = R_1 = {}^Dk_{22}(k_{21}/k_{22}) \quad (8)$$

$$P_{D2}/P_D = R_2 = {}^Dk_{21}(k_{22}/k_{21}) \quad (9)$$

These two equations contain three unknowns, ${}^Dk_{21}$, ${}^Dk_{22}$, and k_{21}/k_{22} and cannot be solved explicitly with the data given here. However, they can be solved in two limiting cases. If k_{21} equals k_{22}, then ${}^Dk_{22}$ equals R_1 and ${}^Dk_{21}$ equals R_2. In this case, if ${}^Dk_1$, the intrinsic isotope effect on k_1, is taken as 0.92 ± 0.03, the ${}^Dk_{cat}$ value of 1.19 ± 0.06 for [4-^{2}H]-phenylalanine and equation 2 yield a value for k_{21}/k_1 of 2.6 ± 1.1. A similar analysis can be done for [3,5-$^2H_2$]-phenylalanine using equation 7, to obtain a k_{21}/k_1 value of 1.1 ± 0.6. Equations 8 and 9 can also be used to obtain the isotope effects and ratios of rate constants if both k_{21} and k_{22} are affected to the same extent by deuterium substitution, i. e., ${}^Dk_{21}$ equals ${}^Dk_{22}$. Then, the isotope effect on either is given by $\sqrt{R_1R_2}$; the data of Table 4 for Δ117PheH give a value for this isotope effect of 5.1 ± 0.3. In addition, if ${}^Dk_{21}$ equals ${}^Dk_{22}$, then k_{21}/k_{22} equals $\sqrt{R_1/R_2}$, 0.75 ± 0.04. Under these conditions, equation 6 and the ${}^Dk_{cat}$ value for [4-^{2}H]-phenylalanine yield a value for k_{21}/k_1 of 1.6 ± 0.9, while equation 7 and the ${}^Dk_{cat}$ value for [3,5-$^2H_2$]-phenylalanine yield a value for k_{21}/k_1 of 1.4 ± 1.0. The values for the second case are in better agreement,

suggesting that $^{D}k_{21}$ and $^{D}k_{22}$ are equivalent, but there is a slight (~34%) preference for loss of the hydrogen originally present at C4. Both analyses are consistent with the overall rate constant for tautomerization ($k_{21} + k_{22}$) being about 4-fold (3.8 ± 2.2) faster than that for initial reaction of the hydroxylating intermediate with the aromatic ring.

The relative values of the tautomerization and hydroxylation steps can also be calculated from the $^{D}k_{cat}$ value for [$^{2}H_5$]-phenylalanine by using equation 10 and 5.1 and 0.92 as the intrinsic isotope effects for these steps. This yields a value for $(k_{21} + k_{22})/k_1$ of 7.5 ± 1.0. Thus, the $^{D}k_{cat}$ values for all three ring-deuterated phenylalanines are consistent with tautomerization being 6-7 fold faster than hydroxylation.

$$^{D}k_{cat} = \frac{^{D}(k_{21}+k_{22}) + {}^{D}k_1\left(\frac{k_{22}+k_{21}}{k_1}\right)}{1+\frac{k_{21}+k_{22}}{k_1}} \qquad (10)$$

In order to determine if the normal $^{D}k_{cat}$ values with phenylalanine as a substrate for Δ117PheH are solely dependent on the substrate, the enzyme, or both, isotope effects were determined with $TrpH_{102-416}$ using phenylalanine as a substrate and with Δ117PheH using tryptophan as a substrate. With $^{2}H_5$ -tryptophan as a substrate for Δ117PheH, there is an inverse isotope effect on $^{D}k_{cat}$ equal to that seen with TrpH (*38*). The stoichiometry shows that $6MePH_4$ oxidation is well coupled with amino acid hydroxylation; thus, $k_1 > k_2$ in Scheme 7. This suggests that tautomerization of a common intermediate is no longer rate limiting when tryptophan is the substrate for Δ117PheH. The eighteen-fold

lower k_{cat} value when tryptophan is the substrate and the inverse isotope effect on $^{D}k_{cat}$ establish that the reaction of the Fe(IV)O intermediate with the indole ring of tryptophan is rate limiting in Δ117PheH, as is the case for TrpH (*90*). The identity of the rate-limiting step is clearly substrate dependent. If the rate constants for hydroxylating intermediate attack were dependent exclusively on the intrinsic reactivity of the amino acid; one would expect an inverse $^{D}k_{cat}$ value with phenylalanine and not tryptophan, since the latter would be more reactive in an electrophilic aromatic substitution. The simplest explanation is that interactions of the enzyme with bound tryptophan are different from those with phenylalanine.

While the substrate inhibition with phenylalanine as a substrate for $TrpH_{102-416}$ greatly limited the precision with which the isotope effects could be measured, the $^{D}k_{cat}$ values are clearly smaller with deuterated phenylalanine as substrates for $TrpH_{102-416}$ than is the case with Δ117PheH. This suggests that the reaction of the Fe(IV)O intermediate with the amino acid substrate is slower in $TrpH_{102-416}$ than Δ117PheH and may be rate-limiting with phenylalanine in addition to tryptophan.

The results presented here are consistent with the mechanism for aromatic amino acid hydroxylation shown in Scheme 3 for PheH. Tetrahydropterin, O_2 and amino acid bind to the active site of the enzyme, triggering the activation of O_2 to form a high valence Fe(IV)O intermediate. Next, this intermediate attacks the amino acid, forming a cationic intermediate. An NIH shift occurs, resulting in high retention of the deuterium initially present at the site of hydroxylation. Lastly, a partially rate limiting proton loss from a tetrahedral intermediate occurs to regenerate the ferrous form of the enzyme and

the hydroxylated product. The results presented here show that the transition state structure for aromatic hydroxylation for PheH is similar to that of the other two enzymes. This study also provides estimates of the relative values of individual rate constants in the reaction of PheH.

CHAPTER V

INVESTIGATION OF THE CHEMICAL MECHANISM OF PHENYLALANINE HYDROXYLASE BY STOPPED-FLOW ABSORBANCE SPECTROSCOPY, MÖSSBAUER SPECTROSCOPY AND RAPID-QUENCH PRODUCT ANALYSIS

INTRODUCTION

The non-heme enzyme phenylalanine hydroxylase (PheH) belongs to the small family of aromatic amino acid hydroxylases (*17*). PheH catalyzes the aromatic hydroxylation of phenylalanine utilizing tetrahydropterin and molecular oxygen (Scheme 2) (*2, 3, 18*). PheH has been extensively studied over the years primarily because mutations that impair its catalytic activity result in phenylketonuria (PKU), a genetic disease that leads to mental retardation (*24, 135*). The crystal structure of the 300 amino acid catalytic domain of PheH is similar to the structures of the catalytic domains of tyrosine hydroxylase (TyrH) and tryptophan hydroxylase (TrpH) (*31-33*). All three enzymes have similar active sites and contain a Fe(II) center facially coordinated by two histidines and a glutamate ($(His)_2$(Asp/Glu)-facial triad motif) (Figure 1 (B)). This arrangement of ligands on the Fe(II) center is found in a large number of non-heme dependent enzymes and is essential for molecular oxygen activation and substrate oxidation (*6, 10*).

The proposed chemical mechanism for aromatic hydroxylation by PheH is typically divided into two partial reactions (*18*), the irreversible activation of O_2 and the

hydroxylation of the amino acid (Scheme 3). In the first partial reaction O_2 is irreversibly activated by the Fe(II) center utilizing two electrons from a tetrahydropterin to form a high valence Fe(IV)O intermediate and 4a-6MePH$_3$OH, the first product. With TyrH the ^{18}O kinetic isotope for this reaction is independent of the character of the amino acid, suggesting that O_2 activation does not involve the amino acid (*35*). The Fe(IV)O intermediate in the second partial reaction reacts with the side chain of the aromatic amino acid though electrophilic aromatic substitution, forming a new carbon-oxygen bond (*38, 41*). Tyrosine is formed following a hydride shift from carbon three to carbon four and tautomerization (Scheme 8) (*39, 128, 136*).

Evidence from absorbance spectroscopy for transient intermediates for several non-heme enzymes that share the (His)$_2$(Asp/Glu)-facial triad motif has emerged over the years (*137-139*). In several cases the identity, oxidation state and role in catalysis of these intermediates have been examined more explicitly (*45, 140-143*). Direct spectroscopic evidence for the involvement of a Fe(IV)O intermediate in the reactions of the aromatic amino acid hydroxylases was lacking until recently. Rapid freeze-quench ^{57}Fe Mössbauer spectroscopy and rapid-chemical quench experiments for TyrH detected a Fe(IV) species which decays concurrently with formation of dihydroxyphenylalanine (dopa) (*45*). The Mössbauer parameters associated with the Fe(IV) intermediate in TyrH are nearly identical to those previously reported in several members of the alpha-ketoglutarate-dependent family, most notably taurine:α-ketoglutarate dioxygenase (TauD), alpha-ketoglutarate halogenase (CytC3) and prolyl-4-hydroxylase (P4H) (*139, 140, 144, 145*).

In the present study using Δ117PheH, the catalytic core of rat phenylalanine hydroxylase, an analysis of the chemical mechanism of this important enzyme using pre-steady state kinetic methods is presented. The goal here is to detect intermediates under single turnover conditions. In addition, the intrinsic rate constants obtained from these data can be related to the mechanistic picture presented in Schemes 3 and 8 in order to address the nature of the rate-limiting step in the hydroxylation of phenylalanine.

EXPERIMENTAL PROCEDURES

Materials. 6-Methyltetrahydropterin ($6MePH_4$) was from B. Schircks Laboratories (Jona, Switzerland). Ampicillin was from USB Corporation (Cleveland Ohio). Dithiothreitol (DTT) and isopropyl β-thiogalactopyranoside were from Inalc (Milano, Italy). L-Tyrosine, L-phenylalanine, ethylenediamine tetraacetic acid (EDTA), nitrilotriacetic acid (NTA), glycerol, sodium chloride, sodium hydroxide, and monobasic and dibasic sodium phosphate were from Sigma-Aldrich Chemical Co. (Milwaukee, WI). Ferrous ammonium sulfate, ammonium sulfate, ferric chloride, LB broth and Hepes were from Fisher (Pittsburgh, PA). The analytical GEMINI reverse-phase C18 column was purchased from Phenomenex (Torrance California).

Expression and purification of Δ117PheH. Δ117PheH, the catalytic domain of rat phenylalanine hydroxylase, was expressed and purified according to previously published methods (*39, 54, 90, 91*) with several modifications. Typically, a single colony from the bacterial strain BL21DE3 which contains the vector pERPHΔ117 (*54*) was allowed to grow in one hundred milliliters of LB broth containing 100 μg/mL

ampicillin for about 12 hours; 10 mL of the overnight culture was used to inoculate 2 liters of LB broth containing 100 μg/mL ampicillin, 1 mM ferric chloride and 4 mM magnesium sulfate. Supplementing the media with ferric chloride and magnesium sulfate resulted in a thirty to forty percent increase in the weight of the cell pellet (*146*). The cultures were grown until the A_{600} of the cells was between 0.3 and 0.5. The temperature was decreased to 20 °C, and the cells were permitted to grow until the optical density was 1.0-1.3. At this point isopropyl-β-thiogalactoside was added to a final concentration of 500 μM; induction and growth continued for 20 hours. Typically 1-1.3 grams of enzyme were obtained from 24 liters following the protocol outlined above. Unless otherwise stated, all purification steps for PheH were performed at 4 °C and have been described previously (*39, 56, 90*).

Preparation of apo-PheH. Purified PheH was precipitated with 65% ammonium sulfate and resuspended in 100 mL of 150 mM Hepes/NaOH, 200 mM sodium chloride, 20% glycerol, 20 mM NTA, and 20 mM EDTA, pH 7.0 (buffer A). The enzyme pellet was dialyzed against 1 L of buffer A three times over 24 hours. To remove the metal chelators, the enzyme was dialyzed four times over 24 hours against 800 mL of 150 mM Hepes/NaOH, 100 mM sodium chloride, 20% glycerol, pH 7.0 (buffer B). PheH treated this way has about 10 percent residual activity in the absence of ferrous ammonium sulfate in the assay mix.

Rapid reaction kinetics. These experiments were performed using an Applied Photophysics SX-18MV stopped-flow spectrophotometer. Solutions of water and buffers were made anaerobic using 30 cycles of argon and vacuum. The stopped-flow

instrument was initially flushed with anaerobic water several times and then it was incubated for 1 to 2 hours with 50 mM sodium dithionite. The instrument was flushed with anaerobic water followed by anaerobic buffer B immediately prior to use. Apo-PheH was placed in a tonometer with one to two equivalents of amino acid. The enzyme sample was made anaerobic by performing 20 to 30 cycles of vacuum and argon gas at 5 °C. The anaerobic apo-PheH•phenylalanine complex was then mixed with a stoichiometric amount of ferrous ammonium sulfate prepared in 5 mM HCl. $6MePH_4$ was prepared by weight and either one or two equivalents were exposed to vacuum and argon cycles for several minutes. The anaerobic $6MePH_4$ was dissolved in buffer B and placed in the side arm of the tonometer. Additional vacuum and argon cycles were performed prior to mixing with the PheH•Fe(II)•phenylalanine complex. The anaerobic PheH•Fe(II)•phenylalanine•$6MePH_4$ complex was then mounted on the stopped flow instrument. The solution containing the complex was mixed with buffer containing different concentrations of O_2. These different O_2 concentrations were obtained by mixing argon and O_2 with a modified MaxBlend medical oxygen blender (Maxtec) and bubbling the mixture of gasses directly into the buffer. Data were collected at multiple wavelengths and typically three to four different shots were acquired per wavelength.

Rapid freeze-quench Mössbauer spectroscopy. For these experiments, an anaerobic solution containing 2.6 mM PheH•^{57}Fe(II)•6 mM L-phenylalanine•6 mM $6MePH_4$ was prepared in an anaerobic glove box. This solution was loaded into a syringe and moved to the rapid-quench apparatus. An oxygen-saturated solution of 150 mM Hepes/NaOH, 100 mM sodium chloride, 20% glycerol, pH 7.0 was placed in the

second syringe. The two solutions were then mixed together, allowed to react for a predetermined amount of time, and then rapidly quenched by freezing it to -150 °C with cryosolvents. The frozen samples were then transferred to a Mössbauer sample cup. Samples ranging from 0-390 ms were collected and analyzed.

Pre-steady state formation of tyrosine. Rapid chemical-quench reaction measurements were performed at 5 °C with a BioLogic quench-flow QFM-400 instrument calibrated using the reaction of dinitrophenylacetate with hydroxide (*147*). The instrument and the PheH•Fe(II)•phenylalanine•6MePH$_4$ complex were prepared anaerobically as described for the stopped-flow experiments. The reaction was initiated by mixing equal volumes of the PheH•Fe(II)•phenylalanine• 6MePH$_4$ complex with buffer B equilibrated with approximately 1.9 mM O_2 at 5 °C. The reaction was quenched using 5 M HCl after specified aging times. Control samples were also collected in which the ternary complex was reacted with anaerobic buffer B for different times. For the control samples in the absence of O_2, the amount of tyrosine from O_2 contamination did not vary with aging time, but 10-15 % turnover was always present. This amount of tyrosine was subtracted from the reaction samples with O_2. The time of the reaction ranged from 30 milliseconds to 5 seconds; two to four samples were collected for each time point. The precipitated enzyme was removed from the quenched sample by centrifugation. The supernatant (100 μL) was diluted 10-20 fold with 1 M HCl. It was subsequently injected into the C18 Phenomenex HPLC column (250 x 4.60 mm) using a 350 μL sample loop. Tyrosine and phenylalanine were separated with a mobile phase of 15 mM sodium phosphate, pH 7.0, at a flow rate of 1.0 ml/min.

Tyrosine and phenylalanine were detected using a Waters 2475 Multi λ Fluorescence Detector with excitation at 270 nm and emission at 310 nm.

Analysis of data. The single wavelength stopped-flow kinetic traces were analyzed globally using the program Spectfit32 (spectrum Software Associates) with the model in Scheme 9 in which three intermediates accumulate in consecutive irreversible steps. The program KaleidaGraph (Synergy Software) was utilized for linear regression analysis of the chemical quench data and for single or double exponential analysis of single wavelength stopped-flow traces. The program KinTek (Explorer Pro) was used for kinetic simulations.

Scheme 9

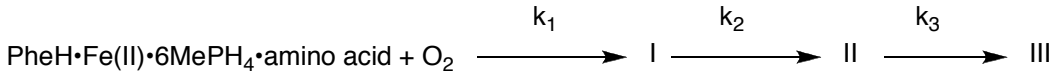

RESULTS

Stopped-flow kinetic analysis of the reaction between PheH•Fe(II)•6MePH4 •phenylalanine and O2. Stopped-flow experiments were performed to establish the kinetics of O_2 addition to PheH and to investigate its chemical mechanism in the transient state. Rather high concentrations (400-1000 μM) of PheH•Fe(II) were normally prepared in a tonometer anaerobically with 1.0-1.5 equivalent of L-phenylalanine and 1.5-2 equivalents of $6MePH_4$. The reaction was initiated by mixing the anaerobic PheH•Fe(II)•$6MePH_4$•phenylalanine complex with buffer equilibrated

with different O_2 concentrations. The reactions were monitored at 248, 318, 335, 400 and 450 nm. Figure 11 (A) shows the absorbance change at 248 nm where the 4a-hydroxypterin (4a-6MePH$_3$OH) product absorbs maximally (*43, 90, 148*). The wavelengths 318 and 335 nm were specifically selected for the potential appearance of a Fe(IV)O intermediate (*139, 149*). However, the single wavelength traces at 318 and 335 nm (Figure 11 (B-C)), exhibit decreases at early time scales; this is consistent with the decrease in extinction coefficient for the enzymatic conversion of 6MePH$_4$ to 4a-6MePH$_3$OH. Kinetic traces at 400 and 450 nm did not reveal any significant transient intermediates (not shown).

The absorbance traces at 248, 318, and 335 nm for each O_2 concentration were fit globally to Scheme 9 using the program Spectfit32 (solid lines Figure 11 (A-C)). Addition of a 4th step resulted in a poor fit and worse residual plots, suggesting that the full kinetic course for the PheH reaction at the selected wavelengths is composed primarily of three phases. The global fit allowed for an estimate of the rate constants and their variation with O_2. In Figure 11 (A-C) pseudo-first-order conditions were not employed since the concentration of O_2 and the quaternary complex are comparable. Despite this limitation, the rate constant (k_1) for the first phase (Scheme 9) showed a linear dependence on the concentration of O_2 (Figure 11 (D)). A second order rate constant of 1.00 ± 0.08 x 10^5 M^{-1} s^{-1} and an off rate constant of 23 ± 5 s^{-1} were obtained from a fit of these data to a linear equation. The linear dependence suggests that the reaction between O_2 and the quaternary complex is strictly second order. The lack of saturation kinetics suggests that a non-covalent complex between the quaternary

complex and O_2 prior to the first chemical step is not formed. Nevertheless, saturation at higher O_2 concentrations cannot be ruled out at this point. The second step k_2 (Scheme 9) for the kinetic traces at 248, 318 and 335 nm (Figure 11 (A-C)) is accommodated by a significant change in absorbance (90% of the total amplitude) at 248 nm likely due to the enzymatic conversion of $6MePH_4$ to the first product 4a-$6MePH_3OH$. However, the value of k_2 decreases hyperbolically with O_2 from a value of about 11 s^{-1} to 2 s^{-1} at 1.0 mM O_2 (Figure 11 (E)). This is readily apparent at 248 and 318 nm (Figure 11 (A-B)) where the absorbance at later time scales decreases (248 nm) and vice versa (318 and 335 nm), but is delayed as the O_2 concentration increases. A plot of the total amplitude change corresponding to the second phase versus O_2 at 248 nm (Figure 11 (E) inset) reveals a poor correlation to a linear equation, but a good fit to a hyperbola, arguing against the second exponential phase being solely due to the formation of 4a-$6MePH_3OH$ (vide infra). The third exponential phase (k_3) is accompanied by a decrease in absorbance at 248 nm with a simultaneous increase at 318 and 335 nm (Figure 11 (A-C)). The value of k_3 is 0.32 ± 0.10 s^{-1} and does not depend on the O_2 concentration. The value for k_3 is less than the turnover number of 1.1 ± 0.2 s^{-1} at 5 °C for PheH. Therefore, it is likely to be a non-enzymatic reaction associated with the 4a-$6MePH_3OH$ product (see discussion).

In order to validate the non pseudo-first-order approximation used to fit the data; the O_2 concentration dependence for the first rate constant k_1 (Figure 11 (D)) obtained from fitting Figures 11 (A-C) to Scheme 9 was estimated by generating kinetic traces with the program KinTek. Similar analysis have been done previously for other

enzymatic systems with excellent results (*150, 151*). The conditions and constraints used here in generating the theoretical traces were as follows: the PheH•Fe(II)•phenylalanine•6MePH$_4$ complex was 0.4 mM and the O_2 concentration

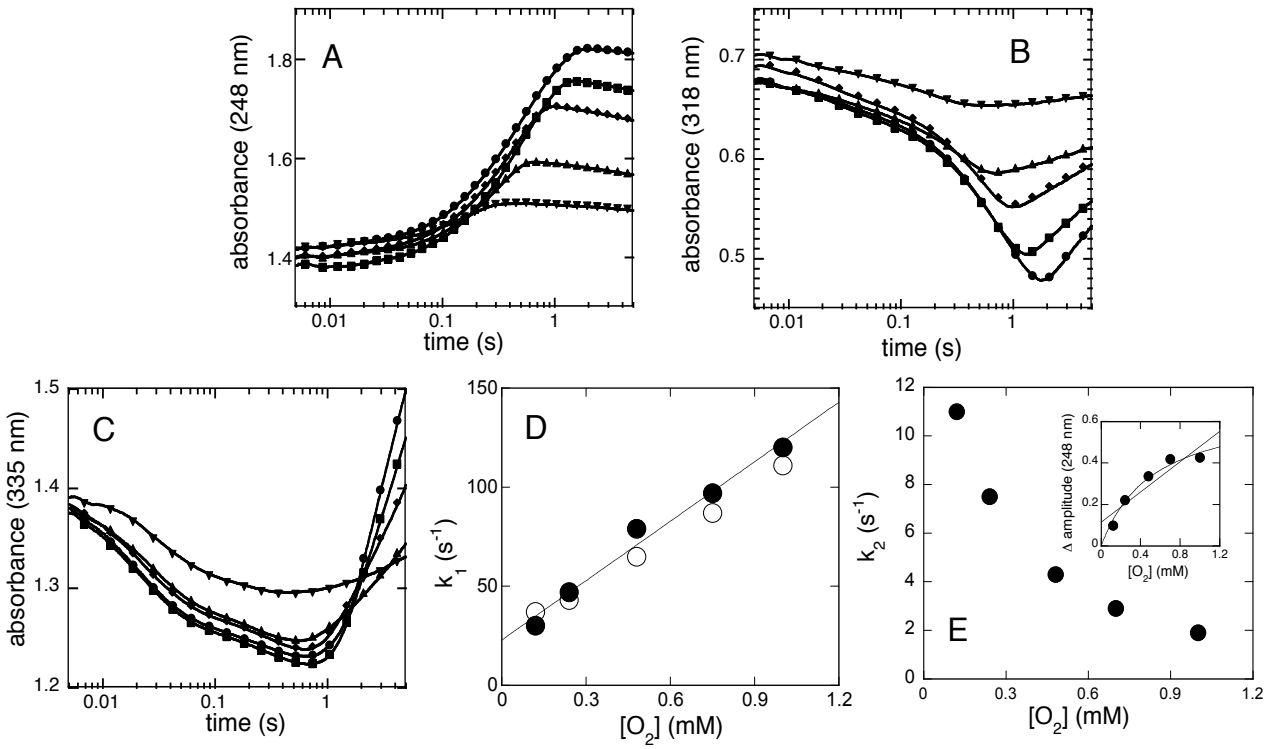

Figure 11: A-C. Stopped-flow single wavelength kinetic traces for the reaction between 0.40 mM PheH•Fe(II)•0.70 mM L-phenylalanine•1.5 mM 6MePH$_4$ and 1.0 mM (●), 0.75 mM (■), 0.48 mM (◆), 0.240 mM (▲) and 0.120 mM (▼) O_2 at 5 °C (final concentrations are listed). The solid lines are global fits to Scheme 9 using Spectfit32. D. plot of the k_1 values obtained from 11 (A-C) versus the concentration of O_2 (●). The line is fit to a linear equation with a slope of 1.0 x10^5 M^{-1} s^{-1} and y intercept of 23 s^{-1}. The open circles are k_1 values obtained by simulating the reaction using Scheme 9 and fitting the resulting traces to three first-order processes (see text for details). E. Oxygen concentration dependence of the second phase (k_2). Inset: The change in amplitude at 248 nm for the second phase versus O_2; the solid lines are fits to a hyperbolic or a linear equation.

varied as shown in Figure 11 (D). For the theoretical traces the values for k_2 ranged from 9 to 2 s^{-1} and $k_3$was 0.30 s^1. The simulated traces were subsequently fit individually using Kintek to three sequential first order processes (Scheme 9) with k_1 as the only variable. The k_1 values obtained (Figure 11 (D), open circles) closely match the

experimental (k_1) values (Figure 11 (D), solid circles). The analysis shows that while the conditions for the reactions in Figure 11 (A-C) do not satisfy pseudo-first order conditions, the k_1 values obtained from the theoretical analysis match very close those obtained from the global fit using Specfit32. This shows that the values of the second order rate constant and the dissociation constant (slope, y-intercept Figure 11 (D)) are unlikely to be affected significantly by violating pseudo-first order conditions.

As noted above the second phase (I → II Scheme 9) contributes to about 90 percent of the total absorbance change at 248 nm; therefore, this step can be assigned to the formation of the 4a-6MePH$_3$OH product from the reactive PheH•Fe(II)•6MePH$_4$• phenylalanine•O_2 complex (vide supra). However, as discussed previously, the magnitude of k_2 decreases inversely with the O_2 concentration (Figure 11 (E)). This inverse dependence can be attributed to several possibilities: multiple turnovers, the oxidation of the Fe(II) center or the oxidation of free 6MePH$_4$ by O_2. In order to determine k_2 more accurately, stopped-flow experiments were performed in which the concentration of the PheH•Fe(II)•6MePH$_4$•phenylalanine complex exceeded that of O_2. Figure 12 shows two such experiments monitored at 248 nm (open symbols) and 318 nm (closed symbols), in which 500 or 300 μM PheH•Fe(II)•6MePH$_4$ •phenylalanine was reacted with buffer containing 90 or 180 μM O_2 (final concentrations). These conditions should allow one turnover, but more importantly the amount of 4a-6MePH$_3$OH formed should equal the concentration of the limiting reactant O_2. The absorbance traces in Figure 12 were modeled using Kintek and Scheme 10. Scheme 10 is a variation of Scheme 9, but the absorbance from intermediates I, II and the product III from Scheme 9

are related to the different pterin species that absorb at 248 and 318 nm (*43, 90, 148*). The model assumes that the first step is reversible formation of a non-covalent complex between the PheH•Fe(II)•6MePH$_4$•phenylalanine complex and O_2 for which the extinction coefficient change is negligible. The second step is the formation of the 4a-6MePH$_3$OH product and the high valence Fe(IV)O intermediate. No spectral signature is associated with the Fe(IV)O intermediate, but the mechanism in Scheme 3 predicts that it forms concurrently with the 4a-6MePH$_3$OH product. The third step is not catalytically competent; ($k_3 < k_{cat}$) therefore, this step must be non-enzymatic, and can be attributed to a rearrangement of the 4a-6MePH$_3$OH product which gives rise to a decrease at 248 nm concurrently with an increase in absorbance at 318 nm respectively (Figures 11 (A-B), 12). The rate constant corresponding to the decay of the Fe(IV)O intermediate and tyrosine formation are not included, but as indicated above the turnover number for PheH is 1.1 ± 0.2 s^{-1} at 5 °C; therefore, k_3 must follow hydroxylation and regeneration of the free enzyme. In addition, the absorbance traces in Figures 11 (A-C) do not reveal spectral changes associated with tyrosine formation (hydroxylation).

In fitting the data in Figure 12 to Scheme 10, the dissociation constant (K_d) of 230 μM for O_2 determined from Figure 1 (D) was held constant. The solid lines in Figure 12 show the simulated data, which superimpose reasonably well on the actual data (symbols). The value of k_2 is 7.4 and 5.4 s^{-1} at 90 and 180 μM O_2 respectively. The

Scheme 10

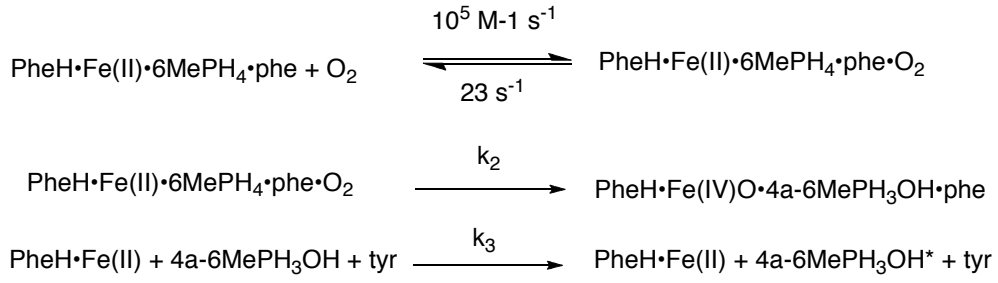

value of k_3 is 0.45 s^{-1} and 0.26 s^{-1} at these concentrations. These two values agree well with the rate constant of 0.32 ± 0.10 s^{-1} determined from the initial multiple exponential fitting using Spectfit (vide supra). The values for k_2 and k_3 from the two independent experiments are slightly different; this is likely due to experimental discrepancy. It is logical to propose that the actual values are the averages (k_2 = 6.4 s^{-1} and k_3 = 0.32 s^{-1}).

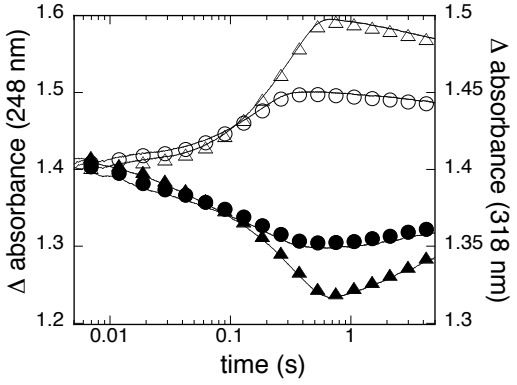

Figure 12: Stopped-flow single turnover experiments monitored at 248 (open symbols) and 318 nm (closed symbols). For the first experiment, 500 μM PheH•Fe(II)•1000 μM $6MePH_4$•800 μM phenylalanine was mixed with an equal volume of buffer containing 90 μM O_2 (circles). For the second experiment 300 μM PheH•Fe(II)•600 μM $6MePH_4$•600 μM phenylalanine was mixed with an equal volume of buffer containing 180 μM O_2 (triangles) at 5 °C (all concentrations listed are final). The absorbance traces (symbols) were fit to the mechanism in Scheme 10 with a K_d value for O_2 set constant at 230 μM (Figure 11(D)). The lines are the fits generated by the model.

The simulations enable the calculation of changes in molar extinction coefficients corresponding to the second phase at 90 and 180 μM O_2: $\Delta\varepsilon_{248}$ = 5.5 and 6.1 mM^{-1} cm^{-1}, $\Delta\varepsilon_{318}$ = -0.42 and -0.47 mM^{-1} cm^{-1}. It is important to note that as long as O_2 is the limiting reactant, the kinetic traces can be modeled by Scheme 10, and by that account Scheme 10 is a reasonable model of the single turnover reaction catalyzed by PheH. Furthermore, the ability to simulate the stopped-flow kinetic traces at two different wavelengths strongly suggests that the changes in absorbance at 248 and 318 nm are due solely to the formation of 4a-6MePH$_3$OH. The changes in the molar extinction coefficients at 248 and 318 nm at pH 7.0 in solution for the conversion of 6MePH$_4$ to 4a-6MePH$_3$OH have been determined previously to be 10-13 mM^{-1} cm^{-1} at 248 nm and -2 mM^{-1} cm^{-1} at 318 nm (*38, 148*). The molar extinction coefficients determined in these experiments at 248 and 318 nm are about one half and one fourth of the published values. It is reasonable to propose that the spectrum of 4a-OH6MePH$_3$ has a much higher absorbance in solution and the protein environment attenuates its absorbance to some extent.

Rapid freeze-quench Mössbauer spectroscopy. The rapid freeze-quench Mössbauer spectroscopy experiment in which 1.3 mM PheH•^{57}Fe(II)•3 mM L-phenylalanine•3 mM 6MePH$_4$ reacted with 1 mM O_2 (final concentrations). The spectrum at 0 ms (Figure 13) contains two obvious features, both of which are consistent with an S=2 Fe(II) species. Only one of these features (~30%) appears to be reactive; yielding accumulation to about 8% at 0.02 seconds of a signal corresponding to the Fe(IV) oxidation state. By 0.1 seconds half of the Fe(IV) signal is left and by 0.390

seconds it has decayed completely (Figure 13). A major reason for low Fe(IV) yields observed in the time-course is the low yield of the reactive complex. From these experiments it is difficult to assign a specific character to the unreactive form of the enzyme; however, it seems to be the final state after turnover (Figure 13: 0.390 seconds). The quadrupole doublet and the isomer shift (δ) could not be determined accurately, but appeared to be similar to those determined for TyrH (*45*). The same experiment carried out with 0.5 mM of the PheH•Fe(II)•6MePH$_4$•phenylalanine complex revealed no change in the quadruplet doublet of the resting enzyme (not shown).

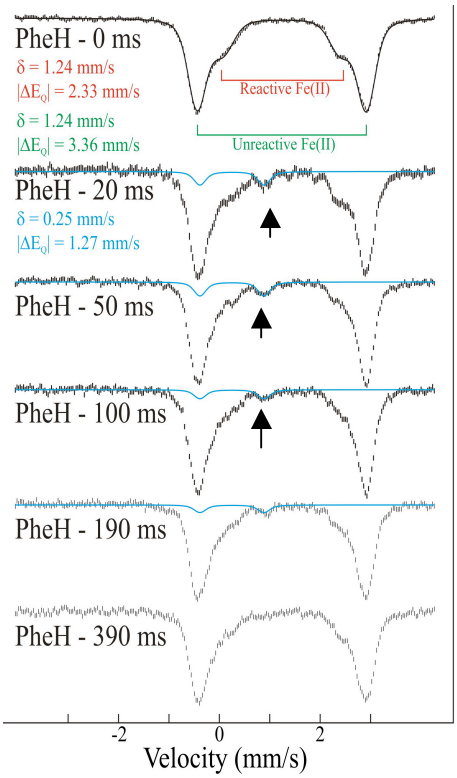

Figure 13: Mössbauer spectra for the reaction between the anaerobic 1.3 mM PheH•^{57}Fe(II)•3 mM 6MPH$_4$•3 mM L-phenylalanine complex with 1 mM oxygen (final concentrations listed). The time course shows the development and decay of a signal corresponding to the Fe(IV) oxidation state with the Mössbauer parameters listed. The time point at 0 ms clearly shows the Fe(II) oxidation sate corresponding to the reactive and unreactive complexes. The arrow denotes the position of the signal from the proposed Fe(IV) intermediate.

The formation of tyrosine was monitored by rapid-chemical quench experiments under conditions where the phenylalanine and $6MePH_4$ were in excess and the final concentration of PheH was 1 or 0.5 mM respectively. The initial rate of tyrosine formation was only 0.28 ± 0.03 sec^{-1} and 0.59 ± 0.07 sec^{-1} respectively. These values are 30 and 60 percent of the expected value of 1.3 ± 0.1 sec^{-1} (vide infra). This shows that the failure to detect higher accumulation of the intermediate is due to PheH becoming inactive at higher concentrations.

Pre-steady state and multiple turnover kinetics for the formation of tyrosine by rapid-mixing chemical quench. In order to determine if steps subsequent to hydroxylation are rate limiting, rapid quench experiments were performed. An anaerobic solution containing 150 μM PheH•Fe(II)•3 mM phenylalanine•3 mM $6MePH_4$ complex was mixed with an equal volume of buffer equilibrated with approximately 1.0 mM O_2 (final concentrations). Reactions were rapidly quenched between 0.03 and 5 seconds with 5 M HCl. Figure 14 shows a time course obtained from a typical chemical quench experiment. The data were well fit by a straight line yielding a rate constant of 1.3 ± 0.1 sec^{-1} with a y-intercept of 0.066 ± 0.005. Fitting the data in Figure 14 (not shown) with the y-intercept as zero does not alter the slope of 1.3, suggesting that the value of 0.066 is more or less zero. The pre-steady state rate of 1.3 sec^{-1} agrees well with the turnover number of 1.1 ± 0.2 sec^{-1} at 5 °C. The lack of a burst rules out the release of either of the two products (4a-$6MePH_3OH$ or tyrosine) or a slow conformational change following hydroxylation as rate limiting for turnover.

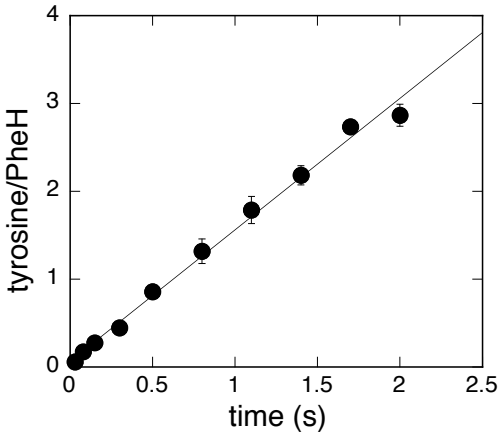

Figure 14: Pre-steady state and multiple turnovers for the formation of tyrosine by rapid-mix chemical quench for a reaction in which 150 μM PheH•Fe(II)•1.5 mM phenylalanine•1.5 mM $6MePH_4$ and approximately 1 mM O_2 reacted at 5 °C (concentrations listed are final).

DISCUSSION

In the present study the reaction mechanism of PheH was investigated using a transient kinetic approach with the goal of detecting intermediates. The proposed chemical mechanism for the hydroxylation of phenylalanine by PheH (Scheme 3) and the identification of the rate limiting step has come about from experiments involving the three aromatic amino acid hydroxylases (*18*). These experiments entailed steady-state kinetics, steady-state kinetics, isotope effects and the use of alternate substrates (*38-41*). Experimental evidence for a hydroxylating intermediate other than a tetrahydropterin-based species comes from studies with the mutant S395A in TyrH and the use of 4-methyl-phenylalanine as a substrate for the wild type enzymes (*42, 43, 52*). S395A-TyrH catalyzes the formation of 4a-$6MePH_3OH$ in the same manner as wild type TyrH, but does not form dihydroxyphenylalanine suggesting that a species, most likely a

Fe(IV)O intermediate, forms following heterolysis of the O-O bond and is responsible for electrophilic aromatic substitution (Schemes 3 and 8) (*43*). The use of 4-methyl-phenylalanine as a substrate for TyrH, PheH and the catalytic cores of PheH and TrpH allowed the determination of the intrinsic kinetic isotope effects for benzylic hydroxylation (Table 3). The intrinsic kinetic isotope effects are consistent with a mechanism involving hydrogen atom abstraction by a high valence iron-based intermediate (Scheme 5) (*42, 52*). These experiments strongly support the involvement of an Fe(IV)O species and not a tetrahydropterin derived intermediate as the hydroxylating species. In spite of this, direct spectroscopic evidence for the involvement of an Fe(IV)O intermediate for the aromatic amino acid hydroxylases was lacking until recently. Rapid freeze-quench ^{57}Fe Mössbauer spectroscopy and rapid-chemical quench experiments for TyrH detected an Fe(IV) signal, whose decay correlated well with the formation of dopa (*45*). A similar intermediate has been detected by Mössbauer and stopped-flow absorbance spectroscopy in several members of the α-KG-dependent family, most notably taurine:α-ketoglutarate dioxygenase (TauD), alpha-ketoglutarate-dependent halogenase (CytC3) and prolyl-4-hydroxylase (P4H) (*139, 140, 145*).

In the present study a kinetic analysis of the reaction between the reactive PheH•Fe(II)•6MePH$_4$•phenylalanine complex and O_2 in the transient state was carried out. The linear dependence on the first step from Scheme 9 on the concentration of O_2 suggests that this step corresponds to O_2 binding to the PheH•Fe(II)•6MePH$_4$• phenylalanine complex. Furthermore, the linear dependence and lack of a lag in the stopped-flow kinetic traces displayed in Figure 11 (A-C) suggests that phenylalanine and

$6MePH_4$ do not have to dissociate for O_2 to react. At this point, there is no consensus agreement on the steady-state kinetic mechanism of PheH (*152, 153*). X-Ray absorption spectroscopy experiments on PheH support a model in which the coordination number changes from 6 to 5 only when L-phenylalanine and a tetrahydropterin are bound, suggesting that once the PheH•Fe(II)•tetrahydropterin•phenylalanine complex is formed a coordination site becomes available for the binding of O_2 (*113*). The stopped-flow absorbance experiments reported here suggest that O_2 is the last substrate to bind to PheH.

The magnitude of the second order rate constant reported here for O_2 addition is nearly identical to that of (4-hydroxyphenyl)-pyruvate dioxygenase (HPPD), extradiol dioxygenase homoproto-catechuate 2,3-dioxygenase and the novel diiron enzyme *myo*-inositol oxygenase (*138, 139, 154, 155*). Once bound, the fate of O_2 in the corresponding reactive complex in the reactions catalyzed by HPPD, homoprotocatechuate 2,3-dioxygenase, and PheH diverge significantly. It is reasonable to propose that when substrate and/or co-substrate are bound the initial collisional binding reaction of the first iron-oxygen species is probably not very different among HPPD, homoprotocatechuate 2,3-dioxygenase and PheH. For homoprotocatechuate 2,3-dioxygenase the dissociation constant for O_2 of the reactive Fe(II) center is about 340 μM compared to 230 μM for PheH. However, for the former the reported dissociation constant is for an active site mutant with a substrate analog (*138*). For homoprotocatechuate 2,3-dioxygenase, O_2 is proposed to bind end-on to the ferrous center followed by electron transfer from the catechol substrate to form ferric superoxide $Fe(III)O_2^{\bullet-}$ (Scheme 1) (*138, 156*). The

transient ferric superoxide, can be detected at 450 nm and is proposed to subsequently initiate substrate oxidation (*138*). Accordingly, a plot of the first relaxation time versus O_2 for the homoprotocatechuate 2,3-dioxygenase active site mutant with 3,4-dihydroxyphenylacetate, the natural substrate, is linear with a y-intercept that crosses the origin, consistent with the irreversible formation of the ferric superoxide. For PheH, O_2 most likely binds end-on to the ferrous center, but in this case an inner sphere electron transfer will most likely occur from $6MePH_4$. A species with the formal oxidation state of $Fe(III)O_2^{\bullet-}$ with electron transfer from the Fe(II) center is unlikely to form transiently. We expect that formation of $Fe(III)O_2^{\bullet-}$ should result in a change in absorbance over the visible region (>450 nm) as seen in homoprotocatechuate 2,3-dioxygenase and such an intermediate is expected to be irreversibly formed, in contrast to what is observed with PheH.

As demonstrated above Scheme 10 accounts well for the single turnover reaction catalyzed by PheH. In the model O_2 can bind reversibly to the PheH•Fe(II)•$6MePH_4$• phenylalanine complex. It is reasonable to assume that O_2 binds directly to the Fe(II) center in the vacant coordination site (vide supra). This assumption is reasonable for the following reasons: the inability to observe saturation kinetics on the plot of k_1 versus O_2 suggests that O_2 reacts directly with the Fe(II) center in a second order reaction that is limited by the diffusion of O_2 into the active site. Divergence of second order behavior in the form of saturation kinetics would imply the accumulation of a non-covalent complex between the PheH•Fe(II)•$6MePH_4$•phenylalanine complex and O_2 prior to a slower first order process likely to be the reaction between O_2 and the Fe(II) center. The

significant value for the y-intercept on the plots in Figure 11 (D) and the reproducibility of the k_1 values by modeling kinetic traces to three first order processes (Scheme 9) suggests that O_2 can readily dissociate from the PheH•Fe(II)•6MePH$_4$•phenylalanine•O_2 complex. This implies that electron transfer to O_2 or a subsequent irreversible step is slower than the dissociation rate of O_2. This is consistent with the limiting value of 6 s^{-1} for the activation of O_2 determined from the single turnover experiments (Figure 12).

The rate constant k_2 in Scheme 10 is written as a microscopic rate constant, but it is reasonable to assume that it is a series of irreversible steps in which O_2 is reduced by 2 electrons provided by 6MePH$_4$. This leads directly to the formation of 4a-6MePH$_3$OH and the Fe(IV)O intermediate. Therefore, it is safe to propose that k_2 is an irreversible rate constant and should be independent of the concentration of O_2. The magnitude of k_2 was determined readily when single turnover conditions were forced by limiting the concentration of O_2 relative to that of the quaternary complex (Figure 12). In contrast fitting kinetic traces for each O_2 concentration independently to Scheme 9 reveals an inverse dependence of k_2 on the O_2 concentration. The inverse dependence is unlikely due to multiple turnovers, as the concentration of L-phenylalanine is nearly stoichiometric with that of PheH•Fe(II). At this point the simplest explanation for the variation of k_2 with O_2 is the non-enzymatic oxidation of free 6MePH$_4$ and/or the oxidation of the ferrous center in PheH to the ferric state. Even though the latter two reactions are known to be slower than 2 s^{-1} at 1 mM O_2 (*157, 158*), they depend on O_2 and probably affect the spectral changes at 248, 318 and 315 nm. A kinetic mechanism,

which included conformational changes, additional steps, and two forms of the enzyme, also failed to fit the data properly.

In the model (Scheme 10) the rate constant k_3 is attributed to the non-enzymatic conversion of 4a-6MePH$_3$OH to 4a-6MePH$_3$OH*. This rate constant as noted above is not catalytically competent and on the stopped-flow traces is readily noticeable at later times when the absorbance at 248 nm decreases with simultaneous increases at 318 and 335 nm. The oxidation state or the character of the species denoted as 4a-6MePH$_3$OH* cannot be inferred utilizing stopped-flow absorbance spectroscopy only. We can only hypothesize that 4a-6MePH$_3$OH* is the ionized form (4a-6MePH$_3$O$^-$). A proton transfer to the 4a-position is likely to be essential for its dehydration to the quinonoid 6-methyldihydropterin (q-6MePH$_2$) and H_2O. The rate constant k_3 is unlikely to be dehydration of 4a-6MePH$_3$OH to q-6MePH$_2$ and H_2O even though this reaction is also associated with decreases and increases in absorbance at 248 and 318 nm, respectively. This is because the rate constant for dehydration at 15 and 25 °C, varies slightly and has been determined to be 0.0125 s^{-1} at pH 7.0 (*90, 159*). This value is about 24-fold slower than the value for k_3 determined in this work.

The decay of the Fe(IV)O intermediate (hydroxylation) is not included in Scheme 10. The formation of tyrosine can readily be monitored at 275 nm for steady-state kinetic assays, since reducing conditions are utilized and 6MePH$_4$ is rapidly regenerated (*54, 126*). For the experiments described here the changes in extinction coefficient for the different pterin species prevent the use of 275 nm as a probe to monitor tyrosine formation. Regardless, the turnover number for PheH at 5 °C is 1.1 ±

0.2 sec^{-1} (*39*); and tyrosine must form with a rate constant of at least that magnitude. Therefore, these experiments do not report on the hydroxylation of the amino acid. The data suggest that hydroxylation of the amino acid and regeneration of the free enzyme precede formation of 4a-6MePH_3OH* (k_3).

Schemes 3 and 10 make several predictions regarding the chemical mechanism of PheH and the fate of the proposed Fe(IV)O intermediate. Heterolysis of the O-O bond results in simultaneous formation of 4a-6MePH_3O^- and Fe(IV)O. The formation of the former species is 5-7 fold faster than the turnover number and should also account for formation of the Fe(IV)O intermediate. The lack of a burst in tyrosine formation for the first turnover (Figure 14) strongly supports hydroxylation as the overall rate-determining step. More importantly, the value of 1.3 ± 0.1 s^{-1} for formation of tyrosine under pre-steady conditions must be the rate constant for decay of the Fe(IV)O intermediate. Steady state kinetic isotope effects for hydroxylation of deuterated phenylalanines by PheH are consistent with the overall rate-determining step being a combination of formation of a new C-O bond and cleavage of a C-H bond, with the former step being 5-7 times slower than the latter (Chapter IV) (*39*). The single turnover stopped-flow experiments and rapid chemical quench experiments reported here suggest that the Fe(IV)O intermediate should form with a first order rate constant of about 5-7 sec^{-1} and decay with a first order rate constant of about 1.3 s^{-1}, consistent with its detection by freeze-quench ^{57}Fe Mössbauer spectroscopy.

The Fe(IV)O intermediate in TauD has a molar extinction coefficient at 318 nm of about 1550 M^{-1} cm^{-1} (*139*) and one that is even higher at 365 nm (*150*). A molar

extinction coefficient change of that magnitude should result in significant perturbations in the stopped-flow kinetic traces at 318 and 335 nm for PheH. Simulations of the kinetic traces in Figure 12 to Scheme 10 suggest that the spectral changes corresponding to k_2 are attributed solely to the conversion of $6MePH_4$ to 4a-$6MePH_3OH$. The change in extinction coefficient at 318 is about -400 M^{-1} cm^{-1} as $6MePH_4$ is oxidized to 4a-$6MePH_3OH$ by PheH; a change much lower than the expected -2000 M^{-1} cm^{-1}. This suggests that if the Fe(IV)O intermediate in PheH has an spectral signature at 318 nm, then its extinction coefficient change at 318 nm must be lower than the value of 1550 M^{-1} cm^{-1} for TauD. In TauD α-ketoglutarate chelates the Fe(II) center directly and taurine binding perturbs the spectrum of the enzyme (*160*). Therefore, it is probable that bound substrates or the active site environment in TauD contributes to the absorbance spectrum of the Fe(IV)O intermediate over the UV and the visible regions. In PheH, phenylalanine does not chelate the iron center nor is the absorbance spectrum of the enzyme perturbed upon binding. This may be a reason for the lack of a spectral signature corresponding to a Fe(IV)O intermediate in PheH versus TauD. A low change in extinction coefficient coupled with the spectral changes as 6-$MePH_4$ is converted to 4a-$6MePH_3OH$ will make detection of the Fe(IV)O intermediate in PheH nearly impossible.

In conclusion the transient kinetic analysis reported here provide further insight into the chemical mechanism and the identity of the rate limiting step for PheH. The reaction is initiated by the reversible binding of O_2 to the five coordinate Fe(II) center. The subsequent step(s) is the irreversible activation of O_2, which occurs with a limiting

value of about 5-7 s^{-1}. The hydroxylation of phenylalanine to form tyrosine occurs with a rate constant of about 1.3 s^{-1} that matches k_{cat}. This establishes directly that hydroxylation of the amino acid is fully rate limiting. The step of about 0.30 s^{-1} is not catalytically competent and most likely involves a unimolecular rearrangement of the 4a-6MePH$_3$OH or protonation of the 4a-hydroxyl prior to its dehydration to q6MePH$_2$ and H_2O.

CHAPTER VI

DISSECTION OF THE CHEMICAL MECHANISM OF TRYPTOPHAN HYDROXYLASE BY STOPPED-FLOW ABSORBANCE SPECTROSCOPY AND RAPID-QUENCH PRODUCT ANALYSIS: DETERMINATION OF INTRINSIC RATE CONSTANTS FOR THE ADDITION OF O_2 AND EVIDENCE FOR A NOVEL TRANSIENT INTERMEDIATE

INTRODUCTION

Tryptophan hydroxylase (TrpH) physiologically catalyzes the formation of 5-HO-trp from tryptophan. This is the first and rate-limiting step in the biosynthesis of melatonin and serotonin (*161, 162*). TrpH belongs to the family of non-heme tetrahydropterin dependent aromatic amino acid hydroxylases that also includes phenylalanine hydroxylase (PheH) and tyrosine hydroxylase (TyrH) (*19*). These three enzymes catalyze aromatic hydroxylation of their corresponding substrates utilizing a tetrahydropterin and molecular oxygen (O_2) (Scheme 2) (*2, 3, 18*). The eukaryotic forms of each enzyme are homotetramers, and alignment of sequences from different organisms reveal that each monomer is composed of an N-terminal regulatory domain and a C-terminal catalytic domain (*30*). The latter domains of about 300 amino acids are similar for the three enzymes, and contain the active site where each enzyme has a Fe(II) center facially coordinated by two histidines and a glutamate ($(His)_2$(Glu)-facial triad motif) (Figure 1 (A-B)). Non-heme iron dependent enzymes use this $(His)_2$(Asp/Glu)-facial triad motif to irreversibly activate (O_2) for substrate oxidation (*6, 10, 163*).

Scheme 3 shows the proposed chemical mechanism for the hydroxylation of tryptophan by TrpH (*18*). The initial steps in this mechanism require the irreversible activation of O_2 by the $(His)_2(Glu)$-facial-Fe(II) center utilizing two electrons from a tetrahydropterin to form a high valence Fe(IV)O intermediate and 4a-hydroxypterin (4a-6MePH$_3$OH), the first product (*18*). The $^{18}(k_{cat}/K_m)$ value for O_2 for TyrH is independent of the identity of the amino acid substrate and the amount of productive turnover (*35*). This shows that the reaction up to the first irreversible step in the activation of O_2 does not include amino acid hydroxylation. The Fe(IV)O intermediate subsequently reacts with the side chain of the aromatic amino acid through electrophilic aromatic substitution, forming a new carbon oxygen bond. 5-Hydroxytryptophan is formed following a hydride shift from carbon 5 to 4 and the loss of a proton. In a quantitative structure-activity study, when a series of para-substituted amino acids were used as substrates for TyrH the relative amounts of hydroxylated products (productive turnover) versus the σ parameter of the substituent yielded a negative ρ value (*41*). This strongly suggests that the transition state during formation of the new carbon-oxygen bond is cationic. In addition, the kinetic isotope effect on the ($^{D}k_{cat}$) value when L-indole-$^{2}H_5$-tryptophan or L-5-^{2}H-tryptophan is a substrate for TrpH is inverse (*38*). This is also consistent with formation of a carbocation as the hybridization of carbon 5 of tryptophan changes from sp^2 to sp^3 during formation of a new carbon-oxygen bond.

The experiments outlined above are consistent with the mechanism in Scheme 3, but do not provide insight into the nature of the hydroxylating intermediate. The involvement of the Fe(IV)O intermediate (Scheme 3) in the reactions of the aromatic

amino acid hydroxylases was confirmed by rapid freeze-quench ^{57}Fe Mössbauer spectroscopy and rapid-chemical quench experiments for TyrH (*45*), and PheH (Chapter V). These experiments detected the development and disappearance of a Fe(IV) signal which for TyrH, decays concurrently with formation of dihydroxyphenylalanine (*45*). The quadrupole doublet and the isomer shift (δ) determined for the Fe(IV) intermediate in TyrH and PheH are similar to those previously characterized for several members of the alpha-ketoglutarate-dependent family of non-heme enzymes (*139, 140, 145*).

$TrpH_{102-416}$ is a form of TrpH having just the amino acids of the catalytic domain, and has been demonstrated previously to be suitable for mechanistic studies (*38, 39, 90*). In the present study a detailed analysis of the chemical mechanism of this important enzyme using pre-steady state kinetic methods is presented.

EXPERIMENTAL PROCEDURES

Materials. 6-Methyltetrahydropterin ($6MePH_4$) was from B. Schircks Laboratories (Jona, Switzerland). Ampicillin was from USB Corporation (Cleveland Ohio). Dithiothreitol (DTT) and isopropyl β-thiogalactopyranoside were from Inalc (Milano, Italy). L-Phenylalanine, L-tryptophan, D,L-5-hydroxytryptophan (5-HO-trp), ethylenediamine tetraacetic acid (EDTA), nitrilotriacetic acid (NTA), glycerol, sodium chloride, sodium hydroxide, and monobasic and dibasic sodium phosphate were from Sigma-Aldrich Chemical Co. (Milwaukee, WI). Ferrous ammonium sulfate, ammonium sulfate, ferric chloride, LB broth and Hepes were from Fisher (Pittsburgh, PA). The

analytical GEMINI reverse-phase C18 column was purchased from Phenomenex (Torrance California).

Expression and purification of TrpH. TrpH, the catalytic core of rabbit tryptophan hydroxylase lacking 101 and 28 residues from the amino and carboxyl termini respectively, was purified according to previously published methods (*38, 39, 90*), with several modifications in order to maximize the final yield of the enzyme. The plasmid pEWOHΔ101ΔH encoding $TrpH_{102-416}$ (*90*) was transformed into a bacterial cell strain that allows for a higher growth density (C41DE3). The cells were incubated overnight in a plate containing 100 μg/mL ampicillin at 37 °C. A single colony from the plate was allowed to grow in one hundred milliliters of LB broth containing (100 μg/mL ampicillin) for about 12 hours (overnight) at 37 °C; 15 mL of the overnight culture was used to inoculate 2 liters of LB broth containing 100 μg/mL ampicillin, 1 mM ferric chloride and 4 mM magnesium sulfate. Supplementing the media with ferric chloride and magnesium sulfate resulted in a thirty to forty percent increase in the weight of the cell pellet (*146*). The cultures were grown until the A_{600} was between 0.3 and 0.5. At this point the temperature was decreased to 20 °C, and the cells were permitted to grow until the A_{600} reached a value of 1.0-1.3. At this point isopropyl-β-thiogalactoside was added to a final concentration of 500 μM. Induction and growth continued for 20-24 hours. All subsequent purification steps for TrpH were performed at 4 °C and have been detailed described previously (*39, 56, 90*). Typically between 1.2 and 1.5 grams of pure enzyme were obtained from 24 L following the protocol outlined above.

Preparation of apo TrpH. The purified enzyme obtained from 24 L of LB broth was precipitated with 60% ammonium sulfate. The enzyme pellet was resuspended in 50 to 80 mL of 150 mM Hepes/NaOH, 200 mM ammonium sulfate, 20% glycerol, 20 mM NTA, and 20 mM EDTA, pH 7.0 (buffer A). TrpH was dialyzed with three 1 L changes over 24 h against buffer A. The enzyme was subsequently dialyzed against 800 mL of 150 mM Hepes/NaOH, 100 mM ammonium sulfate, 20% glycerol, pH 7.0 (buffer B) four times in a 28 hour period. TrpH treated this way had no detectable activity in the absence of ferrous ammonium sulfate in assays.

Stopped-flow absorption spectroscopy. Kinetic measurements were performed using an Applied Photophysics SX-18MV stopped-flow spectrophotometer. Solutions of water and buffers were made anaerobic by alternating between argon and vacuum for 30 to 50 cycles over 1 h. The stopped-flow instrument was initially flushed with anaerobic water several times and then incubated for 1 to 2 h with 50 mM sodium dithionite. At this point apo-TrpH was placed in a tonometer without or with 1.3 to 1.8 equivalent of amino acid. The TrpH or the TrpH•amino acid sample was made anaerobic by alternating 20 to 30 vacuum and argon gas cycles at 5 °C for at least 30 min. The anaerobic apo-TrpH or apo-TrpH•amino acid sample was then mixed with a stoichiometric amount of ferrous ammonium sulfate prepared in 5 mM HCl. Additional vacuum and argon gas cycles were performed at this stage. The $6MePH_4$ was prepared by weight and it was placed in a 2 mL Eppendorf tube. The tube was sealed tightly with a rubber septum and was exposed to vacuum and argon cycles for at least 10 min. The anaerobic $6MePH_4$ was dissolved in 1 mL of buffer B (final concentration 50-80 mM),

and a volume corresponding to 1.5 to 2 equivalents was withdrawn with a 1 mL airtight syringe and placed in the side arm of the tonometer. The tonometer was exposed to additional vacuum and argon cycles for 10 min prior to mixing the $6MePH_4$ with the TrpH•Fe(II)•amino acid complex. At this point the sodium dithionite was removed from the stopped-flow instrument by flushing it with anaerobic water followed immediately by anaerobic buffer B. The anaerobic TrpH•Fe(II)•amino acid•$6MePH_4$, TrpH•Fe(II)• tryptophan or TrpH•Fe(II) complex was then mounted on the stopped-flow instrument. The reaction was initiated by mixing the respective complex with buffer B containing different concentrations of O_2. The different O_2 concentrations were obtained by mixing argon and O_2 with a modified MaxBlend medical oxygen blender (Maxtec) and bubbling the mixture of gases directly into an airtight syringe.

Rapid-mix chemical-quench. Rapid mixing chemical-quench experiments were performed at 5 °C with a BioLogic QFM-400 quench-flow instrument. The instrument was calibrated using the reaction of dinitrophenylacetate and hydroxide (*147*). The instrument and the TrpH•Fe(II)•amino acid•$6MePH_4$ complex were prepared anaerobically as described for the stopped-flow experiments. The 2 mM O_2 concentration for these experiment was obtained by placing buffer B in a stirring round bottom flask with a sealed septum in ice and bubbling with 100 % O_2 for at least 30 min. The reaction was initiated by mixing the TrpH•Fe(II)•amino acid•$6MePH_4$ complex with O_2 at 5 °C using a 216 μL sample loop. The reaction was quenched with 5 M HCl.

Control samples were also collected in which the quaternary complex was reacted with anaerobic buffer B at different aging times. For the control samples the

amount of 5-HO-trp or tyrosine formed did not vary significantly with aging time, but about 10-20 % turnover was always present. The percent of turnover for the different anaerobic samples was averaged and subtracted from the actual quenched samples. Two to four samples were collected for each time point. The precipitated enzyme was removed from the samples by centrifugation at 15000 g for at least 10 min. The supernatant (100 μL) was diluted 15-30 fold with 2 M HCl and injected into a C18 Phenomenex HPLC column (250 x 4.60 mm). Tryptophan and 5-HO-trp or phenylalanine and tyrosine were separated with an isocratic mobile phase of 15 mM sodium phosphate, pH 7.0, at a flow rate of 1.0 mL/min and detected using a Waters 2475 Multi λ Fluorescence Detector with excitation at 270 nm and emission at 310 nm.

Analysis of data. The stopped-flow kinetic traces obtained at multiple wavelengths were analyzed globally using the program Spectfit32 (Spectrum Software Associates) using a model with four irreversible steps (Scheme 11). The program KinTek (Explorer Pro) was used for kinetic simulations. The program KaleidaGraph (Synergy Software) was utilized for analysis of stopped-flow kinetic traces at single wavelengths. Equation 11 was used to analyze single or multiple exponential traces; here, A(t) is the absorbance at time t, i is the number of transients, A_i is the amplitude of the ith transient, k_i is the observed rate constant (k_{obs}) for the ith transient, and A_∞ is the absorbance at infinite time. Equation 12 was used to analyze stopped-flow kinetics traces for a reaction in which intermediate (II) accumulates and decays in a sequence of two irreversible steps (R→ I→ II), where reactant (R) and product (II) do not contribute to the change in absorbance and the amplitude change $(R_o)\bullet(\Delta\varepsilon_{nm})$ is only associated

with intermediate (I) (*164, 165*). Chemical-quench experiments showing a burst in product formation were fit to equation 13, where (aa-OH/TrpH) is the burst amplitude, k_{burst} is the rate constant for the burst and k_{linear} is the steady state rate. Mathematically, the burst amplitude (aa-OH /TrpH), k_{burst} and k_{linear} are related to k_3, k_4, the catalytically active enzyme concentration, $[TrpH]_a$, and the initial concentration, $[TrpH]_0$, by equations 14-16 (*166, 167*).

Scheme 11

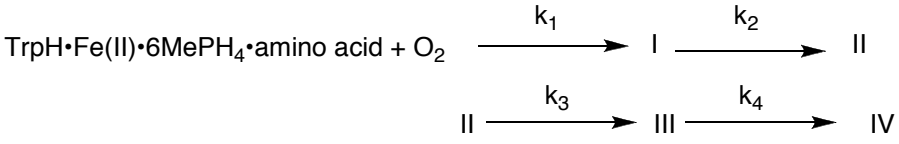

$$A(t) = \sum_i A_i(1-e^{-kit}) + A_\infty \quad (11)$$

$$A(t) = A_0 + R_o(\Delta\varepsilon_{nm})\bullet[k_1/(k_1 - k_2)]\bullet[e^{-k1t} - e^{-k2t}] \quad (12)$$

$$aa\text{-}OH/TrpH_t = (aa\text{-}OH/TrpH)_0\bullet(1-e^{-kburst}) + k_{linear}t \quad (13)$$

$$(aa\text{-}OH/TrpH) = [TrpH]_a/[TrpH]_0\bullet\{k_3/(k_4 + k_3)\}^2 \quad (14)$$

$$k_{burst} = k_3 + k_4 \quad (15)$$

$$k_{linear} = [TrpH]_a/[TrpH]_0 \bullet [k_3 \bullet k_4 /(k_3 + k_4)] \quad (16)$$

RESULTS

Stopped-flow studies of the reaction between TrpH•Fe(II) and O_2. The UV-vis spectrum of the non-heme iron center of TrpH is nearly identical to that of TyrH (*168*). The difference of about 1000 M^{-1} cm^{-1} extending from 300 to about 400 nm for conversion of the ferrous to the ferric state serves as an excellent spectroscopic probe. To determine the reactivity of O_2 against the binary TrpH•Fe(II) or the ternary TrpH•Fe(II)•tryptophan complex, the change in absorbance at 315 nm was utilized. Typically, an anaerobic solution containing 400-600 μM TrpH•Fe(II) was mixed with an equal volume of buffer containing 85-625 μM O_2 (final concentrations). For some experiments stoichiometric concentrations of L-tryptophan were included to determine the effect of the amino acid on the kinetics of TrpH•Fe(II) oxidation. Figure 15 shows stopped-flow traces recorded at 315 nm in the absence (A) or presence (B) of L-tryptophan. These experiments did not use simple pseudo-first-order conditions since the concentrations of O_2 were close to that of TrpH•Fe(II). The absorbance traces in Figure 15 were initially fit to equation 1 with one exponential term to yield estimates of rate constants for the oxidation of TrpH•Fe(II) by O_2.

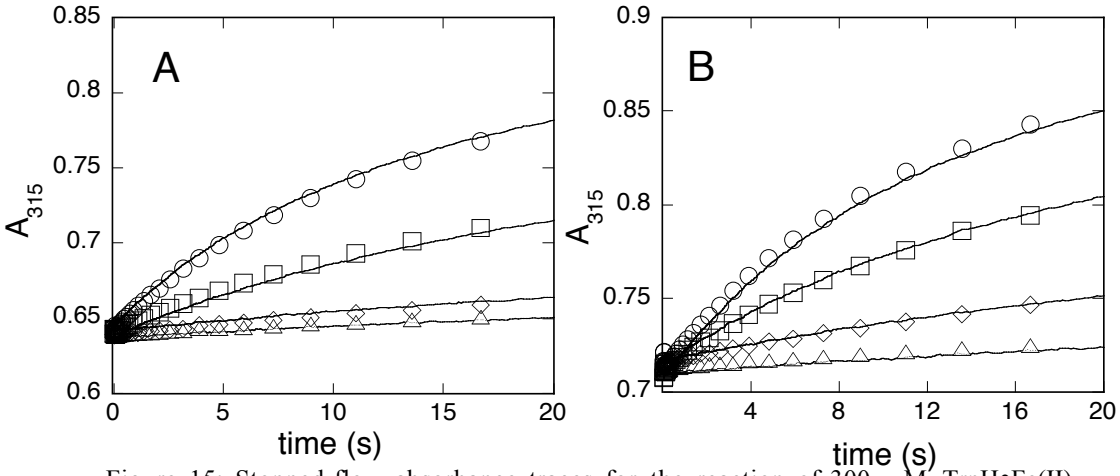

Figure 15: Stopped-flow absorbance traces for the reaction of 300 μM TrpH•Fe(II) containing no (A) or 400 μM L-tryptophan (B) with 600 μM (❍), 300 μM (❑), 125 μM (◊) or 80 μM (Δ) O_2 (all concentrations listed are final) at 5 °C. The solid lines over the data are from simulations to a second order irreversible reaction.

The resulting values were plotted versus the final O_2 concentration (not shown). Linear fits to the data yielded slopes of 155 ± 17 M^{-1} s^{-1} and 137 ± 30 M^{-1} s^{-1} and finite y intercepts of 0.010 ± 0.006 s^{-1} and 0.015 ± 0.010 s^{-1}, in the absence or presence of L-tryptophan, respectively. The stopped-flow kinetic traces were then modeled as a bimolecular reaction using the program KinTek with 140 M^{-1} sec^{-1} as an initial guess for the second order rate constant. The data were fit well (Figure 15) with second order rate constants of 143 M^{-1} s^{-1} and 104 M^{-1} s^{-1} in the absence and presence of L-tryptophan, respectively.

Stopped-flow studies of the reaction between TrpH•6MePH₄•Fe(II)• tryptophan and O_2. Stopped-flow experiments were performed to examine the kinetics of O_2 addition to TrpH under single turnover conditions. A solution containing 200 to 400 μM of the TrpH•Fe(II)•6MePH₄•L-tryptophan was mixed with buffer containing 85-625 μM O_2 (final

concentrations). Absorbance traces were recorded at wavelengths extending from 240 to 500 nm. Figure 16 (A-D) shows selected single wavelength traces at 248, 318, 335 and 400 nm. The wavelength at 248 nm was selected to monitor the formation of the product 4a-hydroxypterin (4a-6MePH$_3$OH) (*43, 90, 148*); an increase at this wavelength is clearly seen. A high valence Fe(IV)O intermediate has been detected at 315 to 365 nm in taurine:α-ketoglutarate dioxygenase (TauD), a mononuclear non-heme enzyme with a Fe(II) center similar to that of TrpH (*139, 149, 150*), so the reaction was followed at 318 and 335 nm. The traces at 318 and 335 nm (Figure 16 (B-C)) do not show evidence of the

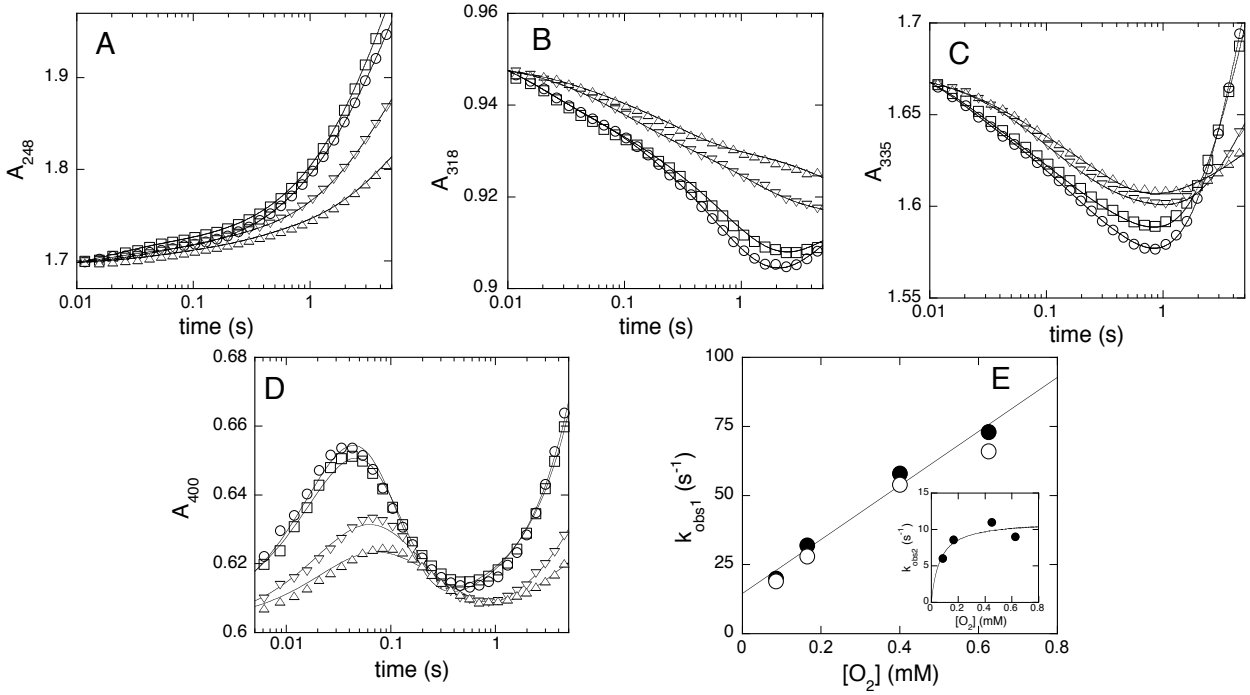

Figure 16: A-D. Absorbance changes during the reaction of 380 μM TrpH•Fe(II) •700 μM•L-tryptophan•1000 μM 6MePH$_4$ and 625 μM (❍), 400 μM (❑), 165 μM (∇) and 85 μM (Δ) O_2 at 5 °C (all concentrations listed are final). The solid lines are from global fits to Scheme 11 using Spectfit32 with rate constants k_2, k_3 and k_4 at fixed values of 11.0 s^{-1}, 1.2 s^{-1} and 0.20 s^{-1} respectively. E. Plot of the first rate constant values (k_{obs1}) versus the concentration of O_2 (solid circles) obtained from the global fits of A-D; the line is a fit to a linear equation. The open circles are k_{obs1} values obtained by simulating the reaction using Scheme 11 and fitting the resulting traces to four first-order processes (see text for details). Inset: the O_2 concentration dependence of k_{obs2}.

transient Fe(IV)O intermediate. Instead, the spectral changes are consistent with the decrease in absorbance accompanying the formation of 4a-6MePH$_3$OH (*78*) or a different pterin species with similar spectral properties. At longer times (> 1 sec) the absorbance at 318 and 335 nm increases, likely due to the formation of the quinonoid dihydropterin (q-6MePH$_2$) by dehydration of the 4a6MePH$_3$OH (*169*). The 400 nm wavelength was randomly selected, but at early times reveals the formation of a novel intermediate that clearly depends on the O_2 concentration (Figure 16 (D)). Following the decay of the intermediate, the absorbance increases in a manner similar to 318 and 335 nm.

A global analysis of the data was carried out using the program Spectfit32. The kinetic traces for each O_2 concentration were fit globally to four sequential first order processes (Scheme 11). A sequence consisting of three sequential first order processes did not fit the data well. The global fit allowed for initial estimates of the rate constants and their variation with O_2. The first phase is associated with small changes in absorbance at 248, 318 and 335 nm, but has a significant increase in absorbance at 400 nm (Figure 16 (D)). A plot of k_{obs1} versus the O_2 concentration is linear with a finite y-intercept, consistent with reversible binding of O_2 (Figure 16 (E) solid circles). The linear dependence suggests that this step is associated with an O_2 binding reaction with a value of 9.8 ± 1.0 x 10^4 M^{-1} s^{-1} for k_{on} (slope) and k_{off} of 15 ± 4 s^{-1} (y-intercept) yielding a dissociation constant (K_d) of 153 ± 56 μM.

The effect of the O_2 concentration on the rate constants for the second phase of the reaction (I → II Scheme 11), which derives primarily from the decay of the 400 nm intermediate, fits to a hyperbola with a limiting value of 11 ± 1.5 s^{-1} and a K_d of 62 ± 38 μM (Figure 16E inset). This type of kinetic behavior suggests that the first and second steps are connected (*166, 170, 171*). Furthermore, the K_d determined for the first and second step are not significantly different. The third phase of the reaction (II → III Scheme 11) is associated with a significant increase in absorbance at 248 nm (50 percent of the total amplitude) and appears to be isosbestic at 318, 335 and 400 nm. The rate constant for this phase appears to be independent of the O_2 concentration, with an average value of 1.2 ± 0.2 s^{-1}. The fact that this rate constant does not depend on the O_2 concentration suggests that this step is irreversible and decoupled from the O_2 binding reaction. The fourth phase of the reaction (III → IV Scheme 11) is readily seen at later times as an increase in absorbance at 335 and 400 nm that does not depend on the O_2 concentration. The average value of 0.20 ± 0.02 sec^{-1} for k_4 agrees with the turnover number of 0.30 ± 0.10 sec^{-1}. Overall, Scheme 11 can account for the absorbance changes occurring in a single turnover reaction by TrpH.

In Figures 16 (A-D) pseudo-first-order conditions were not employed since the concentrations of O_2 used were less than ten-fold over the quaternary complex. This limitation would have the greatest effect on the values determined for k_{on} and k_{off} (Figure 16E). To validate these two rate constants, the traces at each O_2 concentration in Figures 16 (A-D) fit independently to Scheme 3 for each O_2 concentration setting k_2 = 11.0 s^{-1}, k_3 = 1.2 s^{-1}, and k_4 = 0.20 s^{-1} (Figure 16 (E)). The fits (solid lines, Figure 16

(A-D)) reveal that the data can be fit well without significantly altering the value of the rate constants for the first phase (Figure 16 (E) open circles). Furthermore, this analysis strongly supports the conclusion that steps following the O_2 binding reaction are indeed irreversible.

Absorbance spectrum of a novel intermediate. In order to characterize further the intermediate detected at 400 nm, an experiment was carried out in which an anaerobic solution containing 350 μM of the TrpH•Fe(II)•6MePH$_4$•tryptophan complex was mixed with 625 μM O_2 (final concentrations). Three to four shots were collected at 5 nm intervals from 360-500 nm. A spectrum of the intermediate from 360 to 470 nm (Figure 17 (A)) was generated by globally fitting all the data from 0.002 to 0.3 seconds to two irreversible sequential first order processes. The rate constants obtained from the global fit are 77 ± 2 s^{-1} for formation and 10 ± 2 s^{-1} for decay. Figure 17 (B) shows selected single kinetic stopped-flow absorbance traces at 380, 400, 420 and 460 nm (closed symbols) and the fit (lines over the symbols). These same traces were fit independently to equation 12 and average values of 66 ± 4 s^{-1} and 6 ± 2 s^{-1} were obtained for k_1 and k_2, respectively. The values for k_1 and k_2 from using equation 12 are in reasonable agreement with the values obtained from the global fit. It is logical to assume that the evolution and decay of the absorbance between 360 and 470 nm are due to a single intermediate. Overlapping absorbance features due to different species can yield different values for k_1 and k_2 at different wavelengths. The intermediate has its maximum absorbance at about 420 nm with an extinction coefficient of 200 M^{-1} cm^{-1}. The molar extinction coefficient at 420 nm determined from using equation 2 is 180 M^{-1}

cm^{-1}. The global fit was performed only up to 0.3 seconds to eliminate contributions from the third and fourth phases of the reaction, since these last two phases have much higher absorbance changes between 360 and 480 nm. The concentration profile generated from the fit (Figure 17 (C)) reveals that the intermediate accumulates maximally at about 40 ms. Overall, the values of k_1 and k_2 from this experiment match those obtained from the global fit to Scheme 11.

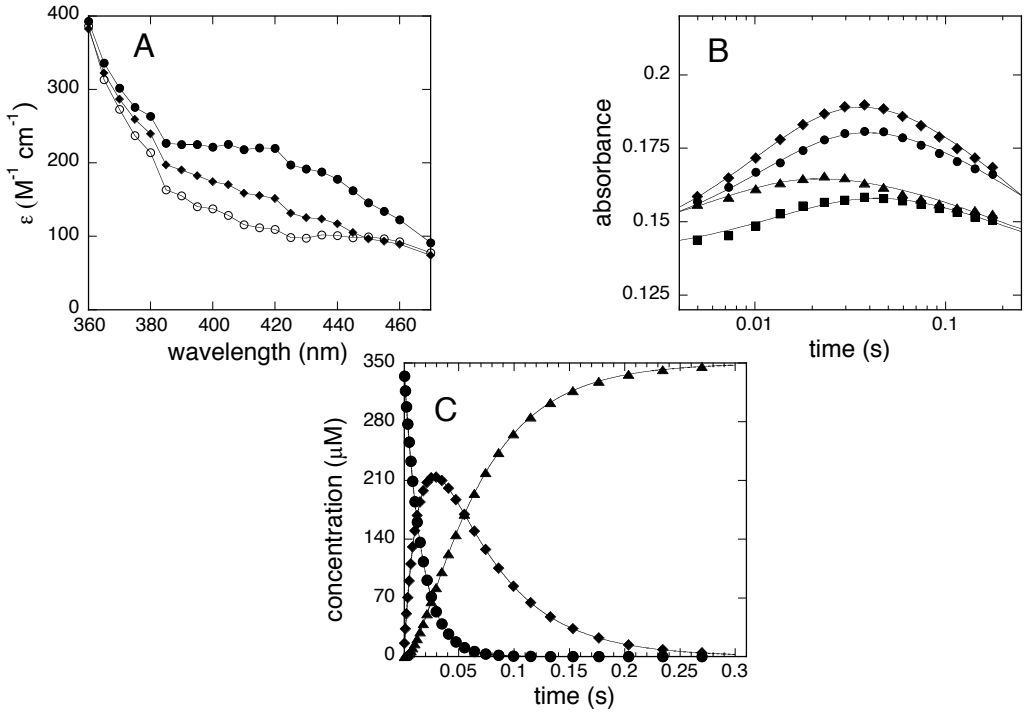

Figure 17: A. Calculated absorbance spectrum of the first intermediate. An experiment similar to that in Figure 16 was performed in which 350 μM TrpHFe(II)500 μM tryptophan1000 μM 6MePH_4 and 625 μM O_2 (final concentrations) were mixed in the stopped-flow instrument. The absorbance was monitored at 5 nm intervals from 360 to 470 nm. The data were fit globally to a two step sequential mechanism using Specfit32 to obtain the spectrum of the starting TrpHFe(II)L-tryptophan6-MePH_4O_2 complex (○), the spectrum of the intermediate (●) and the absorbance spectrum following the decay of the intermediate (◆). B. Single wavelength stopped-flow absorbance traces at 380 (■), 400 (●), 420 (◆) and 460 nm (▲). The solid lines are from fitting the data to a two step sequential mechanism. C. Fractional accumulation of the intermediate I on the basis of the reactant concentrations and the rate constants from the global fit to the two step sequential mechanism: TrpHFe(II)L-tryptophan6MePH_4 (●), Intermediate I (◆) and formation of intermediate II (▲).

Studies of the reaction between TrpH•6MePH$_4$•Fe(II)•phenylalanine and O$_2$. In order to determine if the identity of the amino acid has an effect on the reaction between TrpH and O_2, similar stopped-flow experiments were performed with L-phenylalanine as the amino acid substrate. Previous studies have shown that L-phenylalanine is a good substrate for TrpH, given that all the reducing equivalents from 6MePH$_4$ are utilized in productive turnover (*90*). For these experiments, 350 μM TrpH•Fe(II) was anaerobically combined with 1.5 equivalent of both L-phenylalanine and 6MePH$_4$ (final concentrations). The reaction was initiated by mixing the anaerobic TrpH•Fe(II)• 6MePH$_4$•phenylalanine complex with buffer containing different O_2 concentrations. Absorbance traces were recorded at 248, 318, 335 and 400 nm. The absorbance decreases at 248 nm at times greater than one second, in contrast to the results with L-tryptophan (Figure 18 (A)). This decrease in absorbance is consistent with a change in extinction coefficient for the dehydration of the 4a-6MePH$_3$OH product to quinonoid 6-methyldihydropterin (q-6MePH$_2$) and H_2O (*43, 90, 148*). However, the fact that the kinetic traces at 248 nm are different for the two amino acids and the decrease in absorbance at 248 nm is not seen with tryptophan suggests that hydroxylation of the amino acid is also contributing to the spectral changes at 248 nm. The traces at 318 and 335 were similar to those obtained with L-tryptophan. This shows that the conversion of 6MePH$_4$ to 4a-6MePH$_3$OH dominates the changes in absorbance at early time scales (< 1s) and the bound amino acid perturbs the spectral changes slightly, given that the decrease in amplitude at early time scales is slightly less with phenylalanine (Figure 18 (B)).

The intermediate detected at 400 nm with L-tryptophan has a much lower absorbance with L-phenylalanine (Figure 18 (C)); this suggests that the identity of the amino acid bound contributes significantly to the spectrum of the intermediate. The inset in Figure 18 (C) shows the difference in absorbance at 400 nm under the same experimental conditions with L-tryptophan versus L-phenylalanine. The solid lines are fits to equation 12. The values for k_1 and k_2 are 61 ± 2 s^{-1} and 7.2 ± 0.3 s^{-1} for tryptophan, while for phenylalanine the values are 54 ± 3 s^{-1} and 2.1 ± 0.1 s^{-1}, respectively. The calculated extinction coefficients at 400 nm for the intermediate with tryptophan and phenylalanine under these conditions are 180 M^{-1} cm^{-1} and 35 M^{-1} cm^{-1}, respectively. A complete analysis from 360 to 470 nm of the intermediate with phenylalanine was not carried out. Overall, the data show that the intermediate has a lower extinction coefficient with phenylalanine. It forms and decays with rate constants that are considerably faster than the respective turnover numbers with both amino acids. This strongly suggests that the intermediate is not directly involved in the hydroxylation of the amino acid, but O_2 activation (vide infra).

The data at 248, 318, 335 and 400 nm were fit globally to Scheme 11 for each O_2 concentration. As with tryptophan as the substrate, the rate constant for the first phase of the reaction (k_{obs1}) shows a linear dependence on the concentration of O_2. A plot of k_{obs1} versus the concentration of O_2 yields a second order rate constant of 8.9 ± 0.5 x 10^4 M^{-1} s^{-1}, and an off rate (k_{off}) of 26 ± 2 s^{-1}, yielding a K_d = 290 ± 40 μM (Figure 18 (D)). The second phase of the reaction (k_{obs2}) fits very well to a hyperbolic equation (18 (D) inset) with a limiting value of 9 ± 1 s^{-1} (K_d = 120 ± 30 μM). Unlike with tryptophan, the K_d

value with phenylalanine is well above the lowest O_2 concentration and is better defined. These data also fit to a hyperbolic equation with an offset of 3.2 sec^{-1} ± 0.8 and a K_d

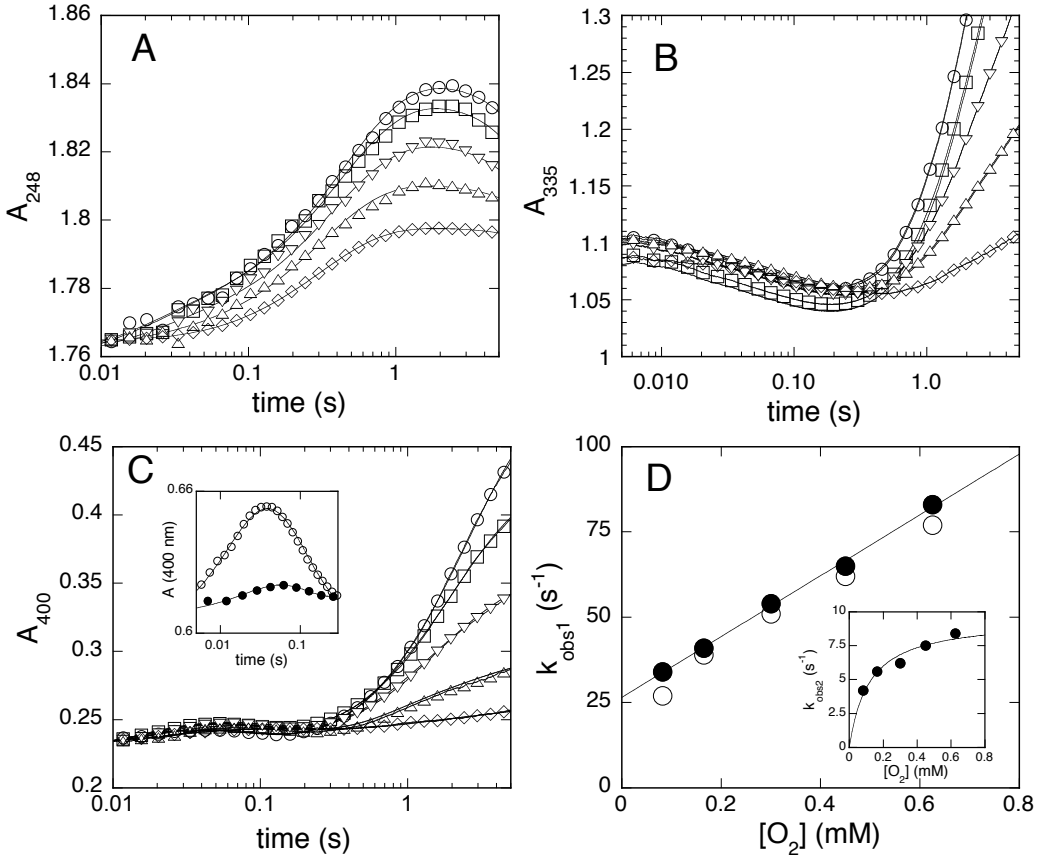

Figure 18: Stopped-flow absorbance traces recorded at 248 nm (A), 335 nm (B) and 400 nm (C) for the reaction of 350 μM TrpH•Fe(II)•550 μM L-phenylalanine•550 μM 6MePH$_4$ with 625 μM (❍), 450 μM (❑), 300 μM (∇), 165 μM (Δ) or 80 μM (◊) O_2 at 5 °C (all concentrations listed are final). The lines in A-C are from global fits for each individual O_2 concentration to a model with four irreversible first-order processes (Scheme 11) using Spectfit32, with the values of the rate constants k_2, k_3 and k_4 set to 6.4 s^{-1}, 1.6 s^{-1} and 0.36 s^{-1}, respectively. C Inset: Absorbance traces at 400 nm versus time when 350 μM TrpH•Fe(II)•700 μM 6MePH$_4$ and 750 μM tryptophan (○) or 550 μM phenylalanine (●) are mixed anaerobically with 625 μM O_2 (final concentrations). D. Solid symbols show the effect of the concentration of O_2 on of the first rate constant (k_{obs1}) obtained from the global fits of A-C and 318 nm to Scheme 11. The open circles are k_{obs1} values obtained by simulating the reaction using Scheme 11 and fitting the resulting traces to four first-order processes (see text for details) Inset: O_2 concentration dependence of k_{obs2}; the line is a fit to a hyperbola.

value greater than 750 μM. However, it is difficult to reconcile a mechanism where the K_d for the second step is significantly larger than the K_d for the initial first fast reaction. Furthermore, a finite y-intercept would mean that O_2 activation is reversible, which is highly unlikely. The hyperbolic dependence on k_{obs2} is consistent with the first kinetic phase being connected to the second, just as is the case when L-tryptophan is the substrate. The rate constants for the third and fourth phases do not depend on the concentration of O_2, with average values of $k_3 = 1.6 \pm 0.2$ s^{-1} and $k_4 = 0.36 \pm 0.05$ s^{-1}; revealing that these steps are unimolecular and decoupled from the O_2 binding reaction. As is the case with L-tryptophan, all four rate constants are catalytically competent. The value for k_4 agrees reasonable well with the turnover number ($k_{cat} = 0.50 \pm 0.15$ s^{-1}).

The traces at 248, 318, 335 and 400 nm were simulated to Scheme 11 with $k_2 = 9$ s^{-1}, its limiting value, $k_3 = 1.6$ s^{-1}, $k_4 = 0.36$ s^{-1}. The fit (Figure 18 (A-C) lines) reproduces the traces without altering significantly the value for the first kinetic phase (Figure 18 (C) open symbols). This shows that the data can be effectively interpreted with steps following the O_2 binding reaction as irreversible, but more importantly the analysis also validates the binding constants determined from the non-pseudo first order conditions. Overall, despite the subtle differences, the values of the rate constants obtained with L-phenylalanine are essentially identical to those obtained with L-tryptophan.

Rapid-mixing chemical quench studies. The rate constants for formation of 5-HO-trp and tyrosine were determined under pre-steady state conditions to establish directly if steps subsequent to hydroxylation limit turnover and to correlate the stopped-

flow kinetic data with the hydroxylation of the amino acid. For these experiments 100 μM TrpH•Fe(II)•1.5 mM $6MePH_4$•1 mM L-tryptophan or 150 μM TrpH•Fe(II)•1.5 mM $6MePH_4$•1.5 mM L-phenylalanine was mixed with an equal volume of buffer B containing 0.9-1.0 mM O_2 at 5 ºC (final concentrations). The reactions were rapidly quenched at different times with 5 M HCl. The data in Figure 19 (A) show a clear burst in the formation of 5-HO-trp. These data were fit to equation 13 to yield values for the burst amplitude (aa-OH/TrpH) and k_{burst} of 0.46 ± 0.19 and 1.3 ± 0.6 s^{-1}, respectively. The value for k_{burst} is about 5-fold faster than the turnover number at 5 ºC and correlates well with the third phase obtained from the stopped-flow experiments. The value determined for k_{linear} is 0.25 ± 0.05 s^{-1} and is equivalent to the value of 0.30 ± 0.10 s^{-1} for k_{cat}. With phenylalanine the values for the burst amplitude (aa-OH/TrpH), k_{burst} and k_{linear} are of 0.53 ± 0.11, 2.6 ± 1.2 s^{-1} and 0.26 ± 0.02 s^{-1}, respectively (Figure 19 (A) inset). The value determined for k_{linear} is in close agreement with the turnover number (0.50 ± 0.15 s^{-1}) and the last phase of the stopped-flow data (0.36 ± 0.05 s^{-1}). Taken as a whole, the parameters obtained from fitting the chemical quench data to equation 13 for tryptophan or phenylalanine are similar, with a significant burst magnitude that suggests that hydroxylation of the amino acid is not fully rate limiting.

To establish the magnitude of the burst more accurately a series of chemical quench experiments were performed with L-tryptophan, in which the final concentration of TrpH varied from 100 to 300 μM. The concentrations of L-tryptophan and $6MePH_4$ were 8 to 10-fold higher than that of TrpH, while the final O_2 concentration was at least 0.9-1.2 mM. The results from six different experiments reveal a burst amplitude (aa-

OH/TrpH) of 0.33 ± 0.15. Additionally, an experiment was performed in which 60 μM TrpH•Fe(II)•1.5 mM $6MePH_4$•1 mM L-tryptophan was mixed with buffer B containing approximately 1.0 mM O_2 at 5 ºC (final concentrations). The lower TrpH concentration allowed for multiple turnovers. A linear regression analysis of these data allows for the determination of k_{linear} (slope) and the burst amplitude (y-axis) (Figure 19 (B)). The slope of the line is 0.10 ± 0.01 s^{-1}, which in close agreement with k_{cat}. More importantly the magnitude of the burst is 0.34 ± 0.05, which agrees well with the value, obtained from averaging the different chemical quench experiments. Combining all these results it is reasonable to conclude that the burst amplitude (aa-OH/TrpH) with tryptophan as substrate is 0.3 ± 0.1.

Using equations 14-16 and the parameters obtained from fitting each of the six different chemical quench experiment to equation 13, the active TrpH concentration $[TrpH]_a$, k_3 and k_4 were obtained (Table 9). This analysis reveals that in all cases TrpH is not fully active ($[TrpH]_a/[TrpH]_0 < 1$). The values for $[TrpH]_a$ vary significantly; this can be explained by taking into account that different preparations of $[TrpH]_0$ were used

Scheme 12

$$\text{TrpH•Fe(IV)O•6MePH}_3\text{OH•trp} \xrightarrow{k_3} \text{TrpH•Fe(II)•6MePH}_3\text{OH•5-OH-trp}$$

$$\text{TrpH•Fe(II)•6MePH}_3\text{OH•5-OH-trp} \xrightarrow{k_4} \text{TrpH•Fe(II)} + 6\text{MePH}_3\text{OH} + \text{5-OH-trp}$$

in these experiments. The parameters $[TrpH]_a$, k_3 and k_4 were subsequently used to simulate each chemical quench experiment to Scheme 12, which assumes that k_{cat} is

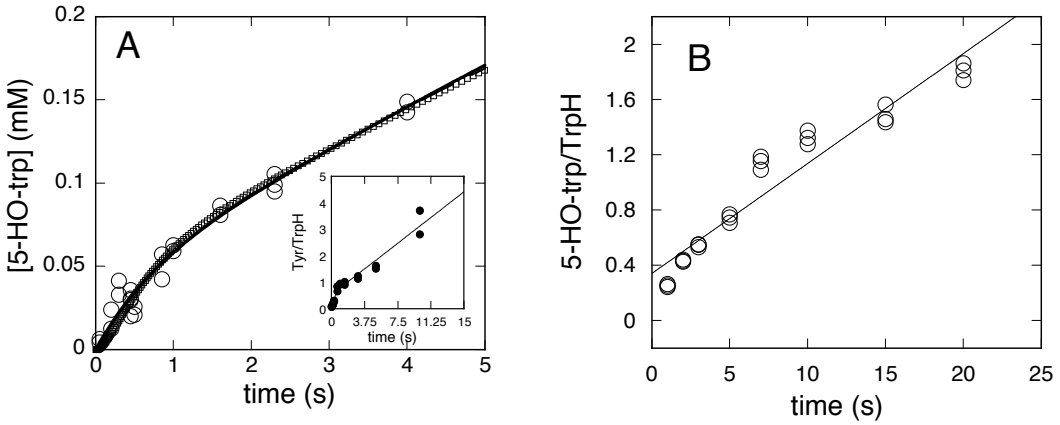

Figure 19: A. Rapid chemical quench analysis of the reaction between 100 μM TrpHFe(II)1.5 mM 6MePH$_4$1 mM L-tryptophan and 1.0 mM O_2 at 5 °C (Final concentrations). The solid line is from a fit to equation 13. The open squares are from simulation of the data to Scheme 12 using KinTek-Explorer with $[TrpH]_{active}$ = 92 μM, k_3 = 1.17 s^{-1} and k_4 = 0.34 s^{-1} (Table 9 and text for details). Inset: Rapid chemical quench analysis of the reaction between 150 μM TrpHFe(II)1.5 mM 6MePH$_4$1.5 mM L-phenylalanine and 1.0 mM O_2 at 5 °C (Final concentrations). The solid line is a fit to equation 13. B. Chemical quench analysis of the reaction between 60 μM TrpHFe(II)1.5 mM 6MePH$_4$1 mM L-tryptophan and 1.0 mM O_2 at 5 °C (Final concentrations). The line is a fit to a linear equation.

Table 9: Magnitudes of Rate Constants k_3 and k_4 Derived from Rapid-Chemical Quench Experiments

$[TrpH]_{Initial}$ μM	$[TrpH]_{active}$ μM	k_3 s^{-1}	k_4 s^{-1}
100	92	1.17	0.34
150	110	1.44	0.28
150	80	0.71	0.15
175	46	2.41	0.53
200	100	2.36	0.18
300	120	1.24	0.33

The values for $[TrpH]_{active}$, k_3 and k_4 were obtained from equations 13-16. Each experiment was simulated to Scheme 12 with $[TrpH]_{active}$, k_3 and k_4 as constants. A typical result is shown in Figure 19A.

limited by rate constants k_3, the hydroxylation step, and k_4, regeneration of free TrpH. A typical result from a simulation is shown in Figure 19 (A) (open squares). The values of k_3 and k_4 for each experiment are listed in Table 9. The average from all of these experiments reveals that k_3 is 1.6 ± 0.7 s^{-1} and k_4 is 0.30 ± 0.14 s^{-1}. This analysis shows that formation of 5-HO-trp is 4-6 fold faster than regeneration of the free enzyme.

DISCUSSION

In the present study, the chemical mechanism of TrpH was investigated using transient stopped-flow and rapid acid-quench approaches. The proposed chemical mechanism for the hydroxylation of tryptophan and the determination of the rate limiting step (Scheme 3) has relied on studies from steady state kinetics, steady state isotope effects and alternate substrates (*38, 39, 51*). The involvement of a hydroxylating intermediate not involving a tetrahydropterin was established by analyzing the products when tyrosine is the substrate; in this case 4a-6MePH$_3$OH is formed, but not dihydroxyphenylalanine, demonstrating that O-O bond cleavage proceeds hydroxylation (*38*). The intrinsic kinetic isotope effects for benzylic hydroxylation of 4-methylphenylalanine by TrpH are consistent with a mechanism involving hydrogen atom abstraction (Chapter II) (*42, 44, 52, 172*). This is consistent with the requirement of a more reactive hydroxylating intermediate than the peroxy-pterin. These results are consistent with formation of a Fe(IV)O intermediate that reacts with the aromatic amino acid (Scheme 3).

Several intermediates in non-heme enzymes, including an Fe(IV)O intermediate, have been detected by various spectroscopic means (*137-139*). The Fe(IV)O intermediates in TyrH, PheH and the alpha-ketoglutarate dependent enzyme TauD could be detected by Mössbauer and absorbance spectroscopy (for TauD) when the reaction with O_2 was carried out in the presence of the reducing substrate and co-substrate (*45, 139*). It is assumed that the Fe(IV)O intermediate forms only in the presence of all substrates, so that reducing equivalents are only consumed in productive turnover. Therefore, reactions between non-heme mononuclear enzymes and O_2 in which one or both substrates are lacking tend to be sluggish. This is consistent with the Fe(II) center becoming much more reactive towards O_2 only when the reducing substrate and the substrate to be oxidized are bound in the active site (*1-3*). For this reason, prior to establishing whether a Fe(IV)O intermediate could be detected in TrpH, it was imperative to determine that the Fe(II) mononuclear center reacts sluggishly when one or both substrates are lacking and becomes reactive towards O_2 only in response to binding of all the substrates. To establish this directly in TrpH a detailed stopped-flow study of the kinetics in which O_2 reacts with the binary TrpH•Fe(II), ternary TrpH•Fe(II)•tryptophan and quaternary TrpH•Fe(II)•6MePH_4•tryptophan complexes was carried out.

For TyrH and PheH the Fe(II) center is readily oxidized by O_2 when no substrates are bound (*168, 173*). An irreversible bimolecular reaction best describes the reaction of O_2 with TrpH•Fe(II) or TrpH•Fe(II)•tryptophan. More importantly a mechanism in which saturation kinetics are displayed would imply the presence of a

non-metal binding site for O_2, for which there is no precedent for any of the aromatic amino acid hydroxylases. In TyrH the mechanism of Fe(II) oxidation is similarly a bimolecular reaction (*168*). In TrpH the binding of tryptophan does not change the reactivity of the Fe(II) center for O_2. The second order rate constant of 210 M^{-1} s^{-1} for TyrH is similar to the values reported in the present work, although the reaction temperature for the former was 20 °C versus 5 °C for the latter. A similar second order rate constant for both enzymes suggests that O_2 diffuses into the active site without the requirement for a binding site. In addition, it can be inferred that the redox potentials of the non-heme Fe(II) centers in TrpH and TyrH are similar.

The oxidation by O_2 of the mononuclear Fe(II) center in (4-hydroxyphenyl)-pyruvate dioxygenase (HPPD), a member of the α-ketoglutarate-dependent dioxygenase family, has been determined to be also an irreversible bimolecular reaction with a second order rate constant of 46 M^{-1} s^{-1} (*154, 174*). This value is similar to the values determined for TyrH and TrpH. In all three cases the reactions are too slow to support the observed rate of catalysis even at O_2 concentrations exceeding physiological concentrations. This suggests that the Fe(II) center is probably never oxidized during normal turnover. The low magnitudes of these second order rate constants suggest that the coordination of the Fe(II) center is not suitable for a reaction with O_2 in the absence of one or both substrates and that its coordination changes only upon binding of both the reducing substrate and the substrate, allowing its reactivity towards O_2 to be enhanced. In the case of TrpH, binding of the amino acid alone does not change the coordination

site of the Fe(II) center; therefore, the reactivity of the Fe(II) center with O_2 is still sluggish, consistent with the requirement for the reducing substrate ($6MePH_4$) (*3, 175*).

The results displayed in Figure 16 reveal that the reactivity of the mononuclear Fe(II) center with O_2 is indeed enhanced in the presence of the reducing substrate ($6MePH_4$) and the target for oxidation (L-tryptophan). The kinetics for the reaction between the quaternary complex TrpH•Fe(II)•6MePH4•tryptophan and O_2 are drastically different from those for TrpH•Fe(II) or TrpH•Fe(II)•tryptophan with O_2. The difference in magnitude of the second order rate constants reveals that the Fe(II) center becomes about 750-fold more reactive, suggesting that the Fe(II) center in TrpH becomes suitable to react with O_2 only in the presence of the reducing substrate and the target for oxidation (*3, 175*).

As indicated above, the reaction between O_2 and the reactive TrpH•Fe(II)•$6MePH_4$•tryptophan complex follows second order kinetics (Figure 16 (E)); since second order rate constants for O_2 addition have been reported previously for several other non-heme enzymes that share the $(His)_2$(Asp/Glu)-facial triad, a direct comparison with TrpH can be made. The magnitudes of the second order rate constants for O_2 addition to HPPD, taurine:α-ketoglutarate dioxygenase (TauD), homoprotocatechuate 2,3-dioxygenase, an extradiol dioxygenase, and more recently the novel diiron enzyme *myo*-inositol oxygenase are very similar to that for TrpH (*138, 141, 154, 155*). One way to reconcile these similarities is to assume that when O_2 binds to the corresponding reactive complexes in HPPD, TauD, homoprotocatechuate 2,3-dioxygenase, and TrpH in the presence of the reducing substrate and the target for oxidation, the initial non-

covalent complex formed or the iron-oxygen species is probably not very different among HPPD, TauD, homoprotocatechuate 2,3-dioxygenase and TrpH, even though the fate of O_2 subsequently diverges significantly. Overall these data highlight that despite the diverse functions of the non-heme enzymes mentioned above, their non-heme Fe(II) centers appear to react initially with O_2 in an analogous manner.

As mentioned before it is clear that the reactivity of the Fe(II) center in TrpH with O_2 is enhanced in the presence of $6MePH_4$ and the amino acid. The first kinetic phase of this reaction is the formation of a reversible complex between TrpH•Fe(II)•$6MePH_4$•tryptophan and O_2 (Scheme 13). We proposed that formation of this complex is associated with the intermediate whose absorbance is maximum at 420 nm (Figure 17). This intermediate to the best of our knowledge is the first one detected by absorbance spectroscopy in the aromatic amino acid hydroxylases. General mechanistic conclusions can be made about this intermediate and species II, III and 1V (Scheme 11) associated with subsequent steps, whether the amino acid substrate is L-tryptophan or L-phenylalanine. First, the clear first order dependence on O_2 suggests that the development of the peak at 420 nm is directly coupled to the O_2 binding reaction; that is, there are no irreversible steps between the O_2 binding reaction and the formation of the 420 nm intermediate (*176*). Secondly, the significant y-intercepts in Figures 16 (E) and 18 (D), argue strongly in favor of a reversible reaction between O_2 and the quaternary TrpH•Fe(II)•amino acid•$6MePH_4$ complex and suggests that electron transfer from the Fe(II) center or $6MePH_4$ to O_2 does not occur in this step. Third, the similar K_d values for O_2 of 153 and 240 μM with tryptophan and phenylalanine suggest that the formation

of the complex does not depend significantly on the character of the amino acid bound. Lastly, since the rate constants k_1 and k_2 for the development and decay of the intermediate with tryptophan or phenylalanine are similar and with k_2 being at least 20 fold faster than the respective turnover numbers of 0.50 ± 0.15 and 0.30 ± 0.10 s^{-1} with tryptophan and phenylalanine, it is reasonable to propose that decay of the intermediate is the first step in O_2 activation. At this point it is not clear why the extinction coefficient of the intermediate at 400 nm with L-phenylalanine is drastically diminished. It may be that the absorbance with tryptophan is enhanced due to the chromophoric character of L-tryptophan.

Scheme 13

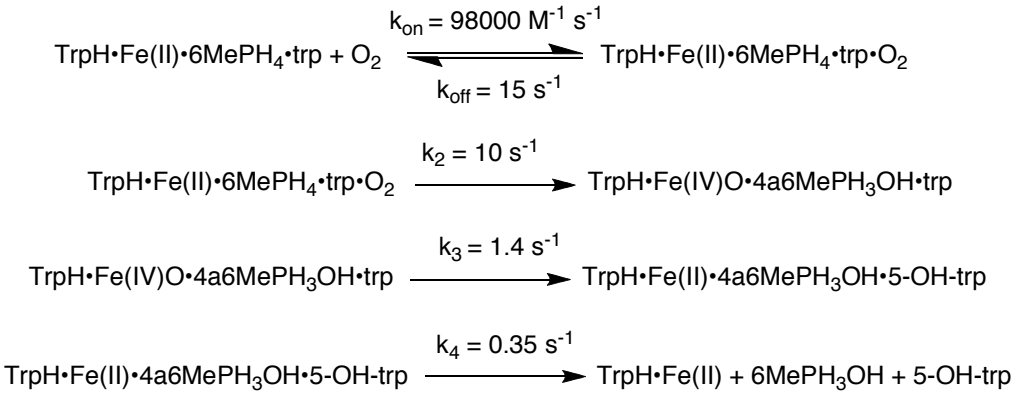

The TrpH•Fe(II)•6MePH$_4$•tryptophan•O_2 complex decays with rate constant k_2 which has a limiting value of about 10 s^{-1} for tryptophan and 9 s^{-1} for phenylalanine. The absorbance change at 248 and 318 nm suggest that first product 4a6MePH$_3$OH is formed in this step. Therefore, intermediate II from Scheme 11 is assigned to the

TrpH•Fe(IV)O•4a6MePH$_3$OH• tryptophan complex (Scheme 13). Scheme 3 predicts that activation of O_2 results in the formation of the TrpH•Fe(IV)O•4a6MePH$_3$OH •tryptophan intermediate complex; thus, a series of irreversible steps is likely to be between the formation of the initial O_2 complex and the TrpH•Fe(IV)O•4a6MePH$_3$OH •tryptophan complex. Formation of the latter is expected to proceed through a peroxy-pterin-iron bridged species (Scheme 3). However, the data suggest that additional steps for the activation of O_2, including the formation and decay of the peroxy-pterin-iron bridged species, do not have absorbance changes at the selected wavelengths or are likely to proceed much faster that 10 s^{-1}.

The TrpH•Fe(IV)O•4a6MePH$_3$OH•tryptophan intermediate complex is assigned as intermediate II. The rapid mix chemical quench experiments and the kinetics simulations further support this. The stopped-flow data show that the decay of the TrpH•Fe(IV)O• 4a6MePH$_3$OH•tryptophan complex occurs with a rate constant of 1.2 s^{-1} or 1.6 s^{-1} with phenylalanine or tryptophan, respectively. These values are in excellent agreement with the average value for k_3 of 1.6 ± 0.7 sec^{-1} determined from the kinetic simulations. This analysis strongly supports the conclusion that hydroxylation of the amino acid occurs in this step. Therefore, k_3 in Scheme 13 is assigned to the decay of the Fe(IV)O intermediate and the formation of 5-HO-trp (TrpH•Fe(II)•4a6MePH$_3$OH •5-HO-trp).

The last steps of the reaction with phenylalanine and tryptophan are also catalytically competent and in both cases the rate constants agree reasonably well with the respective turnover numbers. The value for the last step from the stopped-flow

kinetic traces is in excellent agreement with the value for k_4 obtained from analysis of the chemical quench experiments. This shows that a step following hydroxylation of the amino acid, likely release of 4a6MePH$_3$OH, limits k_{cat} for TrpH with either amino acid substrate (Scheme 13).

Overall, Scheme 13 can account for all the results from stopped-flow absorbance spectroscopy and the rapid-quench product analysis and for that reason is a reasonable model of the single turnover reaction catalyzed by TrpH. Scheme 13 needs to be put in the context of previous results obtained from steady state kinetic isotope effects and the used of tryptophan analogs. An inverse kinetic isotope effect on the turnover number ($^{D}k_{cat}$) with $^{2}H_5$-indole-tryptophan or 5-^{2}H-tryptophan suggests that amino acid hydroxylation is at least partially rate-limiting (*38*). The greater rate for unproductive consumption of tetrahydropterin with different tryptophan analogs in relationship to that for tryptophan suggests that O_2 activation is fast and the Fe(IV)O intermediate decays unproductively due to the at least partially rate limiting hydroxylation reaction with tryptophan or the analogs (*51*). This is consistent with the relative magnitudes of the rate constants in Scheme 13.

Based on the present data, however, the previously observed inverse $^{D}k_{cat}$ value with $^{2}H_5$-indole-tryptophan or 5-^{2}H-tryptophan is not the intrinsic isotope effect on the turnover number, since k_3 (hydroxylation) is 4-6 fold faster than k_4 (regeneration of free TrpH). This will result in a $^{D}k_{cat}$ value less inverse than the intrinsic isotope effect for formation of the new C-O bond. The kinetic mechanism of Scheme 13 assumes that the k_{cat} value is limited by k_3 and k_4. The relationship between these two rate constants and

k_{cat} is given by equation 17. Equation 18 gives the relationship of k_3, k_4 and the isotope effect on the turnover number ($^{D}k_{cat}$) to the intrinsic isotope effect (^{D}k).

$$k_{cat} = (k_3 * k_4)/(k_3 + k_4) \quad (17)$$

$$^{D}k_{cat} = (^{D}k_3 + k_3/k_4)/(1 + k_3/k_4) \quad (18)$$

If the $^{D}k_{cat}$ value is taken to be 0.95 (*38*) and k_3, the rate constant for formation of the new C-O bond is 4-6 faster than k_4, the rate constant for conformational change and/or the release of 4a6MePH$_3$OH, then the intrinsic isotope effect for C-O bond formation is between 0.75 and 0.65. The former value is in reasonable agreement with the calculated equilibrium isotope effect of 0.80 for this reaction (*38*), while the latter value is too inverse. Although, the available data support a ratio for k_3/k_4 between 4-6, it is very unlikely that the kinetic isotope effect for formation of the C-O bond in tryptophan can be as low as 0.7 when one considers that the equilibrium isotope effect for a reaction is generally accepted as the theoretical limit for a secondary kinetic isotope effect (*69*). Therefore, it is more reasonable to propose that the ratio of k_3/k_4 is closer to 4 than 6.

In conclusion the results presented here reveal that TrpH is only suitable to react with O_2 in the presence of both the co-substrate and the amino acid. When both substrates are bound in the active site the ternary TrpH•Fe(II)•6MePH$_4$•trp complex reacts rapidly and reversibly with O_2 forming a species with an absorbance signature that

peaks at 420 nm. This intermediate decays with a rate constant of 9-11 s^{-1}, independent of the identity of the amino acid bound. The value of 9-11 s^{-1} is the lower limit for O_2 activation since no other intermediates accumulate between the initial TrpH•Fe(II) •6MePH_4•trp•O_2 complex and the formation of the 4a6MePH_3OH product and the Fe(IV)O intermediate. The turnover number of the reaction appears to be limited by hydroxylation of the amino acid and release of a product, likely the 4a6MePH_3OH, with the former step being about 4-fold faster than the latter.

CHAPTER VII

SUMMARY

The studies presented here have focused on studying the intrinsic properties of the $(His)_2(Glu)$-facial triad Fe(II) center in the aromatic amino acid hydroxylases. Chapter II showed the advantage of using the unnatural amino acid substrate 4-methylphenylalanine and the isotope effects on the benzylic hydroxylation reaction as a probe to compare the reactivity of the $(His)_2(Glu)$-facial triad Fe(II) center in the three enzymes. The nearly identical isotope effects and their temperature dependence clearly show that the transition state for the benzylic hydroxylation reaction is the same for the three enzymes. Chapter III focused on the activation of H_2O_2 in comparison to normal turnover. The kinetics of the reactions for all three enzymes are slow but similar, revealing that, steps leading to the formation of the Fe(IV)O intermediate from H_2O_2 are the same. The H_2O_2 dependent intermediate that forms catalyzes aromatic, benzylic and aliphatic hydroxylation, suggesting that it is indeed the same Fe(IV)O formed under normal turnover. The results from chapters II and III show that the intrinsic reactivity of the $(His)_2(Glu)$-facial triad Fe(II) center and by that account the Fe(IV)O intermediates that result from $6MePH_4$ and O_2 or H_2O_2 activation are the same.

Chapters IV and V focused on the chemical mechanism of PheH. These two chapters show the power of combining steady state kinetics and rapid reaction techniques, including stopped-flow, rapid-quench product analysis and freeze-quench Mössbauer spectroscopy, to identify the rate-limiting step in the complex reaction

catalyzed by PheH. The ability to carry out the reaction under single turnover conditions and to measure intrinsic rate constants coupled with steady state isotope effects confirms that the irreversible activation of O_2 by PheH is fast relative to turnover. The Mössbauer spectroscopy experiments reveal the existence of a Fe(IV)O intermediate in the catalytic cycle of PheH. Furthermore, the chemical-quench experiments effectively show that the rate-limiting step in the hydroxylation of phenylalanine is the formation of a new C-O bond.

Chapter VI focused on the reactivity of the $(His)_2(Glu)$-facial triad Fe(II) center in TrpH in the absence and presence of substrate(s). In this case the intrinsic rate constants obtained from stopped-flow absorbance spectroscopy and rapid-quench product analysis were put in the context of the state state parameters. The results from this chapter are exciting because for the first time, to the best of my knowledge a transient intermediate was detected in these enzymes by absorbance spectroscopy. The ability to measure intrinsic rate constants via two methods (stopped-flow and rapid-quench) clearly shows the advantage of combing different rapid reaction techniques in order to assign with more confidence the nature of chemical steps. Furthermore, just as is the case with PheH (Chapters IV and V), the rate-limiting step of the reaction in TrpH was identified. In this case, the rate-limting step is a combination of two steps, and the isotope effect on the turnover number determined with steady state kinetics (0.95) is not devoid of kinetic complexity.

REFERENCES

(1) Sono, M., Roach, M. P., Coulter, E. D., and Dawson, J. H. (1996) Heme-containing oxygenases. *Chem. Rev. 96*, 2841-2888.

(2) Solomon, E. I., Brunold, T. C., Davis, M. I., Kemsley, J. N., Lee, S. K., Lehnert, N., Neese, F., Skulan, A. J., Yang, Y. S., and Zhou, J. (2000) Geometric and electronic structure/function correlations in non-heme iron enzymes. *Chem. Rev. 100*, 235-349.

(3) Costas, M., Mehn, M. P., Jensen, P. M., and Que, L., Jr. (2004) Dioxygen activation at mononuclear nonheme iron active sites: enzymes, models, and intermediates. *Chem. Rev. 104*, 939-986.

(4) Ortiz, P. R. (2005) *Cytochrome P450: Structure, Mechanism, and Biochemistry,* 3rd ed. Kluwer Academic/Plenum Publishers, New York.

(5) Abu-Omar, M. M., Loaiza, A., and Hontzeas, N. (2005) Reaction mechanisms of mononuclear non-heme iron oxygenases. *Chem. Rev. 105*, 2227-52.

(6) Lange, S. J., and Que, J., L. (1998) Oxygen activating nonheme iron enzymes. *Current Biology 2*, 159-172.

(7) Elkins, J. M., Ryle, M. J., Clifton, I. J., Dunning Hotopp, J. C., Lloyd, J. S., Burzlaff, N. I., Baldwin, J. E., Hausinger, R. P., and Roach, P. L. (2002) X-ray crystal structure of *Escherichia coli* taurine/α-ketoglutarate dioxygenase complexed to ferrous iron and substrates. *Biochemistry 41*, 5185-5192.

(8) Merkx, M., Kopp, D. A., Sazinsky, M. H., Blazyk, J. L., Müller, J., and Lippard, S. J. (2001) Dioxygen activation and methane hydroxylation by soluble methane monooxygenase: a tale of two irons and three proteins. *Angew. Chem. Int. Ed. Eng. 40*, 2782-2807.

(9) Wallar, B. J., and Lipscomb, J. D. (1996) Dioxygen activation by enzymes containing binuclear non-heme iron clusters. *Chem. Rev. 7*, 2625-2658.

(10) Que Jr., L. (2000) One motif-many different reactions. *Nature Struct. Biol. 7*, 182-184.

(11) Hausinger, R. P. (2004) FeII/alpha-ketoglutarate-dependent hydroxylases and related enzymes. *Crit. Rev. Biochem. Mol. Biol. 39*, 21-68.

(12) Schofield, C. J., and Zhang, Z. (1999) Structural and mechanistic studies on 2-oxoglutarate-dependent oxygenases and related enzymes. *Current Opinion in Structural Biology 9*, 722-731.

(13) Lipscomb, J. D., and Orville, A. M. (1992) Mechanistic aspects of dihydroxybenzoate dioxygenase. *Metal Ions Biol. 28*, 243-298.

(14) Dagley, S. (1986) *Biochemistry of Aromatic Hydrocarbon Degradation in Pseudomonads in the Bacteria*, Academic Press, New York.

(15) Wackett, L. P. (2002) Mechanism and applications of rieske non-heme iron dioxygenases. *Enzyme Microb. Technol. 31*, 577-587.

(16) Wolfe, M. D., Altier, D. J., Stubna, A., Popescu, C. V., Münck, E., and Lipscomb, J. D. (2002) Benzoate 1,2-dioxygenase from *Pseudomonas Putida*: single turnover kinetics and regulation of a two-component rieske dioxygenase. *Biochemistry 41*, 9611-9626.

(17) Fitzpatrick, P. F. (1999) The tetrahydropterin-dependent amino acid hydroxylases. *Ann. Rev. Biochem. 68*, 355-381.

(18) Fitzpatrick, P. F. (2003) Mechanism of aromatic amino acid hydroxylation. *Biochemistry 42*, 14083-14091.

(19) Fitzpatrick, P. F. (2000) The aromatic amino acid hydroxylases, in *Advances in Enzymology and Related Areas of Molecular Biology* (Purich, D. L., Ed.) pp 235-294, John Wiley & Sons, Inc., New York.

(20) Palmer, G., and Massey, V. (1968) Mechanisms of flavoprotein catalysis, in *Biological Oxidation* (Singer, T. P., Ed.) pp 263-300, John Wiley and Sons, New York.

(21) Archer, M. C., and Scrimgeour, K. G. (1970) Rearrangement of quinonoid dihydropteridines to 7,8-dihydropteridines. *Can. J. Biochem. 48*, 278-287.

(22) Bailey, S. W., Rebrin, I., Boerth, S. R., and Ayling, J. E. (1995) Synthesis of 4a-hydroxytetrahydropterins and the mechanism of their nonenzymatic dehydration to quinoid dihydropterins. *J. Am. Chem. Soc. 117*, 10203-10211.

(23) Kappock, T. J., and Caradonna, J. P. (1996) Pterin-dependent amino acid hydroxylases. *Chem. Rev. 96*, 2659-2756.

(24) Udenfriend, S., and Cooper, J. R. (1952) The enzymatic conversion of phenylalanine to tyrosine. *J. Biol. Chem. 194*, 503-511.

(25) Kaufman, S. (1959) Studies on the mechanism of the enzymatic conversion of phenylalanine to tyrosine. *J. Biol. Chem. 234*, 2677-2682.

(26) Nagatsu, T., Levitt, M., and Udenfriend, S. (1964) Tyrosine hydroxylase the initial step in norepinephrine biosynthesis. *J. Biol. Chem. 239*, 2910-2917.

(27) Ludecke, B., Knappskog, P. M., Clayton, P. T., Surtees, R. A. H., Clelland, J. D., Heales, S. J. R., Brand, M. P., Bartholome, K., and Flatmark, T. (1996) Recessively inherited L-DOPA-responsive parkinsonism in infancy caused by a point mutation (L205) in the tyrosine hydroxylase gene. *Hum. Mol. Genet. 5*, 1023-1028.

(28) Boadle-Biber, M. C. (1993) Regulation of serotonin synthesis. *Prog. Biophys. Molec. Biol. 60*, 1-15.

(29) Martínez, A., Knappskog, P. M., and Haavik, J. (2001) A structural approach into human tryptophan hydroxylase and its implications for the regulation of serotonin biosynthesis. *Curr. Med. Chem. 8*, 1077-1091.

(30) Ledley, F. D., DiLella, A. G., Kwok, S. C. M., and Woo, S. L. C. (1985) Homology between phenylalanine and tyrosine hydroxylases reveals common structural and functional domains. *Biochemistry 24*, 3389-3394.

(31) Wang, L., Erlandsen, H., Haavik, J., Knappskog, P. M., and Stevens, R. C. (2002) Three-dimensional structure of human tryptophan hydroxylase and its implications for the biosynthesis of the neurotransmitters serotonin and melatonin. *Biochemistry 41*, 12569-12574.

(32) Erlandsen, H., Fusetti, F., Martinez, A., Hough, E., Flatmark, T., and Stevens, R. C. (1997) Crystal structure of the catalytic domain of human phenylalanine hydroxylase reveals the structural basis for phenylketonuria. *Nature Struct. Biol. 4*, 995-1000.

(33) Goodwill, K. E., Sabatier, C., Marks, C., Raag, R., Fitzpatrick, P. F., and Stevens, R. C. (1997) Crystal structure of tyrosine hydroxylase at 2.3 Å and its implications for inherited diseases. *Nature Struct. Biol. 4*, 578-585.

(34) Windahl, M. S., Petersen, C. R., Christensen, H. E., and Harris, P. (2008) Crystal structure of tryptophan hydroxylase with bound amino acid substrate. *Biochemistry 47*, 12087-12094.

(35) Francisco, W. A., Tian, G., Fitzpatrick, P. F., and Klinman, J. P. (1998) Oxygen-18 kinetic isotope effect studies of the tyrosine hydroxylase reaction: evidence of rate limiting oxygen activation. *J. Am. Chem. Soc. 120*, 4057-4062.

(36) Klinman, J. P. (2001) Life as aerobes: are there simple rules for activation of dioxygen by enzymes? *J. Biol. Inorg. Chem. 6*, 1-13.

(37) Roth, P. J., and Klinman, J. P. (2005) Oxygen-18 isotope effects as a probe of enzymatic activation of molecular oxygen, in *Isotope Effects in Chemistry and Biology* (Kohen, A., and Limbach, H., Ed.) pp 645-670, Marcel Dekker, Inc., New York.

(38) Moran, G. R., Derecskei-Kovacs, A., Hillas, P. J., and Fitzpatrick, P. F. (2000) On the catalytic mechanism of tryptophan hydroxylase. *J. Am. Chem. Soc. 122*, 4535-4541.

(39) Pavon, J. A., and Fitzpatrick, P. F. (2006) Insights into the catalytic mechanisms of phenylalanine and tryptophan hydroxylase from kinetic isotope effects on aromatic hydroxylation. *Biochemistry 45*, 11030-11037.

(40) Frantom, P. A., and Fitzpatrick, P. F. (2003) Uncoupled forms of tyrosine hydroxylase unmask kinetic isotope effects on chemical steps. *J. Am. Chem. Soc. 125*, 16190-16191.

(41) Hillas, P. J., and Fitzpatrick, P. F. (1996) A mechanism for hydroxylation by tyrosine hydroxylase based on partitioning of substituted phenylalanines. *Biochemistry 35*, 6969-6975.

(42) Pavon, J. A., and Fitzpatrick, P. F. (2005) Intrinsic isotope effects on benzylic hydroxylation by the aromatic amino acid hydroxylases: evidence for hydrogen tunneling, coupled motion, and similar reactivities. *J. Am. Chem. Soc. 127*, 16414-16415.

(43) Ellis, H. R., Daubner, S. C., and Fitzpatrick, P. F. (2000) Mutation of serine 395 of tyrosine hydroxylase decouples oxygen-oxygen bond cleavage and tyrosine hydroxylation. *Biochemistry 39*, 4174-4181.

(44) Bassan, A., Blomberg, M. R. A., and Siegbahn, P. E. M. (2003) Mechanism of aromatic hydroxylation by an activated Fe^{IV}=O core in tetrahydrobiopterin-dependent hydroxylases. *Chem. Eur. J. 9*, 4055-4067.

(45) Eser, B. E., Barr, E. W., Frantom, P. A., Saleh, L., Bollinger, J. M. Jr., Krebs, C., and Fitzpatrick, P. F. (2007) Direct spectroscopic evidence for a high-spin Fe(IV) intermediate in tyrosine hydroxylase. *J. Am. Chem. Soc. 129*, 11334-11335.

(46) Bollinger, J. M. Jr., and Krebs, C. (2006) Stalking intermediates in oxygen activation by iron enzymes: motivation and method. *J. Inorg. Biochem. 100*, 586-605.

(47) Krebs, C., Galonic, F. D., Walsh, C. T., and Bollinger, J. M. Jr., (2007) Non-heme Fe(IV)-oxo intermediates. *Acc. Chem. Res. 40*, 484-492.

(48) Hegg, E. L., and Que, L. (1997) The 2-His-1-carboxylate facial triad an emerging structural motif in mononuclear non-heme iron (II) enxymes. *European Journal of Biochemistry 250*, 625-629.

(49) Fitzpatrick, P. F. (1991) The steady state kinetic mechanism of rat tyrosine hydroxylase. *Biochemistry 30*, 3658-3662.

(50) Fitzpatrick, P. F. (1991) Studies of the rate-limiting step in the tyrosine hydroxylase reaction: alternate substrates, solvent isotope effects, and transition state analogs. *Biochemistry 30*, 6386-6391.

(51) Moran, G. R., Phillips, R. S., and Fitzpatrick, P. F. (1999) The influence of steric bulk and electrostatics on the hydroxylation regiospecificity of tryptophan hydroxylase: characterization of methyltryptophans and azatryptophans as substrates. *Biochemistry 38*, 16283-16289.

(52) Frantom, P. A., Pongdee, R., Sulikowski, G. A., and Fitzpatrick, P. F. (2002) Intrinsic deuterium isotope effects on benzylic hydroxylation by tyrosine hydroxylase. *J. Am. Chem. Soc. 124*, 4202-4203.

(53) Siegmund, H. U., and Kaufman, S. (1991) Hydroxylation of 4-methylphenyl-alanine by rat liver phenylalanine hydroxylase. *J. Biol. Chem. 266*, 2903-2910.

(54) Daubner, S. C., Hillas, P. J., and Fitzpatrick, P. F. (1997) Characterization of chimeric pterin dependent hydroxylases: contributions of the regulatory domains of tyrosine and phenylalanine hydroxylase to substrate specificity. *Biochemistry 36*, 11574-11582.

(55) Shiman, R., Gray, D. W., and Pater, A. (1979) A simple purification of phenylalanine hydroxylase by substrate-induced hydrophobic chromatography. *J. Biol. Chem. 254*, 11300-11306.

(56) Daubner, S. C., Hillas, P. J., and Fitzpatrick, P. F. (1997) Expression and characterization of the catalytic domain of human phenylalanine hydroxylase. *Arch. Biochem. Biophys. 348*, 295-302.

(57) Shah, J. A., Biasi, V., Taylor, G. S., Roberts, C., Hemmati, P., Munton, R., West, A., and Routdge, P.C. (1999) Development of a protocol for the automated analysis of amino acids in brain tissue samples and microdialysates. *Journal of Chromatography*, 133-140.

(58) Fitzpatrick, P., F. (2005) Isotope effects from partitioning of intermediates in enzyme-catalyzed hydroxylation reactions, in *Isotope Effects in Chemistry and Biology* (Kohen, A., Limbach, H., Ed.) pp 861-873, Marcel Dekker, New York.

(59) Nelson, D., and Trager, W. F. (2003) The use of deuterium isotope effects to probe the active site properties, mechanism of cytochrome P450-catalyzed reactions, and mechanisms of metabolically dependent toxicity. *Drug. Metabolism and Disposition 31*, 1481-1498.

(60) Hanzlik, R. P., Hogberg, K., Moon, J. B., and Judson, C. M. (1985) Intramolecular kinetic deuterium isotope effects on microsomal hydroxylation and chemical chlorination of toluene-α-d_1 and toluene-α,α-d_2. *J. Am. Chem. Soc. 107*, 7164-7167.

(61) Bell, R. P. (1980) *The Tunnel Effect in Chemistry.* Chapman & Hall, NewYork.

(62) Klinman, J. P. (1991) Hydrogen tunneling and coupled motion in enzyme reactions, in *Enzyme Mechanism from Isotope Effects* (Cook, P. F., Ed.) pp 127-148, CRC Press, Boca Raton, Fl.

(63) Bell, R. P. (1974) Recent advances in the study of kinetic hydrogen isotope effects. *Chem. Soc. Rev. 3*, 513-544.

(64) Kin, Y., and Kreevoy, M. M. (1992) The experimental manifestations of corner-cutting tunneling. *J. Am. Chem. Soc. 114*, 7116-7123.

(65) Kohen, A. (2005) Kinetic isotope effects as probes for hydrogen tunneling in enzyme catalysis, in *Isotope Effects in Chemistry and Biology* (Kohen, A., Limbach, H., Ed.) pp 743-764, Marcel Dekker, New York.

(66) Cook, P. F., Oppenheimer, N. J., and Cleland, W. W. (1981) Secondary deuterium and nitrogen-15 isotope effects in enzyme-catalyzed reactions. Chemical mechanism of liver alcohol dehydrogenase. *Biochemistry 20*, 1817-1825.

(67) Hermes, J. D., and Cleland, W. W. (1984) Evidence from multiple isotope effect determinations for coupled hydrogen motion and tunneling in the reaction catalyzed by glucose-6-phosphate dehydrogenase. *J. Am. Chem. Soc. 106*, 7263-7264.

(68) Huskey, W. P., and Showen, R. L. (1983) Reaction-coordinate tunneling in hydride-transfer reactions. *J. Am. Chem Soc.*, 5704-5706.

(69) Huskey, W. P. (1991) Origins and interpretations of heavy-atom isotope effects, in *Enzyme Mechanism from Isotope Effects* (Cook, P. F., Ed.) pp 37-72, CRC Press, Boca Raton, FL.

(70) Miller, S. M., and Klinman, J. P. (1985) Secondary isotope effects and structure-reactivity correlations in the dopamine ß-monooxygenase reaction: evidence for a chemical mechanism. *Biochemistry 24*, 2114-2127.

(71) Miller, S. M., and Klinman, J. P. (1983) Magnitude of intrinsic isotope effects in the dopamine ß-monooxygenase reaction. *Biochemistry 22*, 3091-3096.

(72) Francisco, W. A., Merkler, D. J., Blackburn, N. J., and Klinman, J. P. (1998) Kinetic mechanism and intrinsic isotope effects for the peptidylglycine α-amidating enzyme reaction. *Biochemistry 37*, 8244-8252.

(73) Klinman, J. P. (1996) Mechanisms whereby mononuclear copper proteins functionalize organic substrates. *Chem. Rev. 96*, 2541-2562.

(74) Groves, J. T., and McClusky, G. A. (1976) Aliphatic hydroxylation via oxygen rebound. Oxygen transfer catalyzed by iron. *J. Am. Chem. Soc. 98*, 859-861.

(75) Brigelius, R., Spottl, R., Bors, W., Lengfelder, E., Saran, M., and Weser, U. (1974) Superoxide dismutase activity of low molecular weight Cu2+-chelates studied by pulse radiolysis. *FEBS Letts. 47*, 72-75.

(76) Eberlein, G. A., Bruice, T. C., Lazarus, R. A., Henrie, R., and Benkovic, S. J. (1984) The interconversion of the 5,6,7,8-tetrahydro-, 7,8-dihydro-, and radical forms of 6,6,7,7-tetramethyldihydropterin. A model for the biopterin center of aromatic amino acid mixed function oxidases. *J. Am. Chem. Soc. 106*, 7916-7924.

(77) Benkovic, S., Wallick, D., Bloom, L., Gaffney, B. J., Domanico, P., Dix, T., and Pember, S. (1985) On the mechanism of action of phenylalanine hydroxylase. *Biochem. Soc. Trans. 13*, 436-438.

(78) Dix, T. A., and Benkovic, S. J. (1985) Mechanism of 'uncoupled' tetrahydropterin oxidation by phenylalanine hydroxylase. *Biochemistry 24*, 5839-5846.

(79) Dix, T. A., Bollag, G., Domanico, P. L., and Benkovic, S. J. (1985) Phenylalanine hydroxylase: absolute configuration and source of oxygen of the 4a-hydroxytetrahydropterin species. *Biochemistry 24*, 2955-2958.

(80) Carey, F. A., and Sundberg, R. J. (2000) *Advanced Organic Chemistry, Chemical Bonding and Structure*, Kluwer Academic/ Plenum Publishers, New York.

(81) Banhson, J. B., and Klinman, J. P. (1995) Hydrogen tunneling in enzyme catalysis. *Methods in Enzymology 249*, 373-397.

(82) Rucker, J., and Klinman, J. P. (1999) Computational study of tunneling and coupled motion in alcohol dehydrogenase-catalyzed reactions: implication for measured hydrogen and carbon isotope effects. *J. Am. Chem. Soc. 121*, 1997-2006.

(83) Bigeleisen, J. W. M. (1958) Theoretical and experimental aspects of isotope effects in chemical kinetics. *Adv. Chem. Physics 1*, 15-76.

(84) Schneider, M. E., and Stern, M. J. (1972) Arrhenius preexponential factors for primary hydrogen kinetic isotope effects. *J. Am. Chem. Soc. 94*, 1517-1522.

(85) Kohen, A., and Klinman, J. P. (1998) Enzyme catalysis: beyond classical paradigms. *Acc. Chem. Res. 31*, 397-404.

(86) Kohen, A., and Klinman, J. P. (1999) Hydrogen tunneling in biology. *Chemistry & Biology 6*, 191-198.

(87) Gustafsson, J. A., Hrycay, E. G., and Ernster, L. (1976) Sodium periodate, sodium chlorite, and organic hydroperoxides as hydroxylating agents in steroid hydroxylation reactions catalyzed by adrenocortical microsomal and mitochondrial cytochrome P450. *Arch. Biochem. Biophys. 174*, 440-53.

(88) Froland, W. A., Andersson, K. K., Lee, S. K., Liu, Y., and Lipscomb, J. D. (1992) Methane monooxygenase component B and reductase alter the regioselectivity of the hydroxylase component-catalyzed reactions. A novel role for protein-protein interactions in an oxygenase mechanism. *J. Biol. Chem. 267*, 17588-17597.

(89) Sura, G. R., Lasagna, M., Gawandi, V., Reinhart, G. D., and Fitzpatrick, P. F. (2006) Effects of ligands on the mobility of an active-site loop in tyrosine hydroxylase as monitored by fluorescence anisotropy. *Biochemistry 45*, 9632-9638.

(90) Moran, G. R., Daubner, S. C., and Fitzpatrick, P. F. (1998) Expression and characterization of the catalytic core of tryptophan hydroxylase. *J. Biol. Chem. 273*, 12259-12266.

(91) Daubner, S. C., Melendez, J., and Fitzpatrick, P. F. (2000) Reversing the substrate specificities of phenylalanine and tyrosine hydroxylase: aspartate 425 of tyrosine hydroxylase is essential for L-DOPA formation. *Biochemistry 39*, 9652-9661.

(92) Daubner, S. C., and Fitzpatrick, P. F. (1999) Site-directed mutants of charged residues in the active site of tyrosine hydroxylase. *Biochemistry 38*, 4448-4454.

(93) Nelson, D. P., and Kiesow, L. A. (1972) Enthalpy of decomposition of hydrogen peroxide by catalase at 25 degrees C (with molar extinction coefficients of H_2O_2 solutions in the UV). *Anal. Biochem. 49*, 474-478.

(94) Shah, A. J., de Biasi, V., Taylor, S. G., Roberts, C., Hemmati, P., Munton, R., West, A., Routledge, C., and Camilleri, P. (1999) Development of a protocol for the automated analysis of amino acids in brain tissue samples and microdialysates. *J. Chromatogr. B. 735*, 133-140.

(95) Nordblom, G. D., White, R. E., and Coon, M. J. (1976) Studies on hydroperoxide-dependent substrate hydroxylation by purified liver microsomal cytochrome P-450. *Arch. Biochem. Biophys. 175*, 524-533.

(96) Gustafsson, J. A., and Ernster, L. (1976) Sodium periodate, sodium chlorite, and organic hydroperoxides as hydroxylating agents in steroid hydroxylation reactions catalyzed by adrenocortical microsomal and mitochondrial cytochrome P450. *Arch. Biochem. Biophys. 174*, 440-453.

(97) Hrycay, E. G., Gustafsson, J. A., Ingelman-Sundberg, M., and Ernster, L. (1975) Sodium periodate, sodium chloride, organic hydroperoxides, and hydrogen peroxide as hydroxylating agents in steroid hydroxylation reactions catalyzed by partially purified cytochrome P-450. *Biochem. Biophys. Res. Commun. 66*, 209-216.

(98) Abu-Omar, M. M., Loaiza, A., and Hontzeas, N. (2005) Reaction mechanisms of mononuclear non-heme iron oxygenases. *Chem. Rev. 105*, 2227-52.

(99) Ribeiro, P., Pigeon, D., and Kaufman, S. (1991) The hydroxylation of phenylalanine and tyrosine by tyrosine hydroxylase from cultured pheochromocytoma cells. *J. Biol. Chem. 266*, 16207-16211.

(100) Dix, T. A., Kuhn, D. M., and Benkovic, S. J. (1987) Mechanism of oxygen activation by tyrosine hydroxylase. *Biochemistry 26*, 3354-3361.

(101) Entsch, B., Ballou, D. P., and Massey, V. (1976) Role of oxygenated flavins in the catalytic reaction of p-hydroxybenzoate hydroxylase, in *Flavins and Flavoproteins* (Badkey, Ed.) pp 111-123, Elsevier, Amsterdam.

(102) Massey, V. (1994) Activation of molecular oxygen by flavins and flavoproteins. *J. Biol. Chem. 269*, 22459-22462.

(103) Entsch, B., Ballou, D. P., and Massey, V. (1976) Flavin-oxygen derivatives involved in hydroxylation by p-hydroxybenzoate hydroxylase. *J. Biol. Chem. 251*, 2550-2563.

(104) Wardman, P., and Candeias, L. (1996) Fenton chemistry: an introduction. *Radiat. Res. 145*, 523-531.

(105) Daubner, S. C., McGinnis, J. T., Gardner, M., Kroboth, S. L., Morris, A. R., and Fitzpatrick, P. F. (2006) A flexible loop in tyrosine hydroxylase controls coupling of amino acid hydroxylation to tetrahydropterin oxidation. *J. Mol. Biol. 359*, 299-307.

(106) Goodwill, K. E., Sabatier, C., and Stevens, R. C. (1998) Crystal structure of tyrosine hydroxylase with bound cofactor analogue and iron at 2.3 Å resolution: self-hydroxylation of phe300 and the pterin-binding site. *Biochemistry 37*, 13437-13445.

(107) Andersen, O. A., Flatmark, T., and Hough, E. (2001) High resolution crystal structures of the catalytic domain of human phenylalanine hydroxylase in its catalytically active Fe(II) form and binary complex with tetrahydrobiopterin. *J. Mol. Biol. 314*, 279-291.

(108) Shiman, R., Xia, T., Hill, M. A., and Gray, D. W. (1994) Regulation of rat liver phenylalanine hydroxylase. II. Substrate binding and the role of activation in the control of enzymatic activity. *J. Biol. Chem. 269*, 24647-24656.

(109) Xia, T., Gray, D. W., and Shiman, R. (1994) Regulation of rat liver phenylalanine hydroxylase. III. Control of catalysis by (6R)-tetrahydrobiopterin and phenylalanine. *J. Biol. Chem. 269*, 24657-24665.

(110) Erlandsen, H., Bjorgo, E., Flatmark, T., and Stevens, R. C. (2000) Crystal structure and site-specific mutagenesis of pterin-bound human phenylalanine hydroxylase. *Biochemistry 39*, 2208-2217.

(111) Andersen, O. A., Stokka, A. J., Flatmark, T., and Hough, E. (2003) 2.0 Å Resolution crystal structures of the ternary complexes of human phenylalanine hydroxylase catalytic domain with tetrahydrobiopterin and 3-(2-thienyl)-L-alanine or L-norleucine: substrate specificity and molecular motions related to substrate binding. *J. Mol. Biol. 333*, 747-757.

(112) Windahl, M. S., Petersen, C. R., Christensen, H. E., and Harris, P. (2008) Crystal structure of tryptophan hydroxylase with bound amino acid substrate. *Biochemistry 47*, 12087-12094.

(113) Wasinger, E. C., Mitic, N., Hedman, B., Caradonna, J., Solomon, E. I., and Hodgson, K. O. (2002) X-ray absorption spectroscopic investigation of the resting ferrous and cosubstrate-bound active sites of phenylalanine hydroxylase. *Biochemistry 41*, 6211-6217.

(114) Neibergall, M. B, Stubna, A., Mekmouche, Y. Münck, E., and Lipscomb, J. D. (2007) Hydrogen peroxide dependent cis-dihydroxylation of benzoate by fully oxidized benzoate 1,2-dioxygenase. *Biochemistry 46*, 8004-8016.

(115) Wolfe, M. D., and Lipscomb. J. D. (2003) Hydrogen peroxide-coupled cis-diol formation catalyzed by naphthalene 1,2-dioxygenase. *J. Biol. Chem. 278*, 829-835.

(116) Groves, J. T., McClusky, G. A., White, R. E., and Coon, M. J. (1978) Aliphatic hydroxylation by highly purified liver microsomal cytochrome P-450. Evidence for a carbon radical intermediate. *Biochem. Biophys. Res. Commun. 81*, 154-160.

(117) Hjelmeland, L. M., Aronow, L., and Trudell, J. R. (1977) Intramolecular determination of primary kinetic isotope effects in hydroxylations catalyzed by cytochrome P-450. *Biochem. Biophys. Res. Commun. 76*, 541-549.

(118) Park, M. J., Lee, J., Suh, Y., Kim, J., and Nam, W. (2006) Reactivities of mononuclear non-heme iron intermediates including evidence that iron(III)-hydroperoxo species is a sluggish oxidant. *J. Am. Chem. Soc. 128*, 2630-2634.

(119) Köster, S., Stier, G., Ficner, R., Hölzer, M., Curtius, H. C., Suck, D., and Ghisla, S. (1996) Location of the active site and proposed catalytic mechanism of pterin-4a-carbinolamine dehydratase. *Eur. J. Biochem. 241*, 858-864.

(120) Kobe, B., Jennings, I. G., House, C. M., Michell, B. J., Goodwill, K. E., Santarsiero, B. D., Stevens, R. C., Cotton, R. G. H., and Kemp, B. E. (1999) Structural basis of intrasteric and allosteric controls of phenylalanine hydroxylase. *Nature Struct. Biol. 6*, 442-448.

(121) Hegg, E. L., and Que, L., Jr. (1997) The 2-His-1-carboxylate facial triad. An emerging structural motif in mononuclear non-heme iron(II) enzymes. *Eur. J. Biochem. 250*, 625-629.

(122) Klinman, J. P. (1978) Kinetic isotope effects in enzymology. *Adv. Enzymol. 46*, 415-495.

(123) Abita, J. P., Parniak, M., and Kaufman, S. (1984) The activation of rat liver phenylalanine hydroxylase by limited proteolysis, lysolecithin, and tocopherol

phosphate. Changes in conformation and catalytic properties. *J. Biol. Chem. 259*, 14560-14566.

(124) Fitzpatrick, P. F. (1994) Kinetic isotope effects on hydroxylation of ring-deuterated phenylalanines by tyrosine hydroxylase provide evidence against partitioning of an arene oxide intermediate. *J. Am. Chem. Soc. 116*, 1133-1134.

(125) Miroux, B., and Walker, J. E. (1996) Over-production of proteins in *Escherichia coli:* mutant hosts that allow synthesis of some membrane proteins and globular proteins at high levels. *J. Mol. Biol. 260*, 289-298.

(126) Shiman, R., Jones, S. H., and Gray, D. W. (1990) Mechanism of phenylalanine regulation of phenylalanine hydroxylase. *J. Biol. Chem. 265*, 11633-11642.

(127) Moran, G. R., and Fitzpatrick, P. F. (1999) A continuous fluorescence assay for tryptophan hydroxylase. *Anal. Biochem. 266*, 148-152.

(128) Guroff, G., Daly, J. W., Jerina, D. M., Renson, J., Witkop, B., and Udenfriend, S. (1967) Hydroxylation-induced migration: the NIH shift. *Science 157*, 1524-1530.

(129) Guroff, G., Reifsnyder, C. A., and Daly, J. (1966) Retention of deuterium in p-tyrosine formed enzymatically from p-deuterophenylalanine. *Biochem. Biophys. Res. Commun. 24*, 720-724.

(130) McKinney, J., Teigen, K., Frøystein, N. A., Salaün, C., Knappskog, P. M., Haavik, J., and Martínez, A. (2001) Conformation of the substrate and pterin cofactor bound to human tryptophan hydroxylase. Important role of Phe313 in substrate specificity. *Biochemistry 40*, 15591-15601.

(131) Fitzpatrick, P. F. (2005) Isotope effects from partitioning of intermediates in enzyme-catalyzed hydroxylation reactions in *Isotope Effects in Chemistry and Biology* (Kohen, A., and Limbach, H., Ed.) pp 861-873, Marcel Dekker, Inc., New York.

(132) Andersen, O. A., Flatmark, T., and Hough, E. (2002) Crystal structure of the ternary complex of the catalytic domain of human phenylalanine hydroxylase with tetrahydrobiopterin and 3-(2-thienyl)-L-alanine, and its implications for the mechanism of catalysis and substrate activation. *J. Mol. Biol. 320*, 1095-1108.

(133) Teigen, K., Frøystein, N. Å., and Martinez, A. (1999) The structural basis of the recognition of phenylalanine and pterin cofactors by phenylalanine hydroxylase: implications for the catalytic mechanism. *Journal of Molecular Biology 294*, 807-823.

(134) Miller, R. J., and Benkovic, S. J. (1988) L-[2,5-H_2]Phenylalanine, an alternate substrate for rat liver phenylalanine hydroxylase. *Biochemistry 27*, 3658-3663.

(135) Surtees, R., and Blau, N. (2000) The neurochemistry of phenylketonuria. *Eur. J. Pediatr. 159*, 109-113.

(136) Guroff, G., and Daly, J. (1967) Quantitative studies on the hydroxylation-induced migration of deuterium and tritium during phenylalanine hydroxylation. *Arch. Biochem. Biophys. 122*, 212-217.

(137) Winters, J. K., Pumpero, V. M., Kavana, M., and Moran, G. R. (2005) Accumulation of multiple intermediates in the catalytic cycle of (4-Hydroxyphenyl)-pyruvate dioxygenase from *Streptomyces avermitilis*. *Biochemistry 44*, 7189-7199.

(138) Groce, S. L., and Lipscomb, J. D. (2005) Aromatic ring cleavage by homoprotocatechuate 2,3-dioxygenase: role of His200 in the kinetics of interconversion of reaction cycle intermediates. *Biochemistry 44*, 7175-7188.

(139) Price, J. C., Barr, E. W., Tirupati, B., Bollinger, J. M., and Krebs, C. (2003) The first direct characterization of a high-valent iron intermediate in the reaction of an alpha-ketoglutarate-dependent dioxygenase: a high-spin Fe(IV) complex in taurine/alpha-ketoglutarate dioxygenase (TauD) from *Escherichia coli*. *Biochemistry 42*, 7497-7508.

(140) Hoffart, L. M., Barr, E. W., Guyer, R. B., Bollinger, J. M. and Krebs, C. (2006) Direct spectroscopic detection of a C-H-cleaving high-spin Fe(IV) complex in a prolyl-4-hydroxylase. *Proc. Natl. Acad. Sci. USA 103*, 14738-14743.

(141) Price, J. C., Barr, E. W., Hoffart, L. M., Krebs, C., and Bollinger, J. M. Jr., (2005) Kinetic dissection of the catalytic mechanism of taurine:alpha-ketoglutarate dioxygenase (TauD) from *Escherichia coli*. *Biochemistry 44*, 8138-8147.

(142) Riggs-Gelasco, P. J., Price, J. C., Guyer, R. B., Brehm, J. H., Barr, E. W., Bollinger, J. M. Jr., and Krebs, C. (2004) EXAFS spectroscopic evidence for an Fe=O unit in the Fe(IV) intermediate observed during oxygen activation by taurine:alpha-ketoglutarate dioxygenase. *J. Am. Chem. Soc. 126*, 8108-8109.

(143) Proshlyakov, D. A., Henshaw, T. F., Moterosso, G. R., Ryle, M. J., and Hausinger, R. P. (2004) Direct detection of oxygen intermediates in the non-heme Fe enzyme taurine/alpha-ketoglutarate dioxygenase. *J. Am. Chem. Soc. 126*, 1022-1033.

(144) Price, J. C., Barr, E. W., Glass, T. E., Krebs, C., and Bollinger, J. M. Jr., (2003) Evidence for hydrogen abstraction from C1 of taurine by the high-spin Fe(IV) intermediate detected during oxygen activation by taurine:α-ketoglutarate dioxygenase (TauD). *J. Am. Chem. Soc. 125*, 13008-13009.

(145) Galonic, D. P., Barr, E. W., Walsh, C. T., Bollinger, J. M. Jr., and Krebs, C. (2007) Two interconverting Fe(IV) intermediates in aliphatic chlorination by the halogenase CytC3. *Nature Chem. Biol. 3*, 113-116.

(146) Studier, F. W. (2005) Protein production by auto-induction in high-density shaking cultures. *Protein Expr. Purif. 41*, 207-234.

(147) Gutfreund, H. (1969) Resolution of optical and sampling methods. *Method. Enzymol. 16*, 229-249.

(148) Davis, M. D., and Kaufman, S. (1989) Evidence for the formation of the 4a-carbinolamine during the tyrosine-dependent oxidation of tetrahydrobiopterin by rat liver phenylalanine hydroxylase. *J. Biol. Chem. 264*, 8585-8596.

(149) Krebs, C., Price, J. C., Baldwin, J., Saleh, L., Green, M. T., and Bollinger, J. M. Jr., (2005) Rapid free-quench Mössbauer spectroscopy: monitoring changes of an iron-containing site during a biochemical reaction. *Inorg. Chem. 44*, 742-757.

(150) Grzyska, P. K., Ryle, M. J., Monterosso, G. R., Liu, J., Ballou, D. P., and Hausinger, R. P. (2005) Steady-state and transient kinetic analyses of tauring/alpha-ketoglutarate variants on the FeIV-oxo intermediate. *Biochemistry 44*, 3845-3855.

(151) Jiang, W., Hoffart, L. M., Krebs, C., and Bollinger, J. M. Jr., (2007) A manganese(IV)/Iron(IV) intermediate in assembly of the manganese(IV)/ iron(III) cofactor of *Chlamydia Trachomatis* ribonucleotide reductase. *Biochemistry 46*, 8709-8716.

(152) Volner, A., Zoidakis, J., and Abu-Omar, M. M. (2003) Order of substrate binding in bacterial phenylalanine hydroxylase and its mechanistic implication for pterin-dependent oxygenases. *J. Biol. Inorg. Chem. 8*, 121-128.

(153) Pember, S. O., Johnson, K. A., Villafranca, J. J., and Benkovic, S. J. (1989) Mechanistic studies on phenylalanine hydroxylase from *Chromobacterium violaceum*. Evidence for the formation of an enzyme-oxygen complex. *Biochemistry 28*, 2124-2130.

(154) Johnson-Winters, K., Pumpero, V. M., Kavana, M., Nelson, T., and Moran, G. R. (2003) (4-Hydroxyphenyl)-pyruvate dioxygenase from *Streptomyces avermitilis*: the basis for ordered substrate addition. *Biochemistry 42*, 2072-2080.

(155) Xing, G., Barr, E. W., Diao, Y., Hoffart, L. M., Prabhu, K. S., Arner, R. J., Reddy, C. C., Krebs, C., and Bollinger, J. M. Jr., (2005) Oxygen activation by a mixed-valent, diiron(II/III) cluster in the glycol cleavage reaction catalyzed by myo-inositol oxygenase. *Biochemistry 45*, 5402-5412.

(156) Groce, S. L., Miller-Rodeberg, M. A., and Lipscomb, J. D. (2004) Single-turnover kinetics of homoprotocatechuate 2,3-dioxygenase. *Biochemistry 43*, 15141-15153.

(157) Haavik, J., Doskeland, A. P., and Flatmark, T. (1986) Stereoselective effects in the interactions of pterin cofactors with rat-liver phenylalanine 4-monooxygenase. *Eur. J. Biochem. 160*, 1-8.

(158) Shiman, R., Gray, D. W., and Hill, M. A. (1994) Regulation of rat liver phenylalanine hydroxylase. I. Kinetic properties of the enzyme's iron and enzyme reduction site. *J. Biol. Chem. 269*, 24637-24646.

(159) Lazarus, R. A., Dietrich, R. F., Wallick, D. E., and Benkovic, S. J. (1981) On the mechanism of action of phenylalanine hydroxylase. *Biochemistry 20*, 6834-6841.

(160) Ryle, M. J., Padmakumar, R., and Hausinger, R. P. (1999) Stopped-flow kinetic analysis of *Escherichia coli* taurine/alpha-ketoglutarate dioxygenase: interactions with alpha-ketoglutarate, taurine, and oxygen. *Biochemistry 38*, 15278-15286.

(161) Jequier, E., Lovenberg, W., and Sjoerdsma, A. (1967) Tryptophan hydroxylase inhibition: The mechanism by which p-chlorophenylalanine depletes brain serotonin. *Molec. Pharmacol. 3*, 274-278.

(162) Lovenberg, W., Jequier, E., and Sjoerdsma, A. (1967) Tryptophan hydroxylation: measurement in pineal gland, brainstem, and carcinoid tumor. *Science 155*, 217-219.

(163) Koehntop, K. D., Emerson, J. P., and Que, L., Jr. (2005) The 2-His-1-carboxylate facial triad: a versatile platform for dioxygen activation by mononuclear non-heme iron(II) enzymes. *J. Biol. Inorg. Chem. 10*, 87-93.

(164) Frost, A. A., and Pearson, R. G. (1963) *Kinetics and Mechanism,* 2nd Ed, John Wiley & Sons, Inc., New York.

(165) Lawrence, M. S., and Massey, V. (1980) Kinetic and mechanistic studies on the oxidation of the meliotate hydroxylase 2-OH-cinnamate complex by molecular oxygen. *J. Biol. Chem. 255*, 5355-5363.

(166) Fersht, A. (1977) *Enzyme Structure and Mechanism,* Second ed., W. H. Freeman and Company, New York.

(167) Kunzelmann S, P. G., Herrmann C. (2006) Transient kinetic investigation of GTP hydrolysis catalyzed by interferon-gamma-induced hGBP1 (human guanylate binding protein 1). *J. Biol. Chem. 281*, 28624-28635.

(168) Frantom, P. A., Seravalli, J., Ragsdale, S. W., and Fitzpatrick, P. F. (2006) Reduction and oxidation of the active site iron in tyrosine hydroxylase: kinetics and specificity. *Biochemistry 45*, 2372-2379.

(169) Lazarus, R. A., DeBrosse, C. W., and Benkovic, S. J. (1982) Structural determination of quinonoid dihydropterins. *J. Am. Chem. Soc. 104*, 6871-6872.

(170) Fierke, C. A., and Hammes, G. G. (1995) Transient kinetic approaches to enzyme mechanisms. *Methods Enzymol. 249*, 3-37.

(171) Hiromi, K. (1979) Analysis of fast enzyme reactions: transient kinetics, in *Kinetics of Fast Enzyme Reactions: Theory and Practice*. pp 187-224, Kodansha Ltd, Tokyo.

(172) Bassan, A., Blomberg, M. R. A., and Siegbahn, P. E. M. (2003) Mechanism of dioxygen cleavage in tetrahydrobiopterin-dependent amino acid hydroxylases. *Chem. Eur. J. 9*, 106-115.

(173) Hill, M. A., Marota, J. A., and Shiman, R. (1988) Reaction of rat liver phenylalanine hydroxylase with fatty acid hydroperoxides. Characterization and mechanism. *J. Biol. Chem. 263*, 5646-5655.

(174) Pumpero, V. M., and Moran, G. R. (2006) Catalytic, noncatalytic, and inhibitory phenomena: kinetic analysis of (4-Hydroxyphenyl)-pyruvate dioxygenase from *Arabidopsis thaliana*. *Biochemistry 45*, 6044-6055.

(175) Bassan, A., Borowski, T., and Siegbahn, P. E. M. (2004) Quantum chemical studies of dioxygen activation by mononuclear non-heme iron enzymes with the 2-His-1-carboxylate facial triad. *Dalton Trans. 20*, 3153-3162.

(176) Valentine, A. M., Stahl, S. S., and Lippard, S. J. (1999) Mechanistic studies of the reaction of reduced methane monooxygenase hydroxylase with dioxygen and substrates. *J. Am. Chem. Soc. 121*, 3876-3887.

VITA

Jorge Alexander Pavon

Department of Biochemistry & Biophysics
103 Biochemistry/Biophysics Building
Texas A& M University
2128 TAMU
College Station, Texas 77843-2128
JApavon999@tamu.edu

Education

Ph.D. Biochemistry, Texas A&M University 2009
B.A. Chemistry, Rutgers University 2003

Honors and Awards

John Mack Prescott Award for Outstanding Research, Texas A&M University, Department of Biochemistry and Biophysics 2007
National Institute of Health Pre-doctoral Fellowship 2005-2010
American Chemical Society Division of Analytical Chemistry Undergraduate Award 2002.

Publications

Pavon, J.A.; Fitzpatrick, P. F. Insights into the catalytic mechanisms of phenylalanine and tryptophan hydroxylase from kinetic isotope effects on aromatic hydroxylation. *Biochemistry* 2006, 45, 11030-7.

Pavon, J.A.; Fitzpatrick, P. F. Intrinsic isotope effects on benzylic hydroxylation by the aromatic amino acid hydroxylases: evidence for hydrogen tunneling, coupled motion, and similar reactivities. *J. Am. Chem. Soc.* 2005, 127, 16414-5.

Papadakis, M.M.; **Pavon, J.A**.; Lalancette, R.A.; Thompson, H.W. The epimeric 9-oxobicyclo[3.3.1] nonane-3-carboxylic acids: hydrogen-bonding patterns of the endo acid and the lactol of the exo acid. *Acta Crystallogr C.* 2003, 59, 167-70.